HYDRIDES AT HIGH PRESSURES; AN EVALUATION OF "CHEMICAL PRECOMPRESSION" ON THE WAY TO METALLIC HYDROGEN

A Dissertation

Presented to the Faculty of the Graduate School

of Cornell University

in Partial Fulfillment of the Requirements for the Degree of

Doctor of Philosophy

by

Paulina Gonzalez Morelos

August 2010

HYDRIDES AT HIGH PRESSURES;
AN EVALUATION OF "CHEMICAL PRECOMPRESSION"
ON THE WAY TO METALLIC HYDROGEN

Paulina Gonzalez Morelos, Ph.D.
Cornell University 2010

In this dissertation, we present a theoretical study of compounds rich in hydrogen, focusing on their crystal structure and potential metallization as pressure is applied.

Chapter 1 is an introduction to metallic hydrogen; it reviews previous studies and suggests a new way of analyzing the geometric changes that ensue as pressure is applied. Chapter 2 describes the search for structures for SnH_4, using chemical intuition and random search algorithms. Chapter 3 deals with the general problem of segregation which arises as SnH_4, a thermodynamically metastable (positive heat of formation from Sn and $2H_2$) but kinetically persistent compound, is compressed. Chapter 3 is a complement to Chapter 2, as layered structures arise naturally in the low pressure regime, prompting us to explore the subject.

Chapter 4 begins an ambitious project which strives to understand the electronic structure and properties of metallic hydrides of the form MH_x, where M= Si, Sn and W, and x = 4, 6, 8, 10, 12. For n > 4, there exist van der Waals complexes at lower pressures, but show great variation in structure as they metallize at higher pressures.

Chapter 5 explores the effect of impurities in the DOS, as swapping of atoms in structures of stoichiometry $Li_{y-1}Be_yH$. The parent LiBe phase is stable at high pressures; here we attempt to lower the pressure for its metallization by H substitution

BIOGRAPHICAL SKETCH

Paulina González Morelos, the author of this dissertation, was born in the spring of 1979 in Ixtlán del Río, in the state of Nayarit, Mexico, the first child of Agueda Morelos and Luis González. Her sister, Laura, nicely completed the family two years later. The love for learning and books came early into Paulina's life as her mom taught her to read and write by the time she was four and ever since then she has found in books great friends.

The family moved a lot in the early years and until the author was 8 years old they finally settled in Tepic. She joined the Girl scouts where she discovered the greatness of the outdoors, and to the relief of her parents, helped her put the books down from time to time. While in High School her father got into Cornell Graduate School -Agricultural Sciences- and the family moved once more, this time to a different country to never-heard-before town of Ithaca, New York. Struggling to adapt to the culture and to the challenge that is learning a new language, Paulina became interested in sciences, joining by her senior year AP Chemistry, the math team, and the National Honor Society.

After High School she decided to return to Mexico to start her undergraduate studies at the University of Guadalajara where she majored in chemistry and physics. During undergrad she worked with Professor Luis Javier González Ortíz researching the chemistry of polymers. She spent time at a summer school at the CINVESTAV which helped her make her mind to continue her studies in sciences, more specifically in the area of theoretical chemistry. She entered the graduate school at the University of Guanajuato working with Professor Juvencio Robles focusing in the research of small metallic clusters. After obtaining

her masters degree Paulina, took a job as a math teacher in Morelia, Michoacan in an elementary school, a small detour while getting ready for the next step.

While at Cornell, she joined the lab of Professor Roald Hoffmann in the winter of 2005. Paulina worked in the general area of high pressure of hydrides, with the goal in mind of obtaining metallic hydrogen at static pressure. Making the most with her time, she also learned salsa dancing, where she met her boyfriend Bruno Rousseau, climbing - becoming later a climbing instructor as part of the Cornell Outdoor Education program- and, kayaking. She also took language classes where she learned the basics of French and German. As the author writes these lines, she wonders how she managed to have time to obtain her degree, but so she did, and in the fall of 2010 Paulina will join the Donostia International Physics Center at San Sebastian-Gipuskuoa, Spain, as a postdoc in the lab of Professor Andrés Arnau.

This thesis is dedicated to my family and to Bruno.

ACKNOWLEDGEMENTS

First and foremost, I would like to thank my advisor, Professor Roald Hoffmann, for allowing me to work in his group. Throughout my 5 years in his lab I have admired his never ending passion for science and teaching science. I have had a great time learning and I will miss it, and vow to remember to keep my audience in mind and not to create mysteries.

Being in his group has been all the richer by allowing me to work with curious and driven scientists such as Eva Zurek, Patryk Zaleski-Ejgierd, Abdel Monem Rawashdeh, Masoud Aryanpour. Special thanks to Vanessa Labet and to Xiaodong Wen. Their comments and insights have taught me a lot and have made a large contribution in my research. The rest of the group, Nick, Anne, Chinmoy, Ji, Rob, Ryan, Katie and Tom were also great bunch.

My great network of friends need to be mentioned in my acknowledgements: Nesha May Andoy, Ankush Gupta and Dominic Olinares. I would not have asked for better friends. The Loring Group who more than once considered me as a honorary member – Scott, Ben, Maicol, Swapna, Paolo and Anne– the same goes to the Hines Group –Brandon, Ian, Debo and Marc– thanks for the good times.

Thanks to my family – my parents Luis, Agueda and my sister Laura– for their support and encouragement. Finally, I would like to thank Bruno Rousseau - Thanks for being so supportive and loving, meeting you was the best part of my experience at Cornell!

I also want to acknowledge the National Science Foundation for supporting this research through Grants No. CHE091063 and DMR-0904505 and to the Cornell Nanoscale Facility for its Intel Cluster, part of the National Nanotechnology Infrastructure Network (NNIN) also funded by the National Science Foundation.

TABLE OF CONTENTS

[1]Reproduced with permission from *ChemPhysChem*, accepted for publication 2010

LIST OF TABLES

LIST OF FIGURES

CHAPTER 1

Metallic Hydrogen, Ever Elusive

1.1 Introduction - Why Metallic Hydrogen?

Metallic hydrogen, a Holy Grail of experimentalists and theoreticians alike, remains elusive [1]. The most abundant element in the Universe is expected to be metallic at planetary core conditions [2], if not superconducting at ambient temperatures [3]. The study of hydrogen at hight pressure is a key problem in modern physics and astrophysics. [4].

H_2 was originally predicted in 1935 to become metallic at 25 Kbar [5]. To help put things in perspective, 100 Gigapascal is equal to one million atmospheres, while the pressure at the core of Earth is ~ 350 GPa. However, it soon became clear that this pressure was not enough for hydrogen to dissociate and display metallic properties. Metallization in a static environment is still out of reach experimentally, even at pressures as high as ~360 GPa [6–9]. But there is evidence for metallization of hydrogen under shock wave conditions [10].

What prevents hydrogen from becoming metallic? As it turns out, there are quite a few barriers to overcome. It is estimated that a drastic reduction in volume, as much as 10-fold, is needed for metallic hydrogen to become a reality. This is very difficult to achieve, given our current experimental limitations [6]. However, the strongest impediment to metallization is perhaps the persistent pairing of the element, into diatomic molecules.

1.2 Solid Hydrogen Under Pressure

Hydrogen at low pressures and at ambient temperature is a molecular diatomic solid. It is made up of freely rotating molecules on a hexagonal close-packed lattice [11]. In solid hydrogen the H_2 molecules have a strong covalent molecular bond (with a bond length unchanged from the free gas phase molecule, R = 0.74Å). There are, of course, weak intermolecular interactions in the crystal; the shortest intermolecular distances are 3.8Å, experimentally [12], while in calculations this distance shrinks to 3.1 Å. With a large band-gap of ~ 16 eV, as measured in a lab, solid hydrogen at ambient temperature is an insulator [13].

The behavior of solid hydrogen at ambient temperature and low pressure is more or less that of a noble gas solid [14]. For comparison the melting point of H_2 is 14 K , while that of He, Ne, Ar, Kr, Xe and Rn are 1, 24, 84, 116, 161, and 202 K respectively. As pressure is applied, hydrogen molecules will come closer together, the interatomic interactions will increase, and, as the molecules dissociate, its behavior should resemble that of an alkali metal, just as predicted back in 1935 [5, 15].

How does solid hydrogen behave under pressure? In the low pressure regime, from 0-100 GPa, solid hydrogen, as described above, consists of freely rotating molecules with their centers arranged in an *hcp* lattice [11]. This state is know as Phase I. As pressure is applied, the molecular axes start to orient,

and the broken-symmetry Phase II occurs at ~110 GPa [14]. At 150 GPa hydrogen undergoes yet another transition; Phase III Raman and IR spectra show a marked change in solid hydrogen at this pressure and low temperatures [16, 17].

The structures of the different phases of hydrogen are not easy to determine. Experiments and theoretical studies on hydrogen come with many challenges. X-ray and neutron scattering data have yet to shed light on possible structures, and predicting new structures involves a laborious search of many different possibilities.

In preparing for a strategy of lowering the metallization pressure of H_2, we first looked into what is known experimentally and theoretically about the element. Here we followed the study done by Pickard and Needs [18] on hydrogen. We chose their most stable structures as initial geometries for theoretical optimization and followed their structural changes as pressure is applied. We analyzed hydrogen at pressures ranging from 0 - 500 GPa, paying attention to H_2 bond lengths and closest interatomic separations.

Throughout this thesis when we say"hydrogen" we mean the element in the form in which occurs at the specified pressure. The expression (hydrogen) does not imply that H_2 molecules persist or distance between them - it just specifies the composition.

1.3 Theoretical methodology

Our ground state calculations were performed with Density Functional Theory (DFT), within the generalized-gradient approximation, [19] with the Perdew-Wang exchange-correlation functional [20].The atomic potentials used in this study were based on Blöch's projector-augmented wave method and a plane wave basis set, as implemented in the Vienna Ab Initio Simulation Package (VASP) codes. For the optimization of the structures, the cell parameters, the atomic positions, and the cell volume were allowed to relax. The stress tensor was also calculated.

A defined stress was added to the stress tensor, setting the calculation into a particular pressure. Once an optimized structure was reached, the electronic density of states (DOS) was calculated. The k-point grids were generated via the Monkhorst-Pack scheme [21]. The calculations are at K = 0, neglecting the zero-point vibrational energy. We are well aware that quantum effects, one consequence of the large zero-point energy of H_2, may play a role in determining the actual state of H_2 [22]. The cutoff of the kinetic energy was set at 650 eV, and for the planewaves we set a self consistent field (SCF) tolerance of 1×10^{-5} eV/unit cell.

1.4 Results

Table 1.1 lists the symmetry groups of the most stable structures at different pressures which ranged from 0-500GPa. The results in Table 1.1. are in good agreement with the values found by Pickard and Needs [18].

Table 1.1: Space groups of the most stable hydrogen structures at pressures ranging from 0-500 GPa

Pressure	Space Group
0	$P6_3/m$
50	$P6_3/m$
100	$C2/c$
150	$C2/c$
200	$C2/c$
250	$Cmca-12$
300	$Cmca-12$
350	$Cmca-12$
400	$Cmca$
450	$Cmca$
500	$I4_1/amd$

1.4.1 $P6_3/m$, the most stable phase of H_2 from 0-100 GPa

As discussed above, hydrogen in Phase I is a molecular solid, in an *hcp* lattice with freely rotating molecules. The most stable structure at pressures ranging

from 0-100 GPa has one such arrangement, with space group $P6_3/m$. It has 8 formula units per cell, with ABAB stacking. Consistent with the rotational solid behavior, rotations of individual molecules within this symmetrical arrangement cost very little. Computations of the rotational reorientation of one molecule in the crystal show a tiny barrier of 0.0012 eV per H_2.

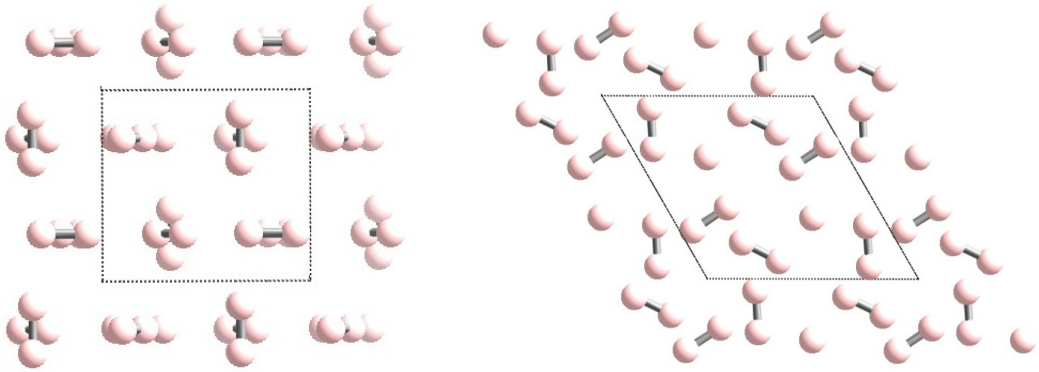

a) b)

Figure 1.1: Top and side view of the most stable structure, $P6_3/m$, of hydrogen at pressures 0-100GPa

1.4.2 *C2/c*, the most stable phase of H_2 from 100-250 GPa

At around 100 GPa and at low temperatures, hydrogen undergoes a phase transition, to the broken-symmetry Phase II. As pressure is applied, the most stable structure becomes a layered arrangement of hydrogen molecules with space group *C2/c*. With 12 formula units per cell, the molecular axes lie mostly on a plane, in contrast with the lower-pressure structure. It is still likely that the barrier to H_2 libration or rotation is small.

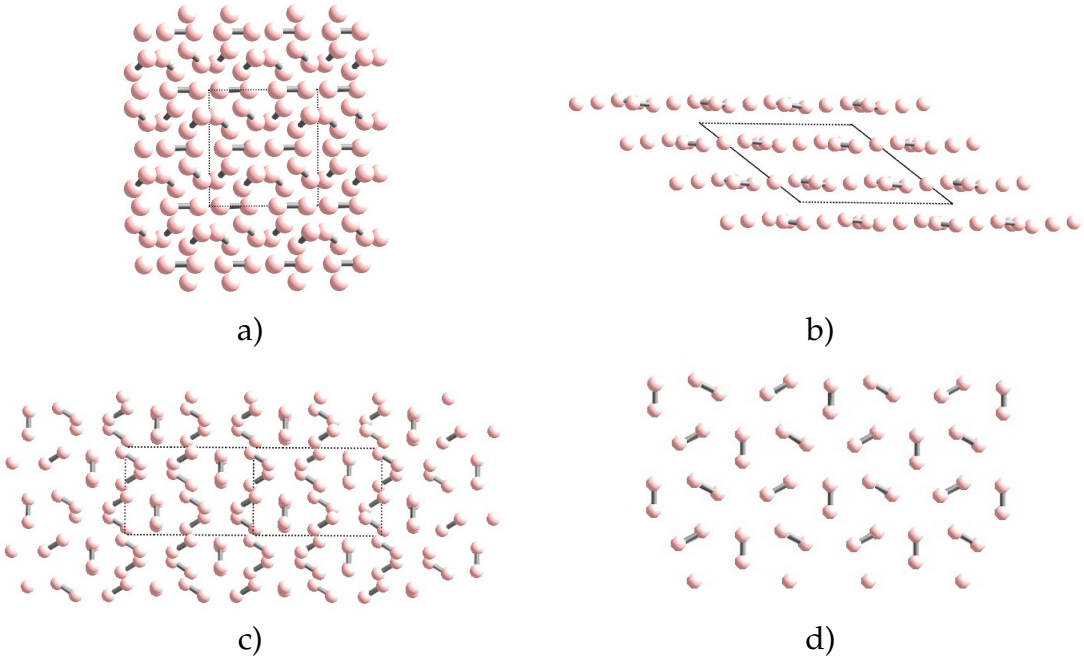

Figure 1.2: Structure *C2/c* of H_2 a)-c) show different view of the unit cell embedded within the structure. d) depicts one of the layers within the structure

1.4.3 *Cmca-12*, the most stable phase of H_2 from 250-350 GPa

This layered structure is arranged in a ABA stacking, with 6 hydrogen molecules per unit cell. This arrangement resembles somewhat the previous system, *C2/c*. The molecule axes lie if anything ”flatter” on the plane. At 300 GPa the H-H bond elongates to 0.77 Å, and the nearest intermolecular distance decreases to 1.09 Å.

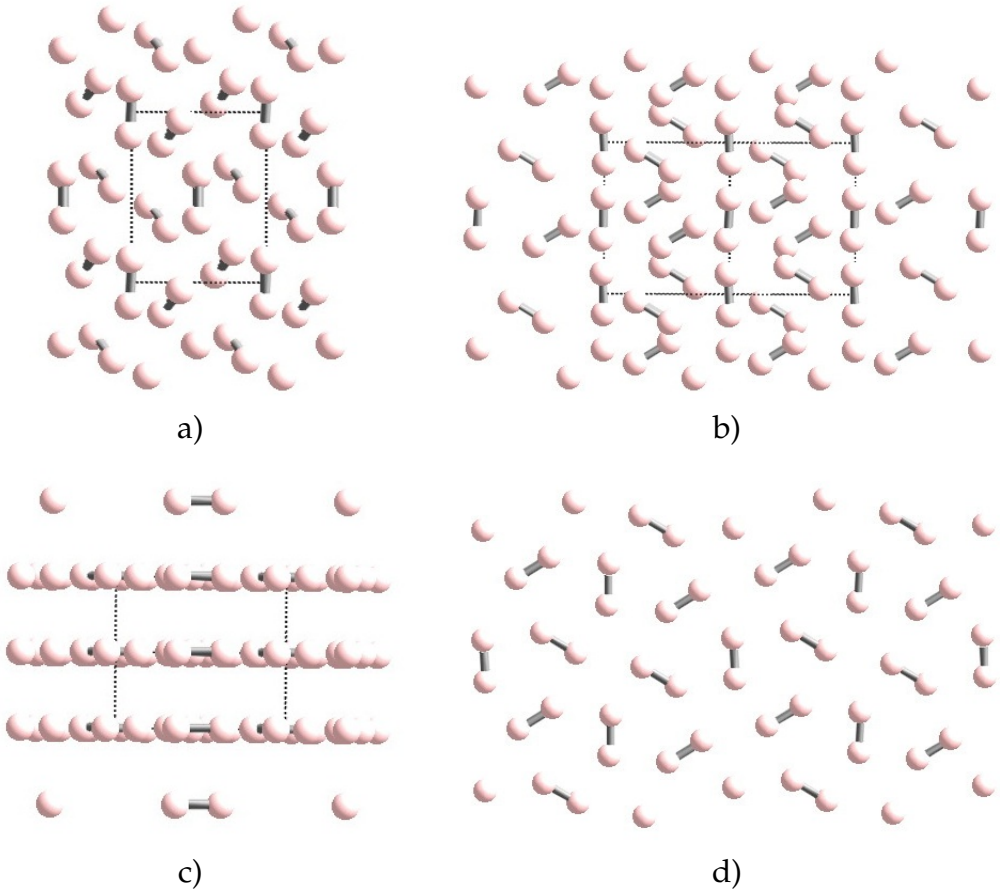

Figure 1.3: Structure *Cmca-12* of hydrogen. a)-c) show different view of the unit cell embedded within the structure. d) depicts one of the layers shown in 1.3b

1.4.4 *Cmca*, the most stable phase of H_2 from 350-500 GPa

Not only do the molecular hydrogen units lie flat on a plane, but the molecules axes orient themselves regularly within the plane in the most stable structure for pressures within the range of 350 - 500 GPa. As we'll see, in this pressure regime it becomes arbitrary to single out H_2 units; the "intermolecular" bonds are as short as 1.1Å in this structure at 350 GPa.

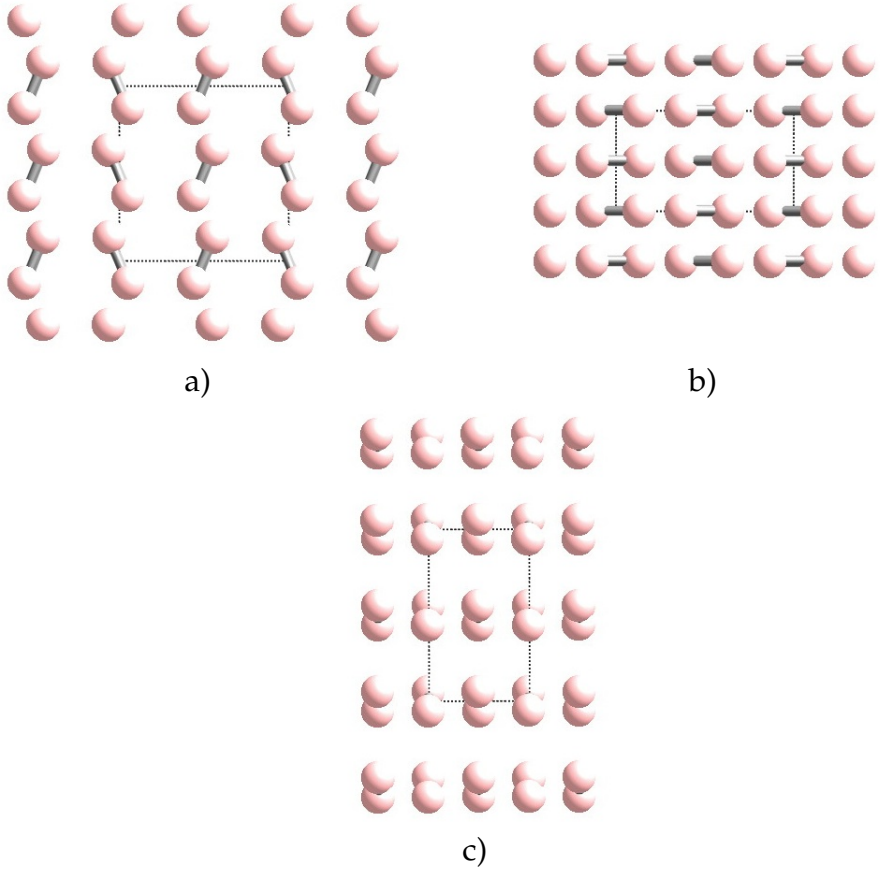

Figure 1.4: Top and lateral view of the most stable structure *Cmca* of hydrogen at pressures 350-500GPa

1.4.5 $I4_1/amd$, the most stable phase of H_2 from 500 GPa-?

At 500 GPa, the most stable structure has 2 formula units per cell. The bond length of the hydrogen molecule is 0.77Å with closest nearest neighbor distance to another "molecule" of 1.05 Å.

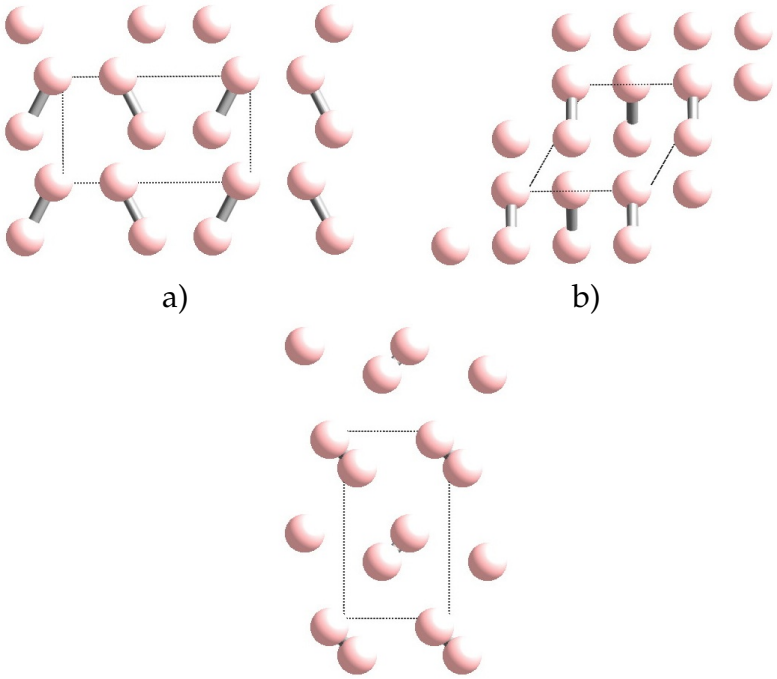

Figure 1.5: Top and lateral view of the most stable $I4_1/amd$ structure of hydrogen at 500 GPa

1.4.6 An Equalization Function

We now wish to compare the distance relationships in the various structures as the pressure increases. Figure 1.6 plots the shortest H-H separation in the lowest enthalpy hydrogen structure at a given pressure.

The separation, call it H_2 bond length, varies in the range of 0.715Å to 0.775 Å in the pressure range studied. The changes are not smooth as a function of pressure, a natural consequence of the phase transitions. But the trend is the expected one, if each H is to increase coordination at higher pressure the H_2 bond must weaken. The 0.015 Å diminution in HH bond length in the low pressure regime ($P6_3/m$) is intriguing.

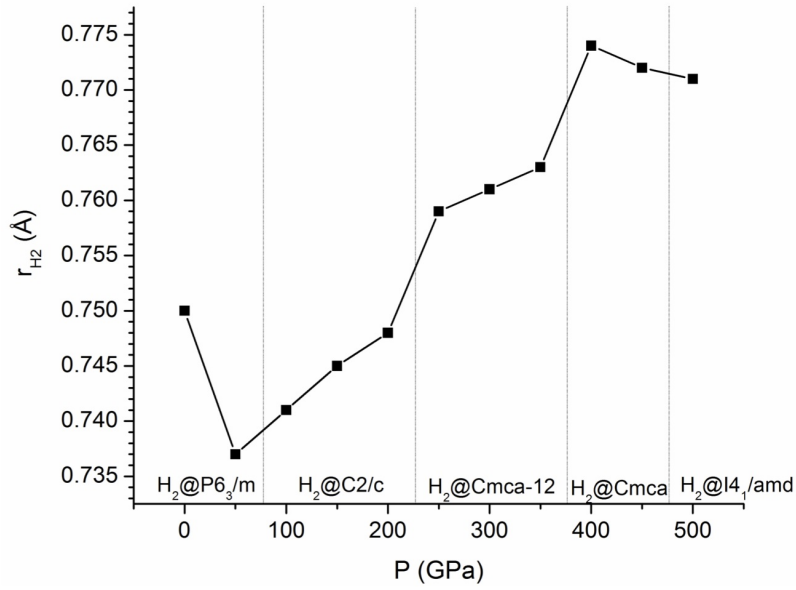

Figure 1.6: Bond length for H_2 in preferred H_2 structures from 0 to 500 GPa

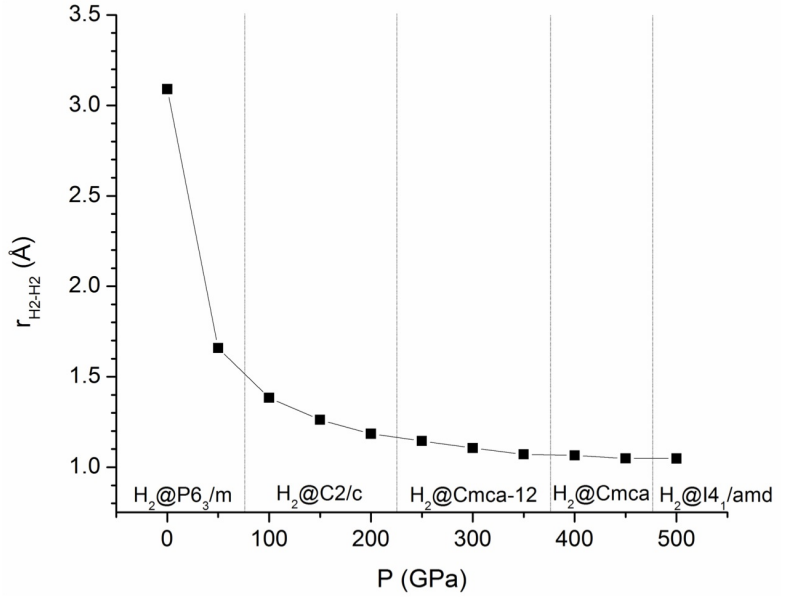

Figure 1.7: Intermolecular distances for H_2 from 0 to 500 GPa

Inter- "molecular" distances as a function of pressure were studied as well. At lower pressures the cell volume is reduced greatly and H_2 - H_2 separations

shorten. As we can see in Figure 1.7 the interatomic distances become consistently lower with pressure. The change is drastic in the lower pressure regime - this is an example of "Van der Waals space squeezed out" an expected phenomenon as pressure is applied to any molecular solid. The effect of phase transitions is smaller on intermolecular H$\cdots$H separations.

Can we characterize more economically the changes that take place on H_2 dissociation and extended network formation? We need a parameter that indicates how distances from a given H atom equalizes - that is how hydrogen makes the transition from molecular hydrogen to a metallic crystal. The following equalization function is proposed for that purpose.

$$\xi(P) = 1 - \frac{r^{P}_{H_2-H_2} - r^{P}_{H_2}}{r^{1atm}_{H_2-H_2} - r^{1atm}_{H_2}}. \tag{1.1}$$

Here $r^{P}_{H_2}$ corresponds to the average bond length of a H_2 molecule at pressure P, $r^{P}_{H_2-H_2}$is the shortest distance between 2 H_2 (H-H $\cdots$ H-H) molecules at pressure P; $r^{1atm}_{H_2}$ is the average calculated bond length in an H_2 molecule at ambient pressure, 0.75 Å (0.01 Å longer than the experimental value); the term $r^{1atm}_{H_2-H_2}$ is also a constant and is the shortest distance between 2 H_2 molecules (that is second nearest neighbors, H - H $\cdots$ H - H) at ambient pressure, 3.1 Å. Therefore, equation (1.1) is set up so that at ambient pressure, the ξ value is 0, and at pressures high enough, when H $\cdots$ H bond equalization occurs, the ξ value converges to 1.

Figure 1.8 plots ξ over the range of pressures considered in our calculations:

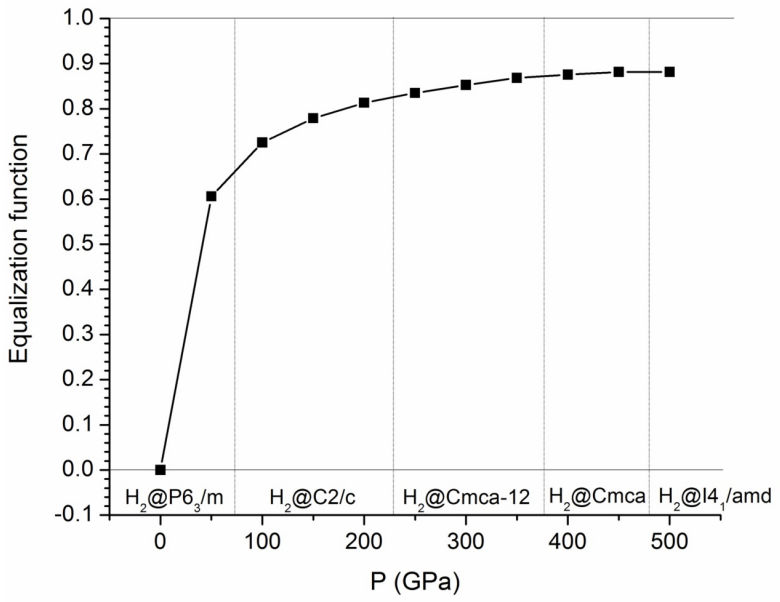

Figure 1.8: Equalization function ξ from 0 to 500 GPa

We see a rapid raise in ξ(P) at low pressures, to plateau at about 400 GPa in which ξ does not change much from what appears to be an asymptotic value of 0.9. The hydrogen structures calculated by us are metallic, *i.e.* have a significant density of states (DOS) at the Fermi level, from 250 GPa on. Note here that experimentally hydrogen is not yet metallic at 350 GPa; DFT methods characteristically underestimate band gaps. It appears that one can have metallic hydrogen without it being an "atomic crystal" with ξ(P) =1 or, to put it in other words, it may be that some of these hydrogen structures are metallic, but are not atomic.

1.5 Conclusions

As part of our research for metallic hydrogen, we analyzed bond length and intramolecular distances for the most stable structures at pressures ranging from 0-500 GPa. We propose an equalization function, ξ, to gauge how hydrogen moves from a molecular solid to metallic hydrogen. ξ takes on the values between 0 (near-neighbor distances much larger than inter- molecular distances) and 1 (near-neighbor distances equal inter-molecular ones). The calculated ξ(P) values for optimized hydrogen phases evolve smoothly from 0 to 0.9. Metallicity (theoretical) sets in at 250 GPa. Though the theoretical values are not reliable, it appears that you can have metallicity in hydrogen without having an "atomic crystal" with ξ =1.

BIBLIOGRAPHY

[1] N. W. Ashcroft. Metallic Hydrogen: A High-Temperature Superconductor? *Phys. Rev. Lett.*, 21:1748–1749, 1968.

[2] D. Saumon, G. Chabrier, W.B. Hubbard, and J.I. Lunine. The Molecular-Metallic Transition of Hydrogen and the Structure of Jupiter and Saturn. *Astrophys. J.*, 391:817–826, 1992.

[3] C.F. Richardson and N. W. Ashcroft. High Temperature Superconductivity in Metallic Hydrogen: Electron-electron Enhancements. *Phys. Rev. Lett*, 78:118–121, 1997.

[4] V. L. Ginzburg. *Key Problems of Physics and Astrophysics*. Mir Publishers, Moscow, 1978.

[5] E. Wigner and H.B. Hungtinton. On the Possibility of a Metallic Modification of Hydrogen . *J. Chem. Phys.*, 3:764, 1935.

[6] P. Loubeyre, F. Occelli, and R. LeToullec. Optical Studies of Solid Hydrogen to 320 GPa and Evidence for Black Hydrogen. *Nature*, 416:613–617, 2002.

[7] A.F. Goncharov, E. Gregoryanz, R.J. Hemley, and H.K. Mao. Spectroscopic Studies of the Vibrational and Electronic Properties of Solid Hydrogen. *Proc. Natl. Acad. Sci. USA*, 98:14234–14237, 2001.

[8] C. Narayana, H. Luo, J. Orloff, and A.L. Ruoff. Solid Hydrogen at 342 GPa, No Evidence for an Alkali Metal. *Nature*, 393:46–49, 1998.

[9] P. P. Edwards and F. Hensel. Will Solid Hydrogen Ever Be a Metal? . *Nature*, 388:621, 1997.

[10] S.T. Weir, A. C. Mitchell, and W.J. Nellis. Metallization of fluid molecular hydrogen at 140 GPa (1.4 Mbar) . *Phys. Rev. Lett.*, 76:1860, 1996.

[11] P. Loubeyre, R. Letoullec, D. Hausermann, M. Hanfland, R.J. Hemley, H.K. Mao, and L.W. Finger. X-ray Diffraction and Equation of State of Hydrogen at Megabar pressures. *nature*, 383:702– 705, 1996.

[12] K.P. Huber and G. Herzberg. *Molecular Spectra and Molecular Structure, IV*. Van Norstrand, N.Y., 1979.

[13] K. Inoue, H. Kanzaki, and S. Suga. Fundamental Absorption Spectra of Solid Hydrogen . *Solid state comm.*, 30:627–629, 1979.

[14] H.K Mao and R.J. Hemley. Ultrahigh-pressure Transitions in Solid Hydrogen. *Rev. Mod. Phys.*, 66:671–692, 1994.

[15] N.W. Ashcroft. Dense Hydrogen: the Reluctant Alkali. *Phys. World*, 8:43–48, 1995.

[16] R.J. Hemley and H.K. Mao. Phase Transition in Solid Molecular Hydrogen at Ultrahigh Pressures . *Phys. Rev. Lett.*, 61:857–860, 1988.

[17] H.E. Lorenzana, I.F. Silvera, and K.A. Goettel. Evidence for a Structural Phase Transition in Solid Hydrogen at Megabar Pressures. *Phys. Rev. Lett.*, 63:2080–2083, 1989.

[18] C. J. Pickard and R.J. Needs. Structure of Phase III of Solid Hydrogen. *Nat. Phys.*, 3:473–476, 2007.

[19] W. Kohn and L.J. Sham. Self-consistent Equations Including Exchange and Correlation Effects . *Phys. Rev.*, 140:A1133–A1138, 1965.

[20] J.P. Perdew, J.A. Chevary, S.H. Vosko, K.A. Jackson, M.R. Pederson, D.J. Singh, and C. Fiolhais. Atoms, Molecules, Solids and Surfaces: Applications of the Generalized Gradient Approximation for Exchange and Correlation . *Phys. Rev. B*, 46:6671–6687, 1992.

[21] H.J. Monkhorst and J.D. Pack. Special Points for Brillouin-zone Integrations . *Phys. Rev. B*, 13:5188–5192, 1976.

[22] I. Tamblyn and S. A. Bonev. Structure and Phase Boundaries of Compressed Liquid Hydrogen. *Phys. Rev. Lett.*, 104:065702, 2010.

CHAPTER 2

Stannane, SnH_4, Under High Pressure

2.1 Introduction - Hydrides as a Way of Obtaining Metallic Hydrogen

Recently, it has been suggested that metallic, hydrogen-dense compounds, such as hydrides, where non-bonded hydrogen atoms are closer together than in elemental hydrogen by itself, might be considered as "chemically precompressed" [1]. And, therefore, such hydrides may be candidates for metallization at relatively low pressures compared to H_2 itself . They might even be high-temperature superconductors. This is the motivation behind the enormous amount of experimental and theoretical research devoted to the (generally unknown) structures under pressure of group 14 tetrahydrides: SiH_4 [2–6], GeH_4 [7], SnH_4 [8, 9]. The present thesis also addresses the problem of the electronic structure of these compounds under pressure.

In this chapter, we look closely to the behavior of one of these hydrides, stannane, SnH_4. Little is known about the structure of solid stannane at any given pressure. Tin tetrahydride is a colorless (and highly toxic) gas at ambient pressure [10]. Its structure in the gas phase is expectedly tetrahedral, with a Sn-H bond length of 1.7Å [11].

2.2 Proposed Structures

Given that the structural data on SnH_4 is scarce, we looked theoretically for alternative geometries in several studies of a similar compound, silane. We began with the structures studied for SiH_4 in the work of Feng *et. al.* [2], and by Pickard and Needs [3], and one structure of SnH_4, which was suggested in a previous theoretical study by Tse *et. al.* [8] The possibilities certainly include structures that are locally tetrahedral at Sn (at ambient pressure), which is the expected geometry for a group 14 compound. We also took into consideration octahedral coordination for the tin, based on the tendency of the element to six-coordination in its chemistry, and on the occurrence of that geometry in structures of SnF_4 and PbF_4 [12, 13]. And in our search for structures with the same stoichiometry we looked into more highly symmetric structures with still higher coordination (not likely candidates at ambient pressure), such as the cubic $PtHg_4$ structure [14].

We have learned from the previous pioneering study of silane in the group [2] that a given coordination type at P= 1 atm may evolve at high pressure into a very different structure. A general expectation is that as pressure increases so does the coordination number of the constituent atoms [15]. Fig 2.1 shows the ten structures we first investigated, in their P=1 atm geometry.

The first three tetrahedrally coordinated models we consider come from placing SnH_4 molecules in different crystal packings: **T1** has a body-center cubic Bravais lattice with Z = 2, **T2** a simple cubic one, Z=1, and **T3** a body-center

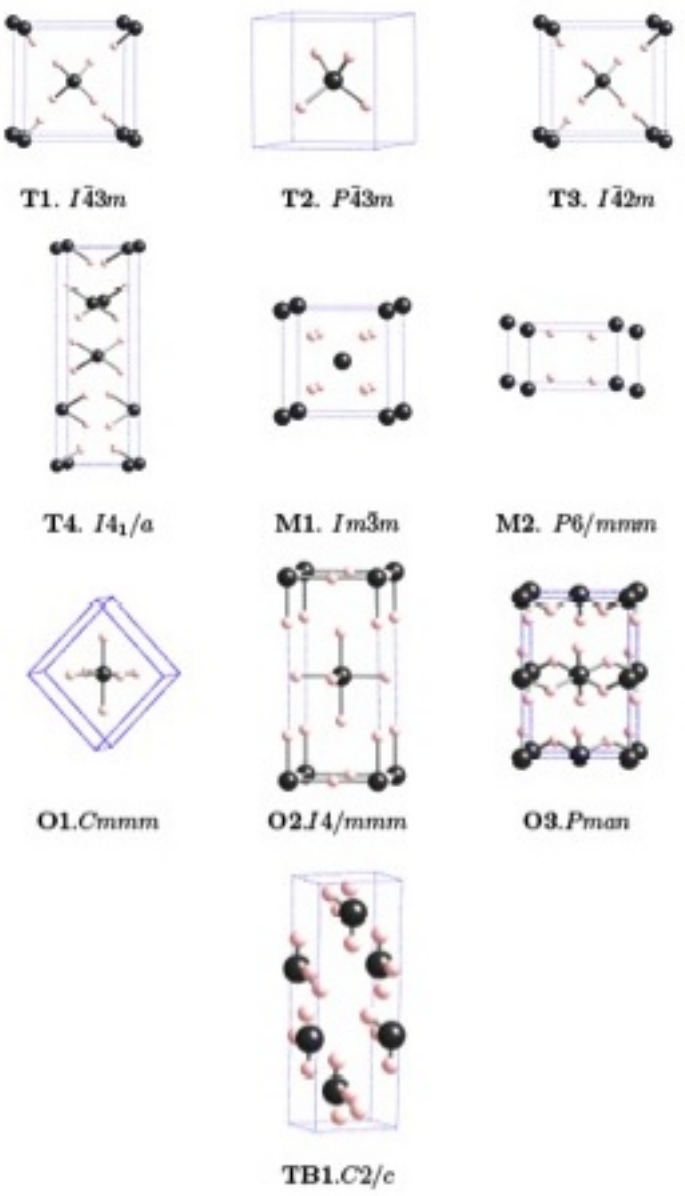

Figure 2.1: Potential structures examined for SnH_4. The structural notation corresponds roughly to the type of coordination around the tin atoms (at ambient pressure); **T** for tetrahedral coordination, **M** for higher symmetry metallic arrangements, **TB** for a trigonal bipyramid coordination, and **O** for octahedral coordination. In our representation, consistently the black spheres are tin atoms and the pink spheres are hydrogen atoms.

tetragonal one with Z = 2. **T4** (Z= 4) shows a Cs-VI-like stacking. **M1** (**M** for metallic) has its hydrogen atoms arranged in cubic coordination at Sn, the tin atoms themselves in a body-center cubic arrangement. **M2** (Z = 1) has tin atoms at the corners of a tetragonal unit cell while the hydrogen atoms form pairs within the cell . This is a structure suggested previously in the literature [8]. **TB1** is a complex packing, with a very distorted trigonal bipyramid coordination at Sn, forming ribbons by sharing the trigonal bipyramid vertices. This geometry derives from the theoretical work of Pickard and Needs, where it was found one of the most stable structures for silane at high pressures. It is not a likely geometry for the low pressure regime, but, as we will see, this structure held a surprise for us. For the octahedrally coordinated structures, **O1** can be described as containing 1-D chains of octahedra sharing edges, while **O2** and **O3** have 2-D arrangements of octahedra sharing corners [2, 3]. The **O2** structure is actually the experimental structure of SnF_4 at P=1 atm [12].

These were the initial structures in our search. The geometries were optimized for unit cell volumes corresponding to pressures which ranged from 0-290GPa. Once optimized, the density of states (DOS) curve was obtained for each structure, so as to gauge its approach to metallicity. In looking at the changes in the structures as pressure is applied, we pay special attention to the distances among hydrogen atoms, as short H-H contacts are likely to accompany metallization.

2.3 Methodology

Density functional theory (DFT) calculations with the Perdew-Wang exchange-correlation functional [16] were performed with Blöchl's projector-augmented wave method and a plane wave basis set, as implemented in the Vienna Ab Initio Simulation Package (VASP) codes. For the optimization of the structures, the cell parameters, the atomic positions, and the cell volume were allowed to relax. The stress tensor was also calculated. A defined stress was added to the stress tensor, converging into a particular pressure. Once an optimized structure was reached, the electronic density of states (DOS) was calculated. The k-point grids were generated via the Monkhorst-Pack scheme [17]. The calculations are for the ground state at zero-temperature, neglecting the zero-point vibrational energy. The cutoff of the kinetic energy was set at 650 eV, and for the planewaves we set a self consistent field (SCF) tolerance of 1×10^{-5} eV/unit cell.

2.4 Results

2.4.1 Structures at High Pressure (290 GPa)

Our calculations covered a range of pressure up to 290 GPa. Some geometries changed little (except for compression), some evolved in complicated ways. As expected [15], high pressure induces higher coordination (with accompanying multi-center bonding) in some of our structures. In order to provide a broad overview of the major structural modifications that arise under high pressure,

it is actually helpful to look at the high pressure structures first, and then fill in the enthalpy landscape in between. The calculated optimum structures at 290 GPa are shown in Figure 2.2.

Structure **T1** approaches with pressure the **M1** structure. This convergence is not surprising, since in the initial **T1** structure hydrogen atoms are coming into the faces of the central tetrahedron, completing the cube as the pressure increases. As we will see, neither structure is energetically competitive as the pressure increases.

For the structures with Z=1 (**T2**, **O1**, **M2**) the only allowed change upon pressurization is the reduction in the size of the unit cell. With it, the hydrogen atoms get closer together; in the case of **T2** the hydrogen atoms form a cubic cluster with a closest H–H distance (at P = 290 GPa) of 1.13 Å, as shown in Fig 2.3. **O1** has its hydrogen atoms forming chains of octahedra (Shown in Fig. 2.4), which share edges; the closest distance between two hydrogen atoms at 290 GPa, is 0.88 Å. The **M2** structure features infinite chains of H atoms; the distances along a chain alternate, at 290 GPa H-H= 0.82, 1.72 Å. The short contacts are intra-unit-cell at high pressures. (Fig 2.5) This structure also remains of relatively high enthalpy throughout the pressure range considered.

Structure **T3** does not follow the same trend as **T1**. While **T1** remains cubic ($a = b = c$), **T3** does not. Within the tetragonal cell ($a = b \neq c$), all three axes contract, but the a/c ratio becomes smaller with pressure. As pressure increases, the Sn-H coordination evolves in **T3**: at P=0 GPa, each Sn has a coordination close to

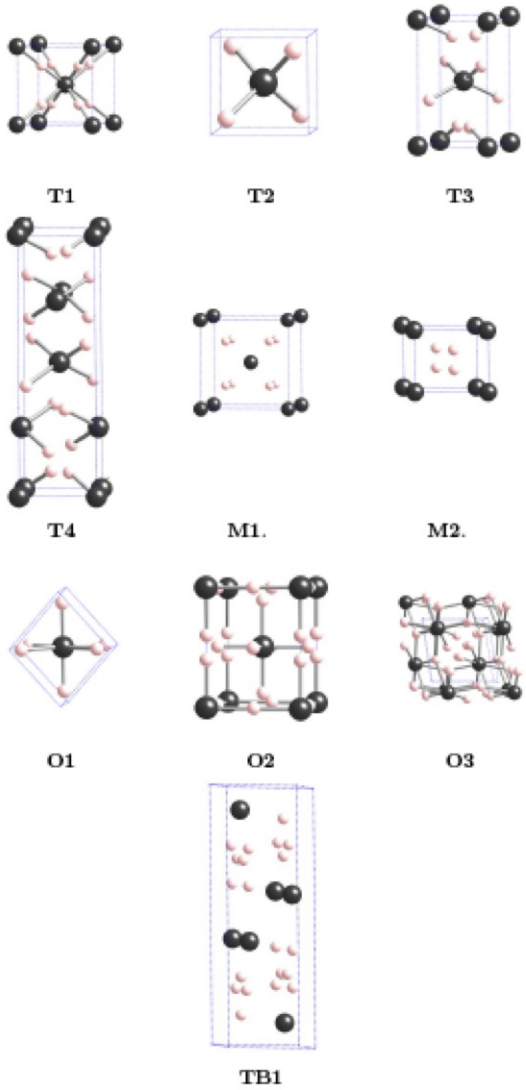

Figure 2.2: Optimized structures at 290 GPa. The structural changes are described in the text; **TB1** and **O3** suffer by far the most pronounced changes in their coordination at Sn as the pressure is increased. TB1 undergoes a separation of elements, with layers of Sn and H atoms (discussed in text), and **O3** increases its coordination number at Sn in a very complex symmetry.

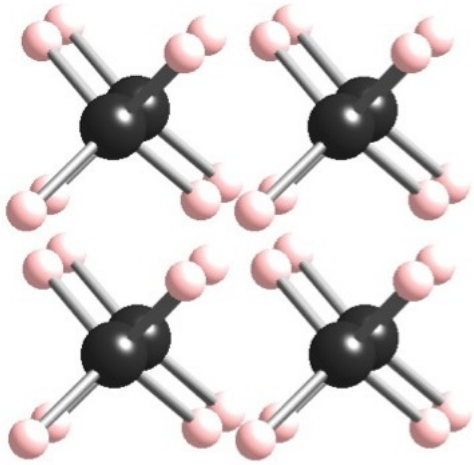

Figure 2.3: Structure **T2**, with several unit cells illustrated so as to show the cubic hydrogen clusters.

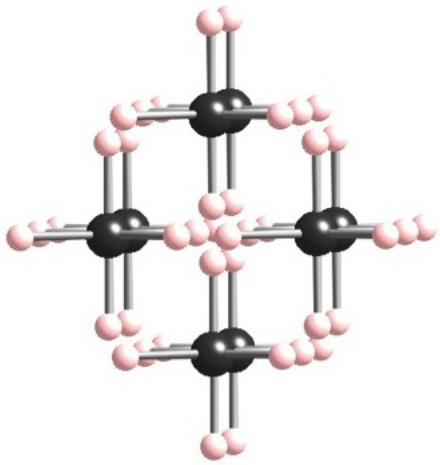

Figure 2.4: Structure **O1** at 290 GPa.

regular tetrahedral, with angles 107° and 114°, whereas at 290 GPa, the tin atoms acquire more hydrogen neighbors. The tin atom moves to a 4 + 4 coordination. The four nearest hydrogen atoms, 1.59Å, form a much flattened tetrahedron, with angles 130° and 100°. The four second-nearest hydrogen atoms, not much further removed (Sn−H distance of 1.78 Å) form pairs of hydrogens with H−H of 0.99Å; these pairs that approach the tin atom on the *c* axis, on top and bottom

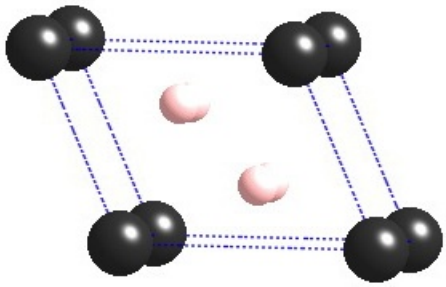

Figure 2.5: Structure **M2** at 290 GPa.

of the flattened tetrahedron. The coordination polyhedra for the tin atoms at 290 GPa are distorted dodecahedra, as may be seen in Fig 2.6. A similar motion to 8-coordination was observed for this structure in the work of Feng *et. al* [2] on silane. However, at the pressures considered they did not find the pairs of hydrogens we see.

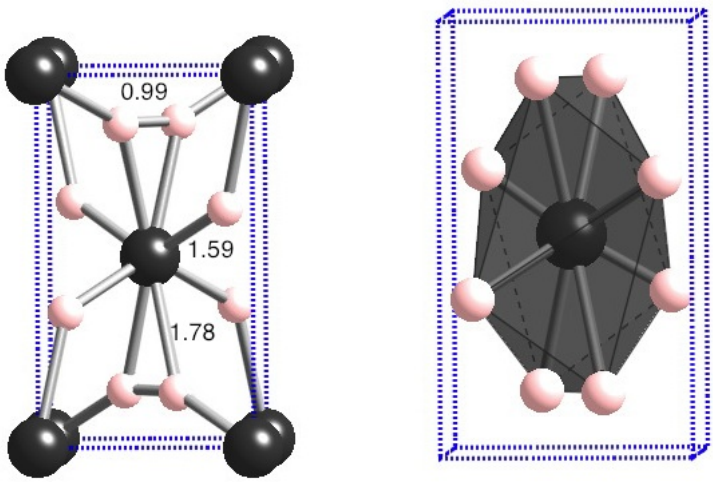

a) b)

Figure 2.6: Structure **T3** a) The structure at 290 GPa; the tin atom increases its coordination to 4 + 4, b) shows the distorted dodecahedron formed by the 8 nearest neighbor hydrogen atoms.

Two of the nine structures described in Figures 2.1 and 2.2 depart still more significantly from their initial P = 1atm geometry: **O3** and **TB1**. The changes predicted (to be described in detail below) are all the more interesting, since these two structures are also calculated as the most stable ones at elevated pressures. Let us in fact turn to the energetics of the various structures.

2.4.2 Energetics as a Function of Pressure

We computed enthalpies of the various structures mentioned as a function of pressure in the range $0 \leqslant P \leqslant 290$ GPa. The structures were studied at small pressure intervals in the regime of low pressures, since the volume decreases considerably in these region (the systems were analyzed at 0, 1, 5, 30, 50, 65, 80 GPa) with $V/V_\circ \sim 0.25$ at 80 GPa. From a pressure of 80 to 290 GPa we use intervals of 30 GPa. The resulting enthalpies in eV per SnH_4 unit, relative to a reference structure, **T3**, are shown in Fig 2.7. This reference structure was chosen because its evolution in enthalpy as $f(P)$ is smooth, as would be expected of a Z=1 geometry.

The first thing we notice in Fig. 2.7 is that some of the structures most certainly do not have smooth enthalpy as F(P) curves. Bumps of the kind observed may indicate computational problems, or they may arise from phase transitions in the structure under consideration, or in the reference structure. As mentioned above, no phase transitions are visible in the **T3** reference. The energy varies smoothly in several of the structures, so that computational anomalies appear

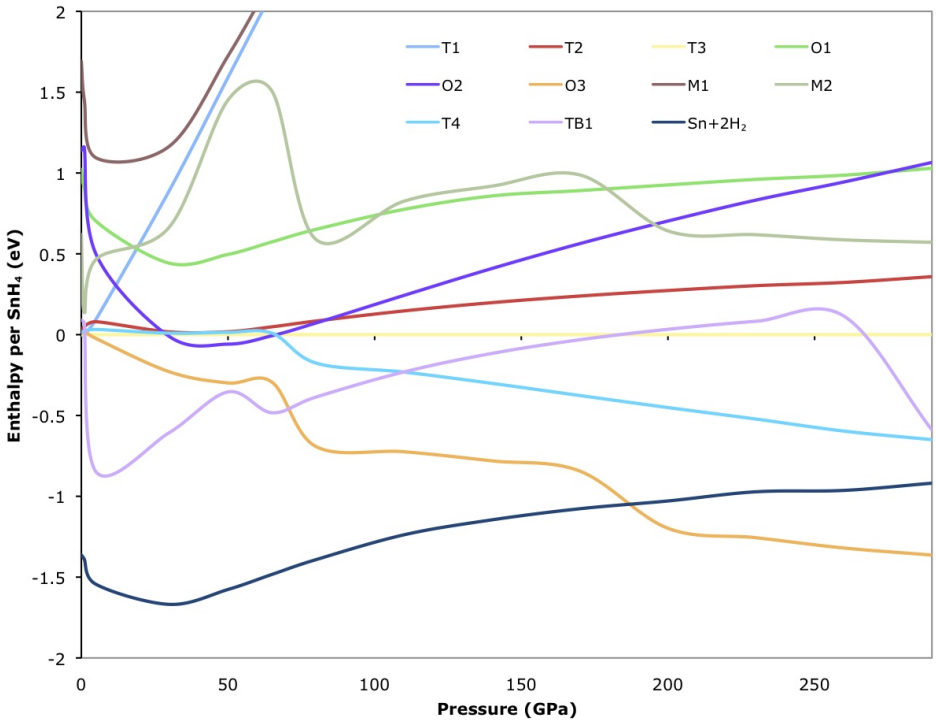

Figure 2.7: Stabilities. Structure **T3** is used as reference. At pressures from 0- 65 GPa the most stable structure is **TB1**, and at higher pressures, **O3** becomes the most stable. Their geometries are discussed in detail in the text.

to be absent. In the case of **O3** and **TB1** curves, the bumps do represent phase transitions, to be described below.

In Fig. 2.7 we also include the sum of the enthalpies of elemental tin and hydrogen. Tin under high pressure undergoes several phase transitions, especially at slightly elevated pressures ($\alpha \rightarrow \beta \rightarrow$ bct $\rightarrow$bcc) [18]; while H_2 evolves from $P6_3/m$, to C2/c, to Cmca-12 [19] (See Chapter 1). These transitions were taken into account, so that the enthalpies are reported relative to the most stable Sn and H_2 structures at a given pressure. The experimental heat of formation

of SnH_4 (g) at P=1 atm is +1.68 eV/ SnH_4 molecule, so the computational result (1.36 eV) is credible. A consequence of this positive heat of formation (in group 14 only CH_4 has a negative $\triangle H_f$) is that stannane is thermodynamically unstable, yet kinetically persistent, to decomposition to H_2 and Sn. This is important to know; it will also help us understand the behavior of some of the unusual high-pressure phases. As Fig. 2.7 shows, it is only at high pressures that one of our proposed structures becomes more stable than the elements.

As shown in Fig 2.7, of the computed alternatives two structures are the most stable over a wide pressure range. In the low pressure region (~2-65 GPa) **TB1** is the most competitive system, while at higher pressures **O3** is of lower enthalpy. Let us look at the evolution of the geometries of these important structures as pressure is applied.

At low pressures **TB1** is calculated to be more stable than any of the **T** structures. Yet SnH_4 is at ambient pressures known to be a tetrahedral gas phase molecule. What is going on? An answer is provided by examining the optimized **TB1** structures.

TB1 is a structure derived from a high pressure SiH_4 candidate. Extrapolated unrelaxed to P= 1 atm (Fig 2.8a), it contains highly distorted SnH_5 bipyramids, with Sn-H distances of 0.9 Å and 1.45 Å. Both distances are unrealistically short (recall the P = 1 atm Sn-H distance of 1.7 Å). A single point calculation shows that this structure at P= 1 atm is very, very high in energy; no wonder that it rearranges. The structure seems not to find

its way to **T1**, **T2**, or **T3**. But it has something better available - segregated Sn and H_2, at lower enthalpy than **T1**. The optimized structure at P= 5 GPa illustrated in Fig. 2.8b is an approach to this. The structure contains layers of Sn atoms and pairs of hydrogen molecules, with H-H distances of 0.79 Å. This a harbinger of things to come - Chapter 3 will show that in the low pressure regime the favored structures are segregated element slabs.

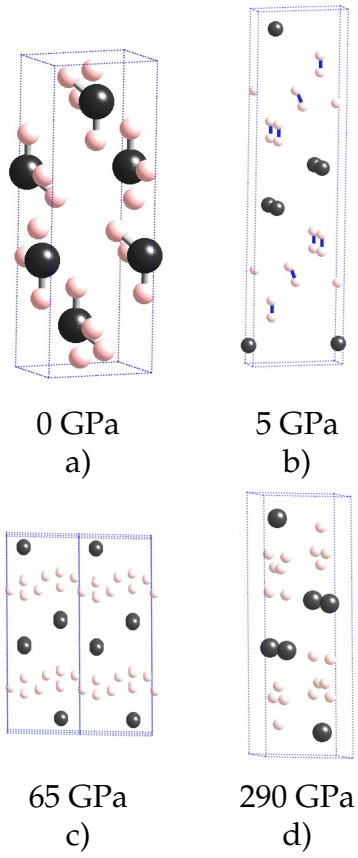

Figure 2.8: Evolution of structure **TB1** as pressure is applied. (a) The initial structure, (b) the structure optimized at 5 GPa, (c) at 65 GPa as the cell becomes smaller, the layer of hydrogen atoms contracts (d) at 290 GPa the layers are still part of the structure.

Interesting things happen to this **TB1** structure with increasing pressure - the two layers are still present but the number of hydrogen atoms pairing up

decreases. At 65 GPa, only two out of three hydrogen atoms form pairs (the H-H bond length is 0.76 Å). Around this pressure another phase transition take place; this time the layer of hydrogen atoms contracts along the *c* axis (Fig. 2.8c). The layers in **TB1** persists with increasing pressure, but it is another highly coordinated structure **O3**, that proves to be more stable in the high-pressure regime.

O3 is by far the most interesting structure of all. It undergoes many changes. The first startling result is that at P= 1 atm the optimized structure goes spontaneously from octahedral coordination of Sn to tetrahedral. This new tetrahedral structures (Fig 2.9b) is not one of the **T** structures calculated by us earlier. The molecular crystal (Z = 2) has a tetragonal lattice, and the Sn-H distances of 1.74 Å in this structure are quite normal. Nothing like this was seen in earlier studies of SiH_4 or GeH_4. Continuing to increase the pressure, at 65 GPa a new phase emerges, the coordination of the Sn atom increases to 6. The Sn environment in this phase is a distorted octahedron.

A second phase transition comes around 140-170 GPa (Fig 2.9d). In this new phase SnH_4 is no longer a molecular crystal. It is now that one sees for the first time pairs of hydrogen (H-H distance 0.89 Å at 140 GPa). The H_2 units axes orient themselves regularly, furthermore the second nearest neighbor lies 1.05 Å away (H-H $\cdots$ H-H). Using the equalization function introduced in chapter 1, ξ = 0.93 at the relatively low pressure of 140 GPa (Pure hydrogen at 140 GPa has a ξ = 0.76). In this pressure range **O3** becomes stable into decomposition of the elements. The distance between the Sn and H also atoms increases with the smallest such separations being 1.82 Å. The coordination number in this struc-

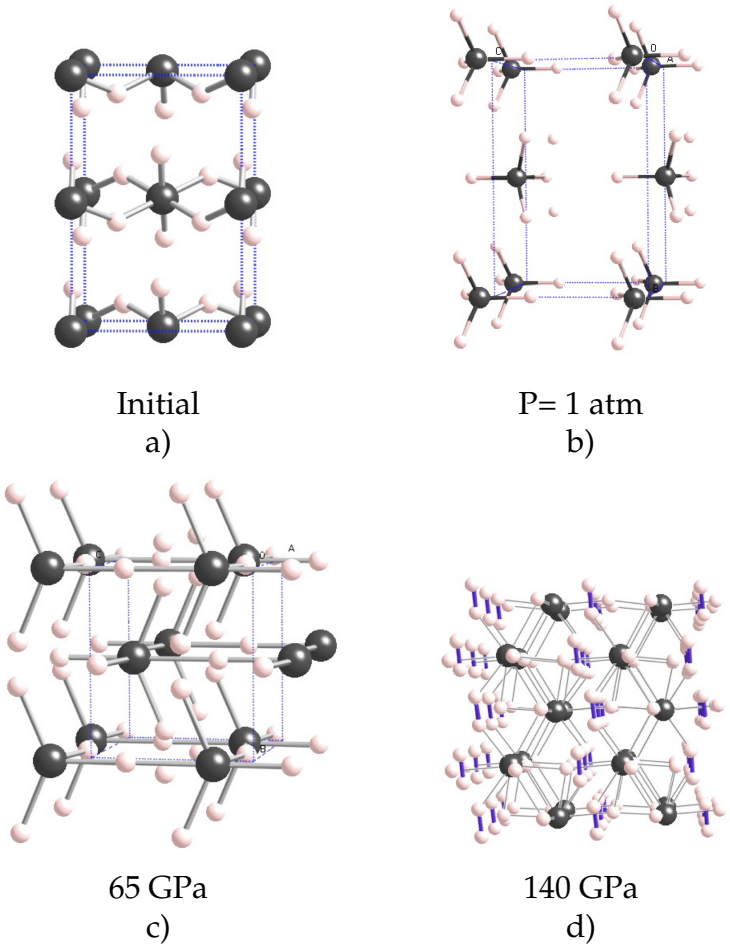

Figure 2.9: Evolution of structure **O3** as pressure is applied (a) The initial structure, (b) the structure optimized at 0 GPa. Notice how it goes from a octahedral coordination to a new tetrahedral, (c) at 65 GPa as the cell becomes smaller, the coordination increases to a distorted octahedral and finally (d) at 140 GPa where we can appreciate the H-H shown in blue in the figure.

ture increases to ten if we use a distance cut off of 2.05Å. The resulting geometry is very complex, as shown in Figure 2.9 and in the histograms in Figure 2.10.

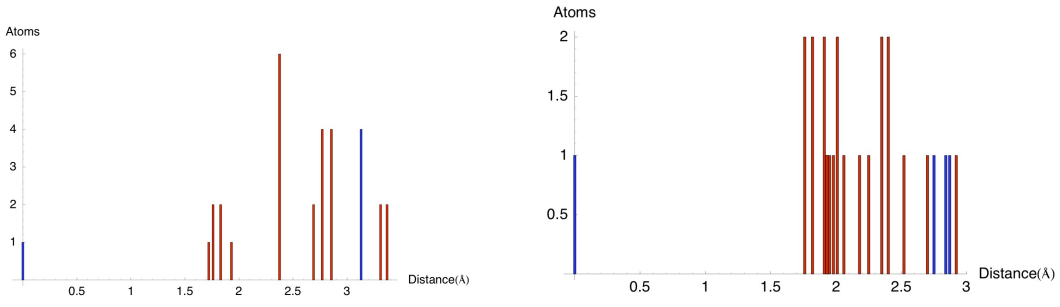

a) b)

Figure 2.10: Histograms for **O3** at a) 65 GPa and b)140, the coordination number increases with pressure and so does the bond length; in blue, tin and in red, hydrogen.

2.5 Other Structures

After we carried out our calculations, a paper appeared detailing an evolutionary algorithm exploration of the SnH_4 structures. In this work several new structures were suggested [20]. The most stable figures, as are shown in Figure 2.11. Using the equalization function, ξ(P) from chapter 1, ξ=0.66 for *Ama*2 at 120 GPa and ξ=0.64 for $P6_3/mmc$ at 200 GPa. At high pressures both of these structures indeed had enthalpies lower than any we had computed, Fig. 2.12 shows the enthalpies of the new structures (checked by us), as well as those of the elements and our two best structures **TB1** and **O3**. In Fig 2.12 the enthalpy of the elements at the given pressures pressure is the reference straight line, not the **T3** structure as in Fig. 2.7.

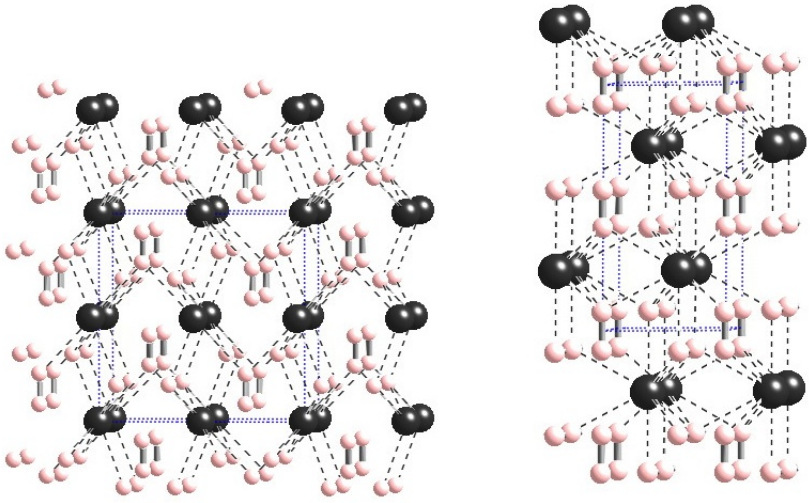

Ama2
120 GPa

P6$_3$/mmc
200 GPa

Figure 2.11: SnH_4 structures suggested by Gao et. al. [20]. The hydrogen bonds are drawn and the dashed lines indicate the closes Sn-H distances.

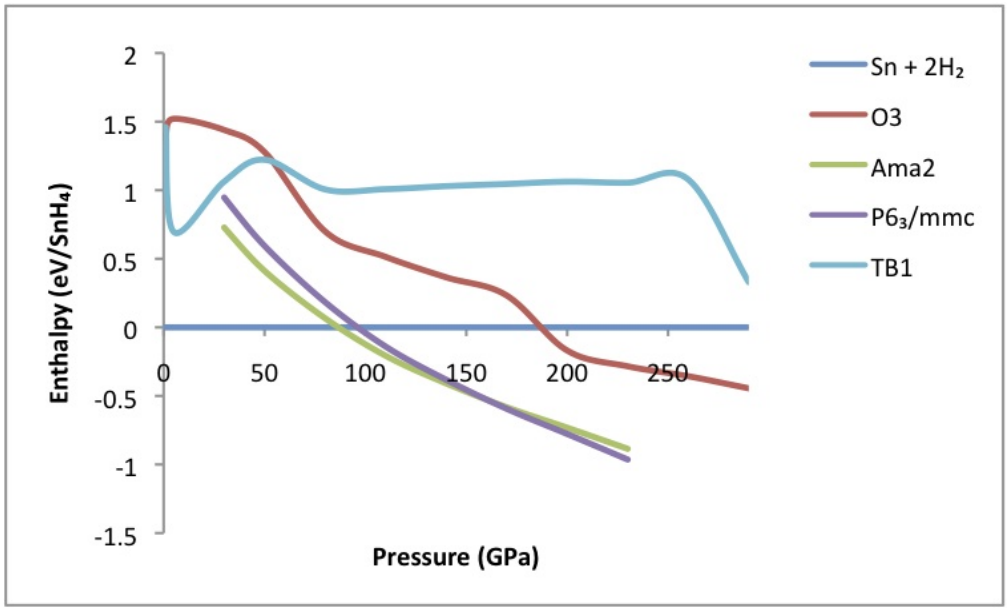

Figure 2.12: Stabilities. The elements in their most stable forms at the pressures considered are used as reference. Our structure as interesting as they are, are not as stable as the ones studied by Gao et. al.

2.6 Density of States, DOS

We were also interested in studying the pressure at which SnH_4 becomes metallic. For that purpose DOS were calculated. The results are summarized in the following table, Table 2.1. Most of our structures become metallic at low pressure. **T1** is an exception, becoming metallic at 230 GPa. It should be noted, however, that these structures are not the lowest enthalpy ones at the indicated pressures - either completely segregated structures or the ones suggested by Gao et. al. will be more stable.

Table 2.1: Pressure in GPa at which the system become metallic.

Structure	Pressure
T3	50
TB1	5
O3	1
T1	230

2.7 Conclusion

We examined some possible structures for stannane and how these structure change under high pressure. Our structures, as interesting as they are, are not as stable as the ones recently proposed by Gao *et. al.* [20]. Our finding of the stability of layered strucctures in the low pressure regime of SnH_4, leads us to tackle that topic in the next chapter.

BIBLIOGRAPHY

[1] N. W. Ashcroft. Hydrogen Dominant Metallic Alloys: High Temperature Superconductors? *Phys. Rev. Lett.*, 92:187002, 2004.

[2] J. Feng, W. Grochala, T. Jaron, R. Hoffmann, A. Bergara, and N.W. Ashcroft. Structures and Potential Superconductivity in SiH_4 at High Pressure: En Route to "Metallic Hydrogen" . *Phys. REv. Lett.*, 2006:017006, 96.

[3] C. J. Pickard and R.J. Needs. High-pressure Phases of Silane . *Phys. Rev. Lett.*, 97:045504, 2006.

[4] M. Martinez-Canales, A. R.Oganov, Y. Ma, Y. Yan, A.O. Lyakhov, and A. Bergara. Novel Structures and Superconductivity of Silane under Pressure. *Phys. Rev. Lett.*, 102:087005, 2009.

[5] D.Y. Kim, R.H. Schericher, S. Lebégue, J. Prasongkit, B. Arnaud, M. Alouani, and R. Ahuja. Crystal Structure of the Pressure-induced Metallic Phase of SiH_4 . *Proc. Natl. Acad. Sci. USA*, 105:16454–16459, 2008.

[6] X-J. Chen, V.V. Struzhkin, Y. Song, A.F. Goncharov, S. Liu M. Ahart, H k. Mao, and R.J. Hemley. Pressure-induced Metallization of Silane . *Proc. Natl. Acad. Sci. USA*, 105:20–23, 2008.

[7] G. Gao, A. R. Oganov, A. Bergara, M. Martinez-Canales, T. Cui, T. Iitaka, Y. Ma, and G. Zuo. Superconducting High Pressure Phase of Germane . *Phys. Rev. Lett.*, 101:107002, 2008.

[8] J. S. Tse, Y. Yao, and K. Tanaka. Novel Superconductivity in Metallic SnH_4 under High Pressure. *Phys. Rev. Lett.*, 98:117004, 2007.

[9] I.J. Maley, D.H. Brown, R.M. Ibberson, and C.R. Pulham. Solid-state Structures of the Covalent hydrides Germane and Stannane. *Acta. Cryst.*, B64:312–317, 2008.

[10] N.N. Greenwood and A. Earnshaw. *Chemistry of the Elements*. Oxford:Butterworth-Heinemann, 1997.

[11] J.E. Huheey. *Inorganic Chemistry: Principles of Structure and Reactivity*. Harper, Row, Pearson, 1983.

[12] M. Bork and R. Hoppe. Zum Aufbau von PbF_4 mit Struktuverfeinerung an SnF_4. *Z. Anorg. Allg. Chem*, 622:1557–1563, 1996.

[13] W.J. Casteel Jr., A.P. Wilkinson, H. Borrmann, R.E. Serfass, and N. Bartlett. Preparation and Structure of Ruthenium Tetrafluoride and a Structural Comparison with Ruthenium Trifluoride and Ruthenium Pentafluoride. *Inorg. Chem.*, 31:3124–3131, 1992.

[14] S.K. Lahiri, J. Angilello, and M. Natan. Precise Lattice Parameter Determination of $PtHg_4$. *J. Appl. Crystallogr.*, 15:100–101, 1982.

[15] Wojciech Grochala, Roald Hoffmann, Ji Feng, and Neil W. Ashcroft. The Chemical Imagination at Work in Very Tight Places . *Angew. Chem. Int. Ed*, 46:3620–3642, 2007.

[16] J.P. Perdew, J.A. Chevary, S.H. Vosko, K.A. Jackson, M.R. Pederson, D.J. Singh, and C. Fiolhais. Atoms, Molecules, Solids and Surfaces: Applications of the Generalized Gradient Approximation for Exchange and Correlation . *Phys. Rev. B*, 46:6671–6687, 1992.

[17] H.J. Monkhorst and J.D. Pack. Special Points for Brillouin-zone Integrations . *Phys. Rev. B*, 13:5188–5192, 1976.

[18] H. Giefers, E.A. Tanis, S.P. Rudin, S. Greeff, X. Ke, C. Chen, M.F. Nicol, M. Pravica, W. Pravica, J. Zhao, M. Lerche, W. Sturhahn, and E. Alp. Phonon Density of States of Metallic Sn at High Pressure. *Phys Rev. Lett*, 98:245502, 2007.

[19] C. J. Pickard and R.J. Needs. Structure of Phase III of Solid Hydrogen. *Nat. Phys.*, 3:473–476, 2007.

[20] G. Gao, A.R. Oganov, P. Li, Z. Li, H. Wang, T. Cui, Y. Ma, A. Bergara, A.O. Lyakhov, T.Iitaka, and G.Zou. High-Pressure Crystal Structures and Superconductivity of Stannane (SnH_4) . *Proc. Natl. Acad. Sci. USA*, 107:1317–1320, 2010.

CHAPTER 3

Segregation into, Layers: A General Problem for Structures under Pressure, Exemplified by SnH_4[1]

3.1 Introduction - Segregation, The Question Emerges for SnH_4

We (and others) have been looking theoretically at the structures under pressure of group 14 tetrahydrides [1–12]. The motivation for examining just this group of compounds is the attractive idea of Ashcroft of chemical precompression [13]. Given the difficulty of metallizing molecular H2 [14, 15] (a potential superconductor and superfluid) [13, 16, 17], the core concept is that the effective repulsion between hydrogen molecules might be reduced by the hydrogen atoms bonding to other atoms [15–17].

The general problem of segregation that we expose in this chapter arose from some very specific considerations of the geometrical and electronic structure of SnH_4 under pressure. We began our studies with some trial structures based on previous experimental and theoretical work on SiH_4, GeH_4, and SnH_4. The way the enthalpy of the structures we calculated with pressure is shown by the colored line of Fig 3.1 (Colored line). The reference [0] enthalpy line in this graph is the enthalpy of Sn + $2H_2$, computed for the most stable structures of the elements at a given pressure, this transitions were already explored in chapter 2.(Sn evolves from diamond α-Sn, $\rightarrow$ β-Sn, $\rightarrow$ bct, $\rightarrow$ bcc; while H_2 evolves from P63/m, $\rightarrow$ C2/c, $\rightarrow$ Cmca-12) [18, 19]. The trial structures we explored (and the bumps in the enthalpy vs. pressure curves that hint at phase transitions) are

[1]Reproduced with permission from *ChemPhysChem*, accepted for publication 2010

of substantial interest, and they were also discussed in chapter 2. Our focus in chapter 3, however, is on the fact that over a wide pressure range (< 180 GPa) the separated elements (blue reference line) may be more stable.

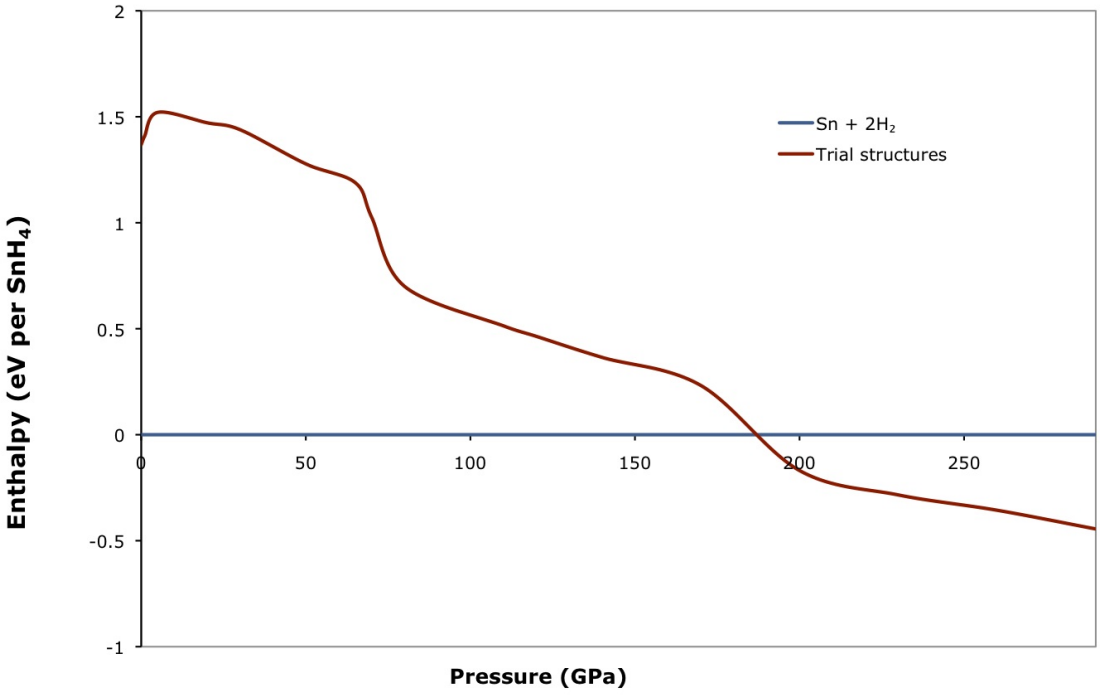

Figure 3.1: Computed relative enthalpies of hypothetical SnH_4 structures as a function of pressure. The zero of enthalpy corresponds to the stable form of the elements, Sn +2H_2, at the given pressure.

Why do we say may and not are? Because there is an enthalpic penalty (for Sn, not so much for H_2) for cutting such layers out of the solid. In forming layers of Sn (at 1 atm of higher pressures) one has created a chemically reactive slab it has low-lying unfilled and high-lying filled orbitals. Such a slab will effectively bond to the H_2 layer, a stabilizing interaction. The new interlayer bonding potentially compensates for this intralayer penalty. But we dont imagine that it

will fully do so.

This simple realization puts a new perspective on the search for optimal structures in this low and medium pressure regime. As we will see, a systematic search in fact finds some layered structures falling in enthalpy between the continuous curve in Figure 1 and those of the separated elements. In quite independent work, a similar trend toward layered structures has been seen theoretically, in silane, [4] and germane, [7] and just recently, stannane, And Gao and coworkers concluded that segregation is also likely in pressurized stannane at P < 96GPa. [20]

3.1.1 The General Problem of Segregation

The favoring of slabs is not surprising when we take a look at the formation energy ($\triangle H_f^\circ$) of group 14 hydrides. Of these hydrides, only CH_4 has a negative heat of formation, $\triangle H_f^\circ$. A molecule of stannane (and so, approximately, the P=1atm solid), with an experimental heat of formation of +1.68 eV/SnH_4 molecule [21] , is thermodynamically unstable, yet kinetically reasonably persistent (at 298K). Gaseous stannane in fact slowly decomposes to the elements at P=1atm [22].

The problem presented by a system under pressure segregating into elements if there is a thermodynamic driving force for the reaction is a very general one. It faces experimentalists in the area continually, but (for reasons of avoiding complexity, we think) has not received sufficient attention from the

theoretical community. This motivates, in part, these chapter.

Many interesting questions arise as one begins to think of segregation. Among them: If segregation to atom slabs is favored, how many layers will there be in each slab? Is a specific ordering of (in our case) tin atoms preferred within a slab? Can this ordering be predicted from our knowledge of existing tin allotropes at high pressure? Will the hydrogen atoms, within a layered structure, always prefer to form molecular pairs? What of their orientations? At what pressure does the formation of a novel three-dimensional tin-hydrogen bonding framework become favored over segregation of the elements?

We address these questions specifically for SnH_4 in this paper. We use reasonably standard DFT computational methodology in these explorations within static lattice approximations initially; the details are provided in the next section.

We restricted ourselves to computations with Z=4, four formula units in a unit cell. If a substance wants to segregate, this limitation favors not especially thick layers, and so potentially an incomplete expression of the tendency to segregate. Nevertheless, we are sure the driving force for segregation manifests itself even within a relatively small unit cell.

3.1.2 Preparing Segregated or Layered Structures for Calculation

We started by first setting up layered structures preserving the bulk SnH_4 stoichiometry, to see if they would optimize to structures closer to the separated elements than the parent compound. In this preparation process we focused mainly on the slabs of tin atoms, our rationale being that Sn-Sn interactions carry greater consequences for the enthalpy than the weaker H_2-H_2 interactions, at least at relatively low pressures where distinct H_2 molecules are likely to be seen.

Within a slab of tin atoms, our starting structures contained 1-4 layers. The number of layers is in some way arbitrary, as two layers can merge into one easily. So Z, the total number of formula units (SnH_4) within a unit cell, will also be specified. Tin changes phases as pressure is applied [19]: α-tin is stable at very low pressures, readily transforming to β-tin, which is energetically more favorable from just above atmospheric pressure to 10 GPa. At higher pressure pure tin undergoes a phase change to bct and at 44 GPa takes on the bcc structure [19].

We focused our attention on the structures that are most stable over a wide range of pressures, namely β-tin in the low pressure regime and bcc at high pressures. For the sake of simplicity, we select one crystal plane per Sn allotrope and form slabs of varying thickness around that plane. Examples are shown in Figure 3.2.

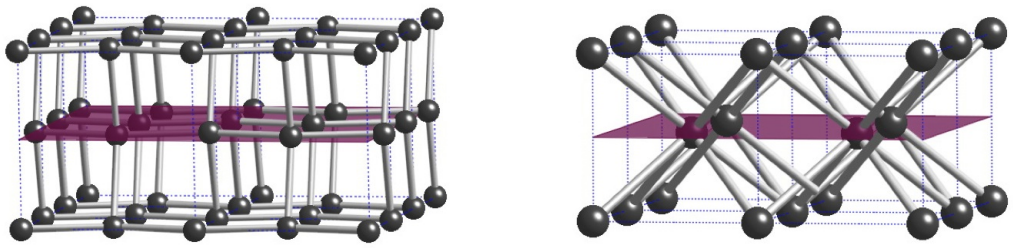

a) b)

Figure 3.2: The Sn elemental structure planes around which further layers were taken to form Sn slabs in trial structures. The reference planes are depicted in purple. a) β-Sn structure, b) bcc Sn, the most stable structure for bulk tin at high pressures

What about possible hydrogen slabs? We knew from preliminary work on high pressure phases of SnH_4 that in some of them H_2 molecules persist, while in others the H-H bond is broken. We wished to give the system a good chance to locate both kinds of structures, and to introduce Sn-H interactions as needed. This led us to start out with two kinds of structures for each hydrogen slab; in one of them we placed dihydrogen molecules at different position in-between two slabs of tin. In the other initial geometry choice, atoms (not molecules) of hydrogen are placed in layers, loosely following a simple tetragonal Bravais lattice. Figure 3.3 shows an illustrative example of these two starting points.

Putting the slabs together, we come to the starting structures for our enthalpy optimization. Figure 4 shows several such arrangements, for the "undimerized" hydrogen atom starting point). In these initial geometries we kept H-H$\geqslant$ 1.2 Å. There may be incipient H-H bonding even at 1.2 Å; there are (a few) molecular H_2 complexes known with that distance, and they show indeed some sign of bonding [23–26]. We also left some additional space among

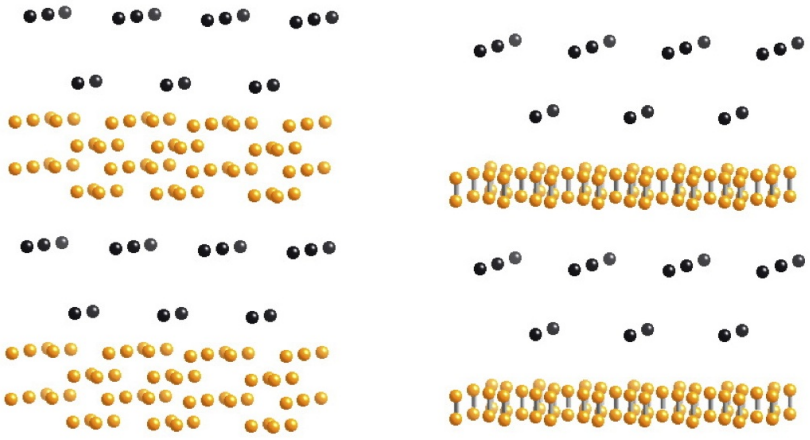

a) b)

Figure 3.3: Two different starting points for slab optimizations. (Sn=black, H=orange). a) Hydrogen atoms are placed in this structure, but not paired; b) All hydrogen atoms are paired

hydrogen and tin atoms (~2 Å) in our starting structures for both cases; the Sn-H bond distance in a tin tetrahydride molecule at ambient conditions is 1.7 Å. The general idea was to start optimizations with structures that allow hydrogens to bond or not bond with each other, and with the tin layer as determined by enthalpy minimization.

3.2 Methodology

Density-functional theory (DFT) calculations with the Perdew-Wang exchange-correlation functional [27] were performed with Blöchl's projector-augmented wave method (PAW) and a plane wave basis set, as implemented in the VASP codes. For tin, the 5*s* and 5*p* were treated as valence state.

For the optimization of the structures, the cell parameters, the atomic po-

sitions, and the cell volume were all allowed to relax. The stress tensor was also calculated. A defined stress was added to the stress tensor, converging into a particular pressure. Once an optimized structure was reached, the electronic density of states per electron (DOS) was calculated. The k-point grids were generated via the Monkhorst-Pack scheme [28]. The calculations are for the ground state at 0K, and neglecting the zero-point vibrational energy. The cutoff of the kinetic energy was set at 650 eV, and for the planewaves we set a self-consistent field (SCF) tolerance of 1 x 10^{-5} eV/unit cell. The Wigner-Seitz radii was oriented along the atomic radii given in the PAW potentials: r(Sn)= 1.566Å, r(H)=0.37 Å.

3.3 Results

3.3.1 Layers at one Atmosphere

SnH_4 Layers at One Atmosphere Pressure: Geometry

In our calculations the most stable layered system at 1 atm emerges from optimizing a starting structure of tin atoms in a slab of 2 bcc layers alternating with an array of initially unpaired hydrogen atoms, and with Z= 4. As seen in Fig 1.4a, the hydrogen atoms do pair in the course of optimization. A layered structure derived from a starting point with paired hydrogen atoms has a slightly higher enthalpy (by 0.21 eV/SnH_4). The final structure in that case has a similar ordering in the tin layer but the axes of the hydrogen molecules assume an aver-

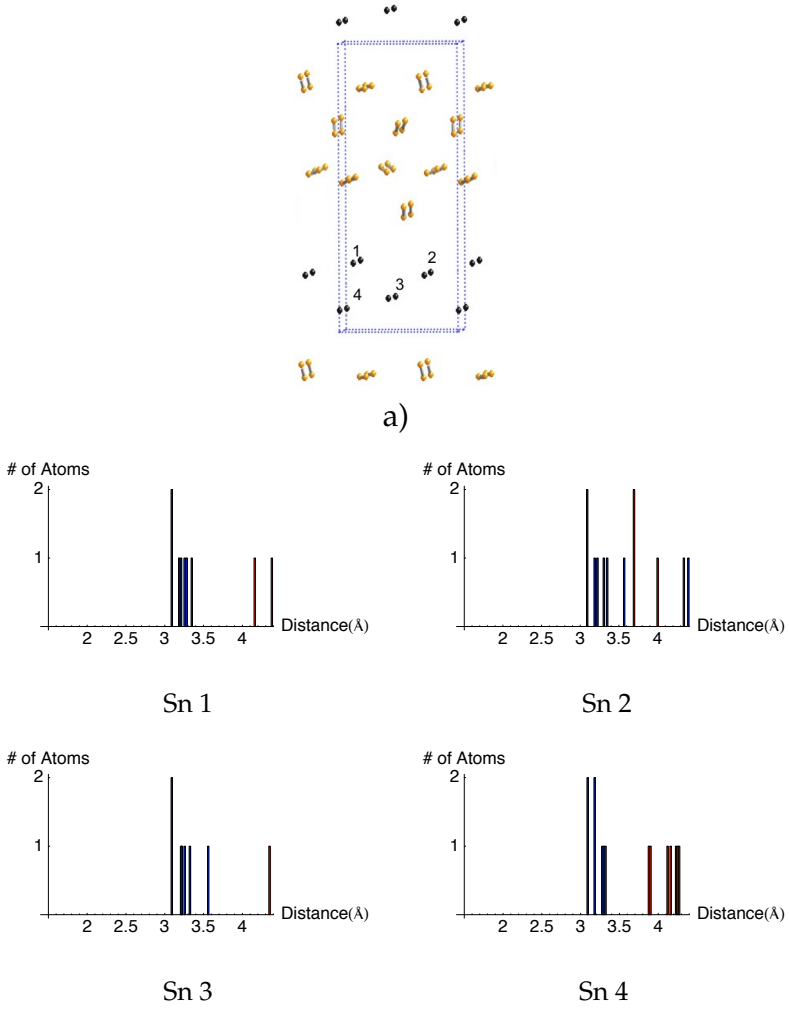

Figure 3.4: The most stable layered structure for tin tetrahydride, at 0 GPa, and the coordination environment of the Sn atoms in it. a) A unit cell embedded in a larger view of the layered system. There are 4 different types of tin atoms (numbered); each has a distinct coordination environment. b) The coordination of each tin atom is shown in portions of distance histograms (in red, distances from the reference Sn atom to hydrogen; in blue, to tin).

age orientation that follows the corrugations of the tin layer. It is not surprising that several structural options are found for the hydrogen layer, differing in H_2 orientation; at low pressure, small dispersion forces (van der Waals bonding) determine the ordering of H_2 molecules in their own layer. Also local approxi-

mations to DFT functionals generally do not give dispersion forces reliably.

There are 4 different types of tin locations in the optimized Z=4 structure. A useful way to gain insight into the geometrics of bonding in an extended structure is to construct histograms of the calculated atom separations, which we do in Figure3.4b. As these diagrams show, each Sn (numbered in Figure3.4a) has a distinct coordination environment. Note the Sn-Sn separations lying between 3.0 and 3.6 Å, similar to those in α-tin (3.02 Å) and β-tin (2.8 and 3.1 Å). The Sn-H distances are long (the shortest is $\sim$ 3.7 Å, longer by far than the normal Sn-H bond length in stannane (1.7 Å). It is clear that in this layered structure there is little manifestation of the Sn-H interaction and just some small reconstruction in the Sn layers. This structure is very different from the molecular crystal system which first comes to mind when we think about SnH_4.

Energetics of Layering at P=1 atm

What is the energetic price that the layered structure has to pay for the arrangement we have found? Using the enthalpies of the most stable allotrope of tin and of molecular hydrogen at 1 atm pressure as a reference, our optimized layered structure is unstable by +0.37 eV per SnH_4.

Lets see if we can take apart the contributions to the enthalpy of the optimum layered structure. We calculate that to excerpt a β-tin layer from the element structure costs +0.31 eV/atom. To cut out $2H_2$ from its element structure costs much less (since only dispersion forces are involved in the process),

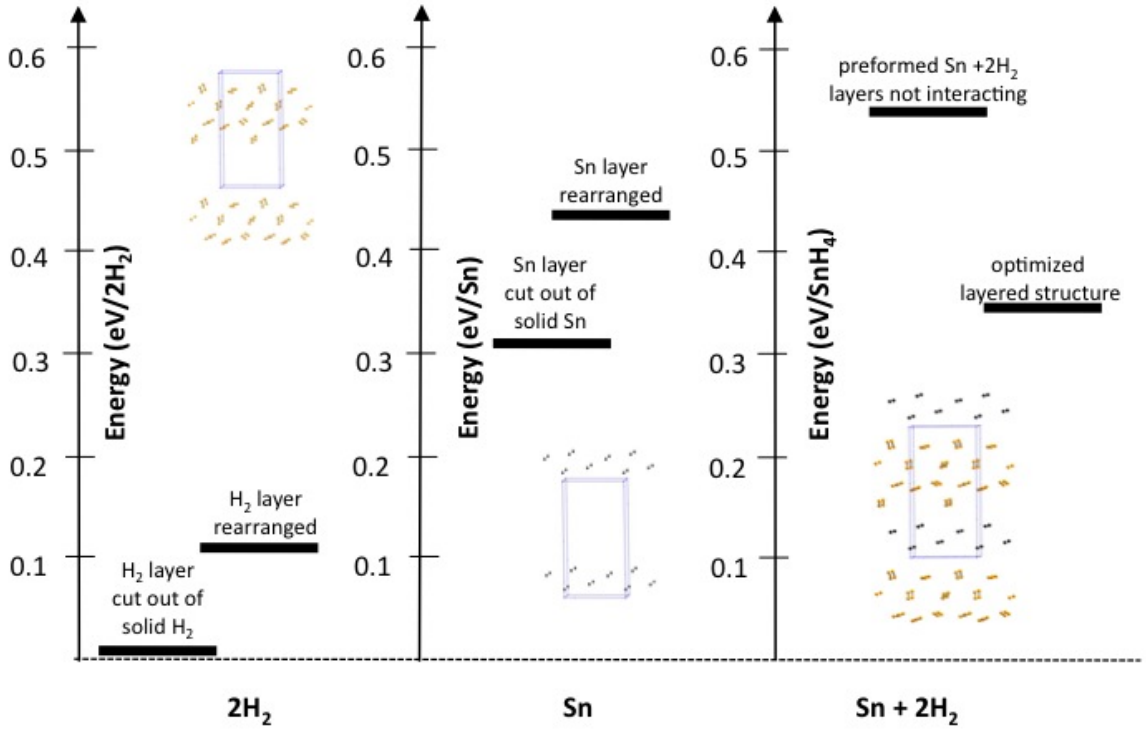

Figure 3.5: Energetics for the tin tetrahydride layered structure. The zero of energy for the right side of the figure is the energy of the separated β-tin and $2H_2$ structures; on the left the zero of energy is of individual Sn or $2H_2$, as appropriate. "Rearranged" means Sn and $2H_2$ layers taking on the geometry they have in the optimized layered structure.

namely +0.03eV. Figure 3.5 at the left shows these energies.To rearrange an isolated β-tin layer to the geometry it has in the optimized layer structure costs 0.10 eV more (a total of +0.43eV); to rearrange the H_2 layer the cost is +0.11eV. Bringing the preformed Sn and H_2 layers together is therefore a stabilizing process, by -0.17eV. These components of the energy are shown graphically in Figure3.5. The general picture holds it costs energy to cut out slabs of Sn and H_2 from their solids, that penalty is compensated in part by Sn-H_2 interactions.

We expect that if we took thicker slabs for Sn and H_2 (higher Z) the enthalpy of the slabs would approach that of the elements, the blue reference line in Figure 3.1.

Electronic Structure of the Layered Material at P = 1atm

The computed structure can be described as Sn (layer)· $2H_2$. What one might expect in its electronic structure are prominent molecular σ_g and σ_u^* derived bands for the H_2 layer, but slightly broadened. The Sn layers are rather thin, and we anticipate them to be metallic, a substantial density of states (DOS) at the Fermi level arising from the "dangling bonds" of the Sn slab carved out of its bulk structure (the next section describes experimental and theoretical work on related Sn surfaces).

Figure 3.6 shows the density of states per electron (DOS) of the P = 1atm Sn(layer)·$2H_2$ arrangement, and the contribution of the Sn and H atoms to that DOS. For this average density the r_s value is 2.67. ($(4\pi/3)r_s^3 a_o^3 = V/N_e$)

From this plot we notice that indeed the tin atom contributions dominate the DOS at the Fermi level. The structure is indeed distinctly metallic. As expected, the contributions to the DOS of the hydrogen atoms have a clear peak for H_2 σ_g at -5.89 eV, overlapping a region of mainly Sn *s* states. The σ_u^* peak is more dispersed. We are not sure this is real, for VASP DOS projections are problematic and more so in the high energy regime. The problem may be seen most clearly

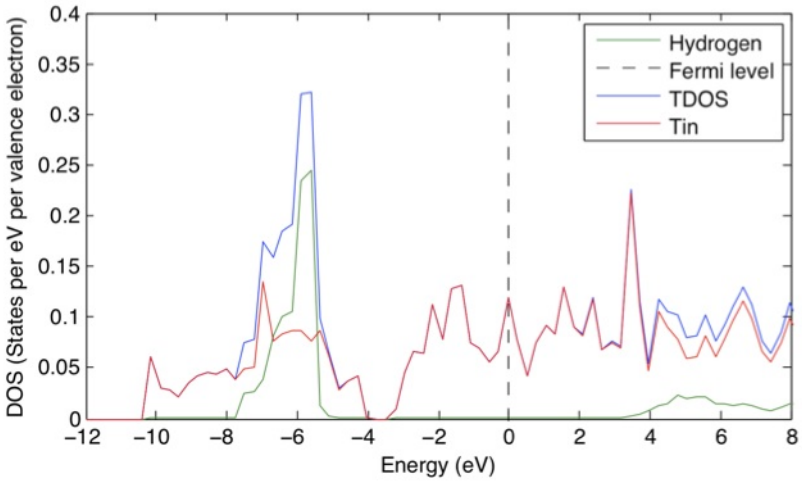

Figure 3.6: Density of States plot for SnH4 at 0 GPa, Z=4, nominal r_s=2.67. In blue, the total DOS (TDOS); in red, contributions to the TDOS from the 4 tin atoms and in green from the 16 hydrogen atoms.

in the high energy region, where the H and Sn contributions to the DOS do not add up to the total DOS.

Information from Low Pressure Studies of Sn Surfaces

Contemporary surface science has provided us with much information on metal and semiconductor surfaces, and their interaction with molecules [29]. Most of such experimental studies are made under high vacuum conditions.

Given how much work has been done on Si and Ge surfaces, surprisingly little is known about Sn surfaces. Tin is widely used, in solders, tin-coated steel, and overlayers on other metals. In fact, while there are many studies of Sn overlayers, we have found little on Sn itself. Apparently such crystals are difficult to

grow.

However, it is possible to grow well-defined overlayers of *alpha*-Sn on CdTe and InSb. Following initial medium and high electron diffraction studies of reasonably thick α-Sn overlayers on these semiconductors [30, 31] , Woodruff and Horne investigated the α-Sn(100) surface, and found a (2 x 1) reconstruction [32, 33]. They also studied the interaction of H2 and H with such overlayers, and argued for the formation of a monohydride phase (contrasted with dihydride on the much better studied Si(100) surface. In another study the same authors reported a progressive reconstruction from (2 x 1) to p (2 x 2) to c (4 x 4).

A thorough theoretical study of the α-Sn(100) surface and its reconstructions by Lu et al [34] found a large buckling of the dimers, a deformation well-known for the Si(100) reconstruction, except for a zero gap region around the zone center [34], and they found the surface to be semiconducting. The Sn layers or slabs that we have studied are derived from β-Sn layers, and are much thinner than the surface models (12 layers) studied by Lu et al. For this reason they are more likely to be metallic.

We have found no experimental studies of β-Sn surfaces in the literature, to date.

3.3.2 Layers at 50 GPa

50 GPa Structures

Moving from 0 GPa to 50 GPa, the volume of the unit cell decreases, prompting shorter distances between elemental layers. The starting point for the lowest enthalpy structure computed at 50 GPa, and Z=4, has the tin atoms cut out of slabs of β-Sn. The final ordering of the tin atoms within the slab is, however, different from β-tin. The hydrogen molecules in this structure have a calculated H-H separation of 0.79 Å, slightly longer than gas phase H_2 separation at 0.74 Å. The H_2 axes are noticeably aligned, as Figure 7a shows; the average orientation of the slab of H_2 diatomics seems to "follow" the way the tin layer folds. We have not studied the energetics of further displacement of the H_2 molecules in their sublattice, or their libration. It is likely that even at 50 GPa the barriers to displacement in the H_2 sublattice are small, and given the inadequacy of our functional for dispersion interactions, we did not explore such motions. Gao et al obtained similar-looking structures at 50GPa, using an evolutionary algorithm structure search. [20]

As in the 0 GPa case, there are four different types of tin locations. Their coordination environments are analyzed by a histogram of Sn-H, Sn distances in Figure 7b. The windows of the histograms at this pressure are from 1.4 to 2.8 Å, smaller than those at 1 atm, shown above in Figure3.4b.

Note that the nearest neighbors for a tin atom are now hydrogen atoms (of hydrogen molecules) at ~1.9 Å, and the nearest tin atom is at ~ 3 Å. The overall compression is apparent, and is by far greater in the H_2 layer, as expected. There

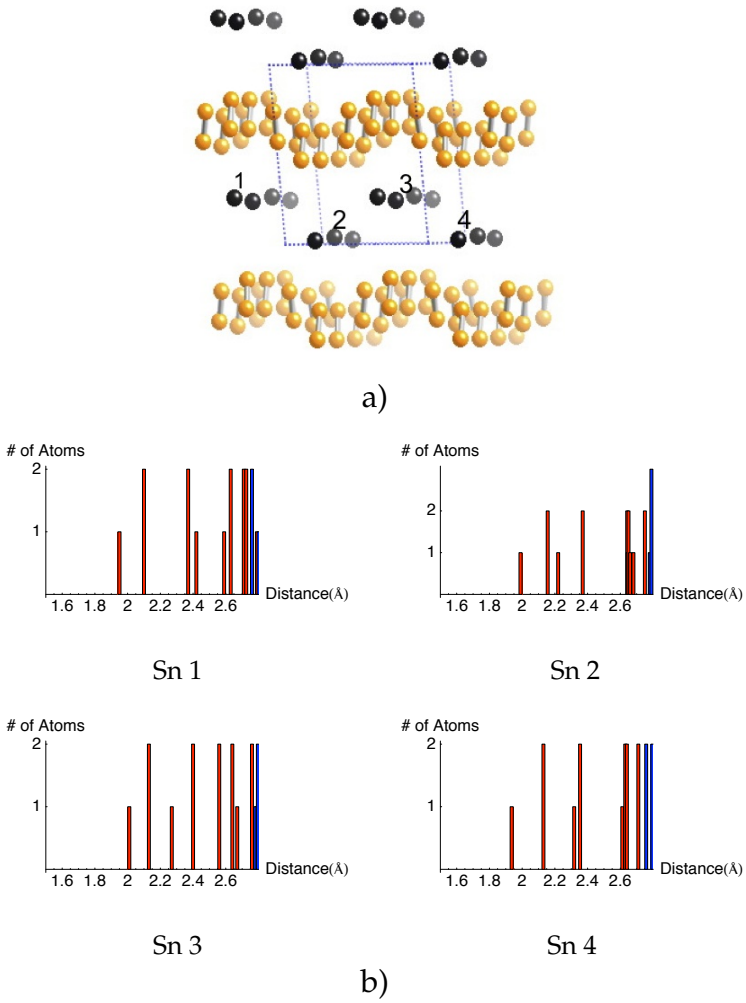

Figure 3.7: The lowest enthalpy structure for SnH_4 computed at 50 GPa and its tin coordination environment. a) The unit cell of the optimized system, extended in this view beyond the unit cell (dashed lines). There are 4 different types of tin atoms, each with a distinct coordination environment (numbered); b) Portions of distance histograms for the different tin atoms in the unit cell, labeled by the number of the tin (In red Sn-H and in blue, Sn-Sn distances).

must be some interaction between Sn layers and H_2 molecules or between H_2's, for the H-H bond stretches a little (0.79 Å) The shortest nonbonded H-H···H-H approaches are 1.72 Å. For calibration, in the 50 GPa structure of elemental H2 ($P6_3/m$ space group [18]), these distances are 1.7-2.0 Å. It is clear that in

this structure the van der Waals space between H_2 molecules is now "squeezed out" [35] while the Sn layers are less affected.

The best 50 GPa structure we calculate is unstable when compared to separation into its elements at the same pressure, by +0.61 eV per SnH_4; it is, however, more stable than the best structures derived by optimizing structures based on other studies of EH_4 molecules where E= Si, Ge and Sn (the red curve in Figure1; details of the structures were given in chapter 2), by 0.66 eV per SnH4. Once again the enthalpy of the layered structure lies in-between the elements and structures that are not layered. If the slabs were thicker, a still more segregated structure is likely to be stabilized.

We thought it possible to go further, and analyze the energetics of the layered structures by decomposing them into their elemental layers, as we did for the P=1 atm structure. This approach proves problematic; it runs into fundamental difficulties of defining appropriate thermodynamic functions and conditions for separate layers as pressure is applied.

Electronic Structure of the Layered 50 GPa System

At 0 GPa the metallic character of layered structure derived from the tin slabs alone. Given what we found in the 50 GPa structure (the relatively short Sn-H distances), we expect this phase to be metallic, but with both elements contributing to the DOS at the Fermi level. Figure 3.8 shows the DOS at P=50 GPa,

with the contributions of tin and hydrogen atoms. Note the hydrogen density dispersed throughout the energy window and the expected increase in overall band dispersion at 50GPa relatively to P=0 GPa,

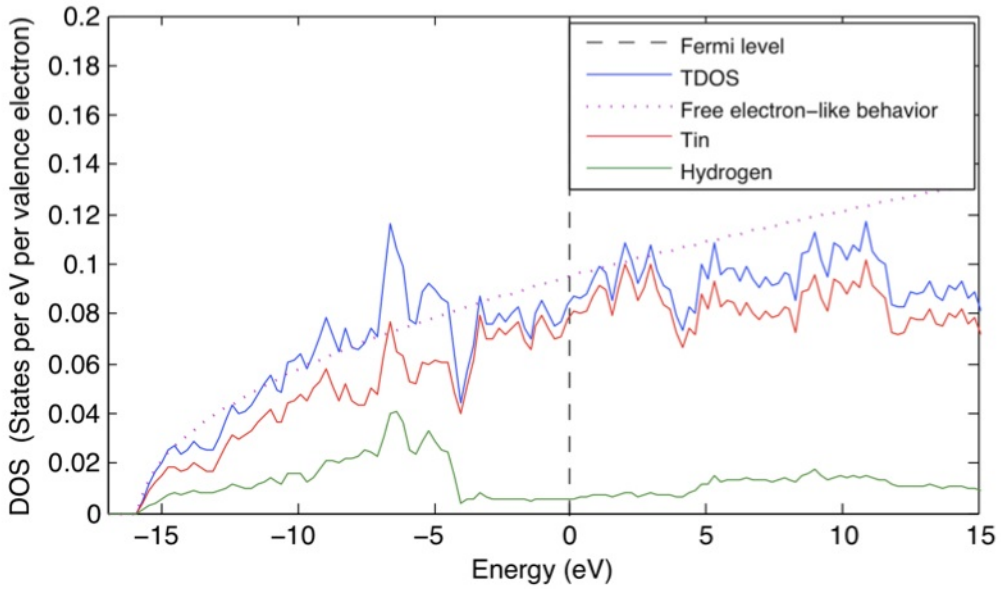

Figure 3.8: . Density of States plot for SnH_4 at 50 GPa, and r_s=1.829. In blue, the total DOS (TDOS); in red, contributions to the TDOS from tin and in green from hydrogen

3.3.3 Layers at 140 GPa

Structures at 140 GPa (V/V_0 = 0.21)

The most stable system calculated by us at 140 GPa (Figure 3.9a) no longer shows elemental slabs (but see below), even though the starting point for geometry optimization was layered. As we will see, hydrogens surround the tin atoms, and the closest distances between hydrogens actually increase (relative to their lower pressure separations). Lets look at the coordination of the Hs first.

A free electron parabola fits the DOS quite well.

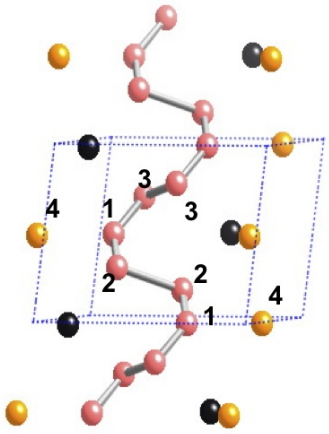

a)

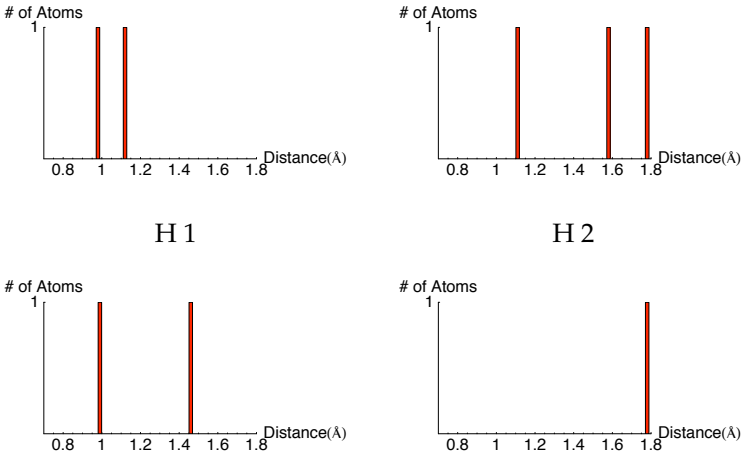

b)

Figure 3.9: The most stable structure for tin tetrahydride (from our sampling of layered structures at 140 GPa) and its H-H separations. a). Hydrogen atoms are no longer simply paired; some hydrogen atoms form a network a helix, here we show them in pink. Distinct hydrogens are numbered. b) Histograms of HH separations by atom type).

Figure 3.9b shows the histogram of HH separations in the 140GPa structure. Note that there are no HH contacts close to the molecular distance of 0.74 Å(or

that in elemental H_2 at this pressure, which has H-H bonds of 0.74 Å, and next-nearest Hs at 1.3 Å). There are four symmetry-distinct hydrogens in the optimal structure. From the histogram we see that one hydrogen atom (H4) is pretty much isolated. That hydride is surrounded by 4 Sn in a tetrahedron, as shown in Figure 3.10a, but its closest neighbor is actually another hydrogen atom at 1.78 Å.

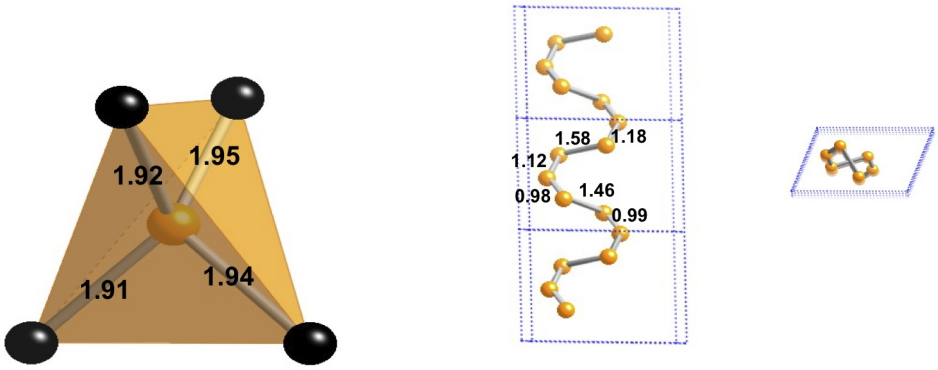

a) b)

Figure 3.10: Hydrogen coordination environment within the most stable structure for tin tetrahydride at 140 GPa. a) Coordination environment for H4; b) Distances within the helix and side view. (Sn=black, H=orange)

Hydrogens 1, 2 and 3 form helices, with separations (all indicative of partial bonding) indicated in Figure 3.10b The nearest interhelix separation is at 2.1 Å. The singling out of a helix is thus somewhat arbitrary (including H - H 1.58, excluding 2.1 Å, as examination of the histogram shows); we really have the beginning of a 3-dimensional hydrogen network. Alternatively one could focus on just the shorter H-H contacts (0.98, 1.12 Å) in which case we would say the structure contains H_3 units.

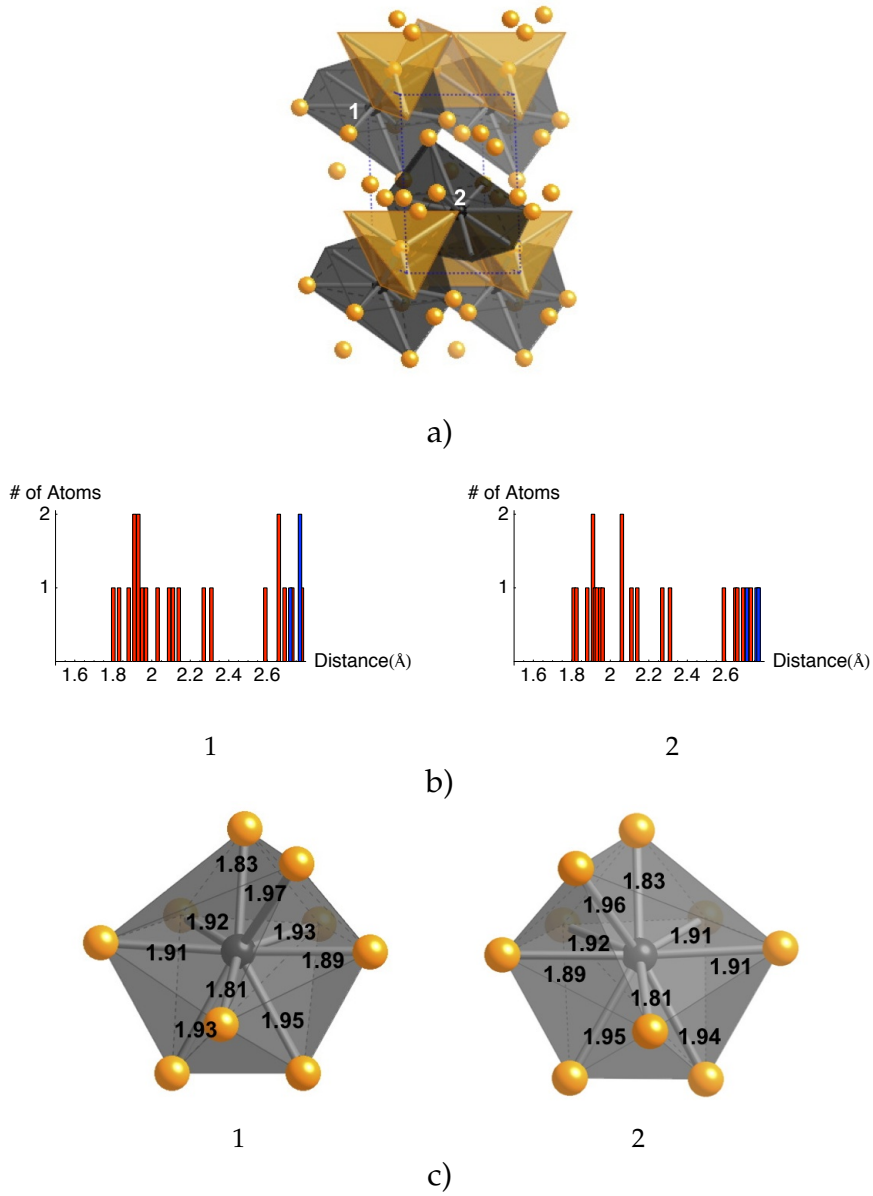

Figure 3.11: The most stable structure for SnH_4, from our sampling of layered structures at 140 GPa, and its tin coordination. Slabs are no longer a feature in this structure. a) The unit cell of the optimized system, extended in this view beyond the unit cell (dashed lines). There are two different types of tin atoms per unit cell (numbered); b) Portions of distance histograms for the different tin atoms in the unit cell. (in red Sn-H and in blue, Sn-Sn distances); c) Coordination polyhedra for the two tin atoms; notice that the two tin atoms coordination environments are almost mirror images.

We now turn to the Sn-H separations, Figure 3.11. There are two distinct Sn atoms in the structure; a histogram of the Sn-H distances is given in Figure 3.11b. It is not easy to define a Sn coordination environment. The closest Sn-H contact is 1.8 Å, but there are many hydrogens not much further away. If one used the large gap at 2.3 - 2.6 Å for both tins as a cut-off for defining coordination, one would have to call the Sn's 15-coordinate. Even though this coordination number seems too high, the general phenomenon of increasing coordination with pressure [35] makes sense. In Figure 3.11a and 3.11c we use an arbitrary Sn-H cut-off of 2.0 Å, which results in much distorted nonahedra for the two symmetry-distinct (yet almost mirror-image) Sn atoms.

Energetics and Electronic Structure at P = 140 GPa

The 140 GPa structure is still unstable with respect to the elements. The difference in enthalpy is now reduced, to +0.17 eV per SnH_4. Could there exist a layered structure (with Z greater than the largest one investigated, Z=4), at still lower energy than the one we found? We dont know, and are prevented from exploring the question by the economics of computation for large Z unit cells.

Subsequent to our calculations, Gao et. al. [20] reported two lower enthalpy candidates for SnH4 structures at high pressures, of *Ama2* and $P6_3/mmc$ symmetry. We calculated these structures over the range of pressures 80-230GPa. The results are shown in the Figure 3.12.

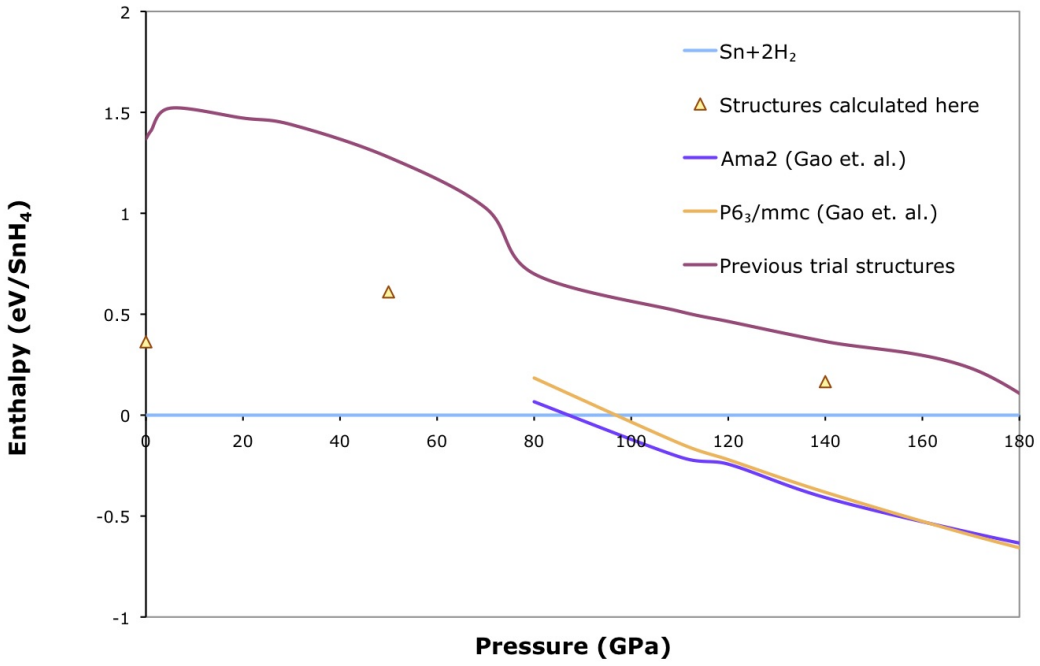

Figure 3.12: Computed relative stabilities of the structures calculated in this paper, and *Ama2* and *$P6_3/mmc$* structures, reported by Gao et. al. [20]

Our structural search at P = 140 GPa was clearly inferior to that of Gao et. al. [20] who found *Ama2* and *$P6_3/mmc$* structures that are more stable than the elements at this pressure. Nevertheless, we feel the "helical" geometry is sufficiently interesting to report here, even if it is not the most stable structure at 140 GPa.

At 140 GPa the electronic structure of the structure we calculated is not only metallic, but the TDOS shows a characteristic free-electron like shape (Figure 3.13). Both Sn and H states contribute to the DOS throughout both filled and unfilled states.

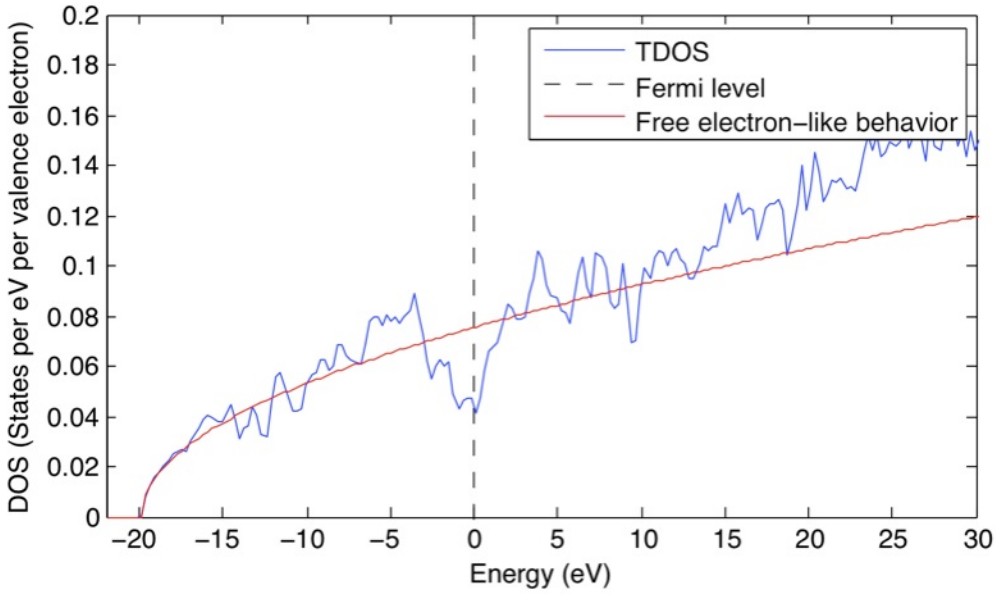

Figure 3.13: Density of States (TDOS) plot for SnH_4 at 140 GPa, and r_s=1.635.

When is a structure layered?

We return to the question of whether this structure is layered or not. In another view of the 140 GPa SnH_4 structure, in Figure 3.11, layers of Sn and H atoms can be seen. The perception of lowered dimensionality in a 3-dimensional structure is much in the eye of the beholder. So layers easily float into view in classical structures such as diamond, β-Sn and bcc, yet these are hardly two-dimensional arrays. The perceived layers are just a symptom of the human addiction to pattern recognition. One has to look at the distribution of distances only when the separations along one axis (perpendicular to the putative layer) are significantly longer than those within a layer could one realistically call the material layered.

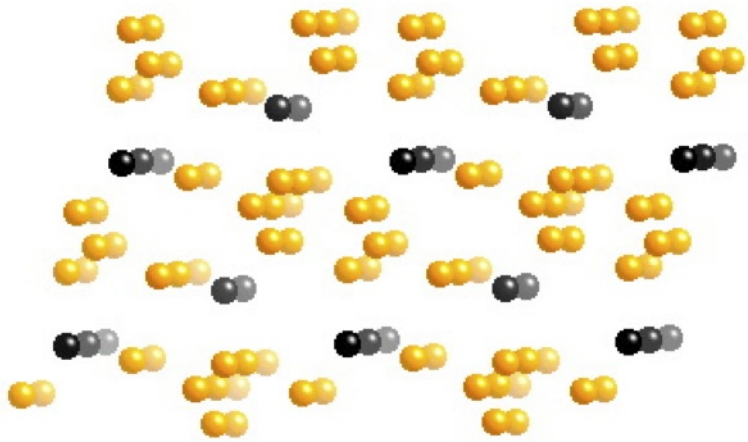

Figure 3.14: The geometry of the SnH_4 structure calculated by us at 140 GPa, r_s=1.635 (Identical to that shown in Figure 3.11.) In a view that emphasizes the structures layered nature.

3.4 Conclusions

When a tetrahydride is thermodynamically unstable with respect to the elements, as is the case for SnH_4, the necessary preconditions are present for segregation in fact, as we propose, to a layering of element slabs. We investigated such layering in SnH_4, making sure that the choice of structures allowed H-H bond formation to occur if energetically allowed.

Our optimum structures at 0 and 50 GPa (r_s= 2.67 and 1.829) show slabs of Sn and molecular H_2. With increasing pressure, van der Waals space is squeezed out, and Sn - H and H_2 - H_2 separations decrease. At 140 GPa, with r_s=1.635

(and we expect the same for greater pressures). Our optimum structures no longer show slabs nor the presence of molecular hydrogen. Interestingly, at 140 GPa, the hydrogen atoms are arranged in H_3 units that form helices. Hydridic isolated atoms also occur. As expected, the coordination of tin and hydrogen increases with pressure. However, still more stable structures than those found here (also with H_2 molecular units) have been reported [20].

One can take apart the contributions to the enthalpy of slab formation: It takes a good bit of energy to cut the metal layer out of its 3-D lattice, less so for the dispersion-force-bound H_2 layer. Bringing the preformed layers together is a stabilizing process, due to what effectively is chemisorption at an interface.

The SnH_4 case maybe extreme in that the heat of formation of the molecules is so positive, creating a large thermodynamic driving force for segregation and layering. But the lesson of our modeling exercise is clear and likely to be valid generally: *Over a wide range of pressures any compound that has a substantial positive enthalpy of formation is likely to segregate to the elements*.

Obviously this does not preclude the possibility (in fact, likelihood) of eventual re-mixing, as the pressure increases, the situation changes, even when there is a driving force for layering. Unsegregated structures with new bonding patterns may be stabilized; this is where the effect of high pressure becomes truly interesting.

BIBLIOGRAPHY

[1] J. S. Tse, Y. Yao, and K. Tanaka. Novel Superconductivity in Metallic SnH_4 under High Pressure. *Phys. Rev. Lett.*, 98:117004, 2007.

[2] J. Feng, W. Grochala, T. Jaron, R. Hoffmann, A. Bergara, and N.W. Ashcroft. Structures and Potential Superconductivity in SiH_4 at High Pressure: En Route to "Metallic Hydrogen" . *Phys. REv. Lett.*, 2006:017006, 96.

[3] C. J. Pickard and R.J. Needs. High-Pressure Phases of Silane . *Phys. Rev. Lett.*, 97:045504, 2006.

[4] M. Martinez-Canales, A. R.Oganov, Y. Ma, Y. Yan, A.O. Lyakhov, and A. Bergara. Novel Structures and Superconductivity of Silane under Pressure. *Phys. Rev. Lett.*, 102:087005, 2009.

[5] D.Y. Kim, R.H. Schericher, S. Lebégue, J. Prasongkit, B. Arnaud, M. Alouani, and R. Ahuja. Crystal Structure of the Pressure-induced Metallic Phase of SiH_4 . *Proc. Natl. Acad. Sci. USA*, 105:16454–16459, 2008.

[6] X-J. Chen, V.V. Struzhkin, Y. Song, A.F. Goncharov, S. Liu M. Ahart, H k. Mao, and R.J. Hemley. Pressure-Induced Metallization of Silane . *Proc. Natl. Acad. Sci. USA*, 105:20–23, 2008.

[7] G. Gao, A. R. Oganov, A. Bergara, M. Martinez-Canales, T. Cui, T. Iitaka, Y. Ma, and G. Zuo. Superconducting High Pressure Phase of Germane . *Phys. Rev. Lett.*, 101:107002, 2008.

[8] M. I. Eremest, I.A. Trojan, S.A. Medvedev, J.S. Tse, and Y. Yao. Superconductivity in Hydrogen Dominant Materials . *Science*, 319:1506–1509, 2008.

[9] O. Degtyareva, M. Martinez-Canales, X-J Chen A. Bergara, Y. Song, V. V. Struzhkin, H k. Mao, and R.J. Hemley. Crystal Structure of SiH_4 at High Pressure. *Phys. Rev. B*, 76:064123, 2007.

[10] Z. Li, W. Yu, and C. Jin. First-principles calculation on Phase Stability and Metallization in GeH_4 under Pressure. *Solid Sate Commun.*, 143:353–357, 2007.

[11] Y.S. Yao, J.S. Tse, Y.Ma, and K. Tanaka. Superconductivity in high-pressure SiH_4. *Europhys. Lett.*, 78:37003, 2007.

[12] M. Marinez-Canales, A. Bergara, J. Feng, and W. Grochala. Pressure Induced Metallization of Germane. *J. Phys. Chem. Solids*, 67:2095–2099, 2006.

[13] N. W. Ashcroft. Hydogen Dominan Metallic Alloys: High Temperature Superconductors? *Phys. Rev. Lett.*, 92:187002, 2004.

[14] C. Narayana, H. Luo, J. Orloff, and A.L. Ruoff. Solid Hydrogen at 342 GPa, No Evidence for an Alkali Metal. *Nature*, 393:46–49, 1998.

[15] P. P. Edwards and F. Hensel. Will solid hydrogen Ever be a Metal? . *Nature*, 388:621, 1997.

[16] N. W. Ashcroft. Metallic Hydrogen: A High-Temperature Superconductor? *Phys. Rev. Lett.*, 21:1748–1749, 1968.

[17] A. Bergara and N.W. Ashcroft. Proceedings of the 20th General Conference of the Condensed Matter Division of the European Physical Society.

[18] C. J. Pickard and R.J. Needs. Structure of Phase III of Solid Hydrogen. *Nat. Phys.*, 3:473–476, 2007.

[19] H. Giefers, E.A. Tanis, S.P. Rudin, S. Greeff, X. Ke, C. Chen, M.F. Nicol, M. Pravica, W. Pravica, J. Zhao, M. Lerche, W. Sturhahn, and E. Alp. Phonon Density of States of Metallic Sn at High Pressure. *Phys Rev. Lett*, 98:245502, 2007.

[20] G. Gao, A.R. Oganov, P. Li, Z. Li, H. Wang, T. Cui, Y. Ma, A. Bergara, A.O. Lyakhov, T.Iitaka, and G.Zou. High-pressure crystal structures and superconductivity of Stannane (SnH_4) . *Proc. Natl. Acad. Sci. USA*, 107:1317–1320, 2010.

[21] D.R.Lide. *CRC Handbook of Chemistry and Physics 85th Edition*. CRC Press, N.J., 2004-2005.

[22] N.N. Greenwood and A. Earnshaw. *Chemistry of the Elements*. Oxford:Butterworth-Heinemann, 1997.

[23] X-L. Luo, H. Liu, and R.H. Crabtree. Separating the Rhenium-Hydride and Proton-proton Dipole-dipole Contributions to the 1H NMR Spin-lattice Relaxation Rate of the Hydride Ligand in mer,trans-$ReH(CO)_3(PPh_3)_2$ by Deuteration . *Inorg. Chem.*, 30:4740–4742, 1991.

[24] F. Maseras, A. Lledos, E. Clot, and O. Eisenstein. Transition Metal Polyhydrides: From Qualitative Ideas to Reliable Computational Studies. *Chem. Rev*, 100:601–636, 2000.

[25] D.M. Heinekey and W.J. Oldham. Coordination Chemistry of Dihydrogen. *Chem. Rev.*, 93:913–926, 1993.

[26] R.H. Crabtree. Transition Metal Complexation of σ Bonds. *Angew. Chem. Int. Ed.*, 32:789–805, 1993.

[27] J.P. Perdew, J.A. Chevary, S.H. Vosko, K.A. Jackson, M.R. Pederson, D.J. Singh, and C. Fiolhais. Atoms, Molecules, Solids and Surfaces: Applications of the Generalized Gradient Approximation for Exchange and Correlation . *Phys. Rev. B*, 46:6671–6687, 1992.

[28] H.J. Monkhorst and J.D. Pack. Special Points for Brillouin-zone Integrations . *Phys. Rev. B*, 13:5188–5192, 1976.

[29] G. A. Somorjai. *Principles of Surface Chemistry*. Prentice-Hall, Englewood Cliffs, N.J., 1972.

[30] R.F.C. Farrow, D.S. Robertson, G.M. Williams, A.S. Curtis, G.R. Jones, I.M. Young, and P.N.J. Dennis. The Growth of Metastable, Heteroepitaxial Films of α-Sn by Metal Beam Epitaxy . *J. Cryst Growth*, 54:507–518, 1981.

[31] H. Höchst and I. Hernández-Calderón. Angular Resolved Photoemission of InSb(001) and Heteroepitaxial Films of α-Sn(001). *Surf. Sci.*, 126:25–31, 1983.

[32] D.P. Woodruff and K. Horn. The Surface Structure of α-Sn100 and the Effect of Hydrogen Adsorption . *Vacuum*, 33:633–637, 1983.

[33] D. P. Woodruff and K. Horn. The Surface Structure of α-Sn (100) . *Philosophical Magazine A*, 47:L5–L8, 1983.

[34] Z.Y. Lu, G.L. Chiarotti, S.Scandolo, and E. Tosatti. Atomic and Electronic Structure of Ideal and Reconstructed α-Sn (100) Surfaces. *Phys. Rev. B*, 58:13698, 1998.

[35] W. Grochala, R. Hofmann, J. Feng, and N.W. Ashcroft. The Chemical Imagination at Work in *Very* Tight Places. *Angew. Chem. Int. Ed. Engl.*, 46:3620–3642, 2007.

CHAPTER 4

SiH_x x = 4, 6, 8 from 0 - 200 GPa

4.1 Introduction: Experimental work on SiH_8

As we discussed in chapter 1, hydrogen by itself refuses to become metallic by just applying static pressure [1, 2] . The idea of using compounds already "chemically precompressed" [3], while attractive, might lead to segregation - as seen in chapter 3 - when the thermochemistry of the materials is not taken into account. But there is another way to approach our goal. Recently there has been appeared an experimental paper by Strobel et. al. [4] which studied a mixture of silane and H_2 at relatively low pressures. This chapter focuses on such mixtures, revealing particular interactions between SiH_4 and H_2.

This work is part of an ambitious overall project that our group has undertaken, to study systems of the form MH_x, where M= Si, Sn and W and x= 4, 6, 8, 10, 12, at pressures ranging from 0 - 250 GPa. In time, we will get to analyze them all. In the present chapter we study SiH_x where x= 4, 6, 8 from 0 - 200 GPa.

4.2 Methodology

For structure prediction, we use the genetic optimization algorithm developed by Oganov and Glass (USPEX) [5, 6]and implemented in the Vienna Ab Initio Simulation Package, VASP. Simulations were performed at 0, 50, 100, 150 and 200 GPa for systems with 2 formula units per unit cell. We selected the

lowest-enthalpy structures and further optimized their structures as a function of pressure using VASP and dense k-point meshes.

Density-functional theory (DFT) calculations with the Perdew-Wang exchange-correlation functional [7] were performed with Blöchl's projector-augmented wave method (PAW) and a plane wave basis set, as implemented in VASP.

For the optimization of the structures, the cell parameters, the atomic positions, and the cell volume were all allowed to relax. The stress tensor was also calculated. A defined stress was added to the stress tensor, converging towards a particular pressure. Once an optimized structure was reached, the electronic density of states per electron (DOS) was calculated. The k-point grids were generated via the Monkhorst-Pack scheme [8]. The calculations are for the ground state at 0K, and neglecting the zero-point vibrational energy. The cutoff of the kinetic energy was set at 650 eV, and for the planewaves we set a self-consistent field (SCF) tolerance of 1 x 10^{-5} eV/unit cell. The Wigner-Seitz radii was oriented along the atomic radii given in the PAW potentials.

4.3 Results

We start by analyzing the structures, showing for each histograms of the coordination environment for Si. The enthalpies of the various structures as a function of pressure will be discussed afterward. The associated DOS and partial DOS

were also calculated, and the normalized plots per valence electron are shown in their respective Appendix. All the structures shown in this chapter are visualized with program CrystalMaker, drawing bonds for Si-H distances ≤ than 1.7 Å and for bond distances H-H up to 1 Å.

4.3.1 SiH_4

Ambient pressure

USPEX was not successful in finding a reasonable structure at ambient pressure. For consistency's sake we decided, to use the lowest-enthalpy structure at 50 GPa for SiH_4 and to optimize it at P=0. We could be using our chemical intuition but we want to exclusively use the algorithm for this study. We are currently working on the optimization of this system. Figure 5.1 shows the initial structure for SiH_4. This structure is unrealistic since at ambient pressure we expect Si to have a tetrahedral coordination and for silane to be a molecular crystal [9].

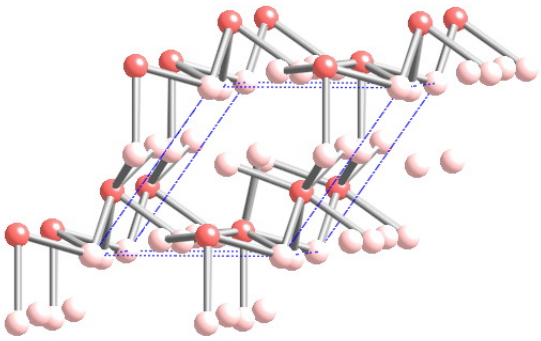

Figure 4.1: Lowest-enthalpy structure for SiH_4 at 50 GPa. This structure is unrealistic at ambient pressure; silane is expected to be a molecular crystal of SiH_4 tetrahedral molecules [9].

50 GPa

At this pressure, the Si coordination is that of a distorted octahedron, the 6 hydrogen atoms are not at equidistant as can be appreciated in the portion of the histogram. The octahedra form a network by sharing vertices, as shown in Figure 5.2. Because of the stoichiometry and coordination of the Si atom, there are no molecular hydrogen, with the closest H – H at 1.75 Å.

Layers are not a feature of this structure. It is likely that at the moderate pressure of 50 GPa, segregation has been overcome for this system or that it was not large enough to lead to the formation of layers. Also missing from it is the classical view of SiH_4 as a tetrahedral molecule, in agreement with previous work done by Feng, et. al. [9] in which they found that at this pressure regime, structures with six-fold coordination for Si atoms are favored.

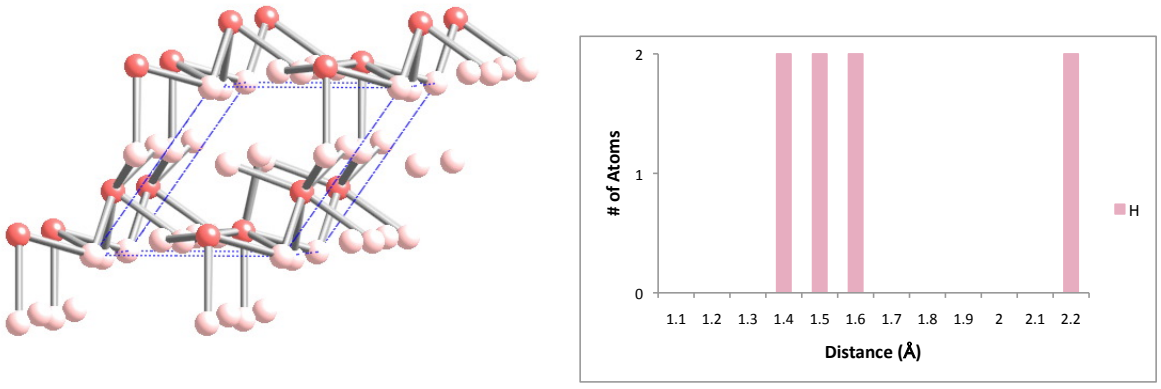

a) b)

Figure 4.2: Lowest-enthalpy structure for SiH_4 at 50 GPa a) The unit cell of the optimized system, extended in this view beyond the unit cell (dashed lines); b) Portions of distance histograms for silicon atoms in the unit cell (in pink Si-H and in red, Si-Si distances).

100 GPa

As 100 GPa pressure is applied to the system, the lowest-enthalpy structure is that shown in Figure 5.3. The coordination environment for the Si atom now is more crowded; it goes from a distorted octahedron to a distorted dodecahedron (in this chapter we will refer to dodecahedron as the polyhedron with 8 vertices). It is easy to define a Si coordination, just by looking at the histogram, Figure 5.3b, where we appreciate a large gap at 1.6 - 2.2 Å. These dodecahedrons are connected with each other not by sharing vertices but by sharing edges. Again, this results are in agreement with previous work [9, 10]; Si atoms are 8 coordinated and polymeric chains Si-H-Si are formed.

The nearest H-H distance is 1.50 Å, these hydrogens are not coordinated to the same Si atom.

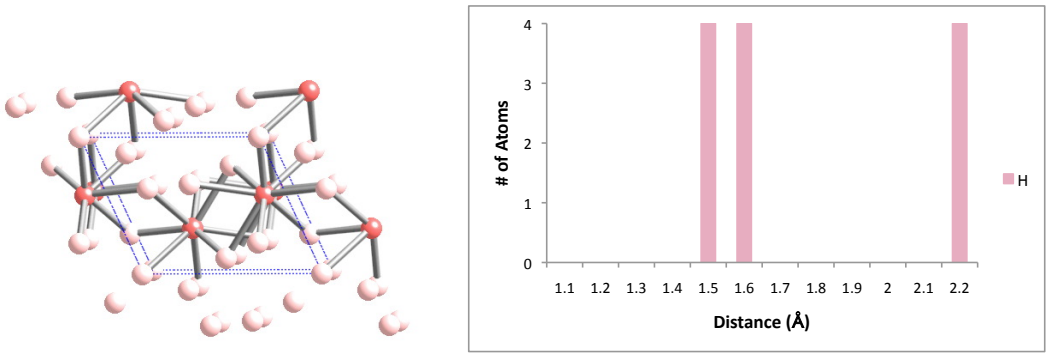

a) b)

Figure 4.3: Lowest-enthalpy structure for SiH_4 at 100 GPa a) The unit cell of the optimized system, extended in this view beyond the unit cell (dashed lines); b) Portions of distance histograms for silicon atoms in the unit cell (in pink Si-H and in red, Si-Si distances).

150 GPa

At 150 GPa, the lowest-enthalpy structure, Figure 5.4a is very much similar to the one described at 100 GPa. Si is clearly 8-coordinated to hydrogen, forming distorted dodecahedrons which share edges with their neighbors. The gap observed in the partial distance histogram, Figure 5.4b, is now from 1.5 to 2.1 Å. The closest H-H distance in this geometry is 1.47 Å, the hydrogen atoms are bonding to different Si.

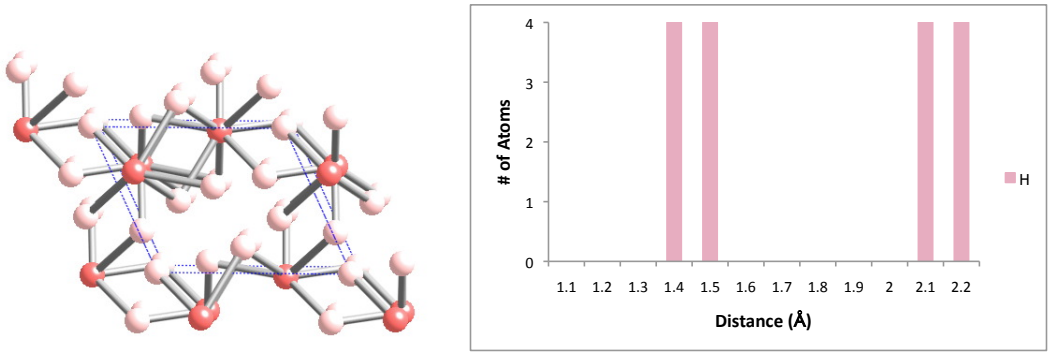

a) b)

Figure 4.4: Lowest-enthalpy structure for SiH_4 at 150 GPa a) The unit cell of the optimized system, extended in this view beyond the unit cell (dashed lines); b) Portions of distance histograms for silicon atoms in the unit cell (in pink Si-H and in red, Si-Si distances).

Throughout the remainder of our study we compare the stability of our systems not with respect to the elements but with respect to the silane structures as shown in this subsection and to molecular hydrogen in its most stable form at the given pressure, as described in chapter 1. Taking a look into our DOS, shown in the Appendix A, Silane at 150 GPa it is still not a metal. Work is being done at the moment for SiH_4 at 200 GPa.

4.3.2 SiH_6

Ambient pressure

At ambient pressure, the most stable structure for SiH_6, Figure 5.5, is clearly a molecular crystal composed of silane weakly bound with molecular hydrogen. Si is tetra-coordinated, with a Si-H bond length of 1.5 Å, and the closest H-H is 0.75 Å. Using the equalization function introduced in chapter 1, ξ = 0.108. Metallicity is not expected for this system; this is confirmed by the gap at the DOS at the Fermi level shown in Appendix B.

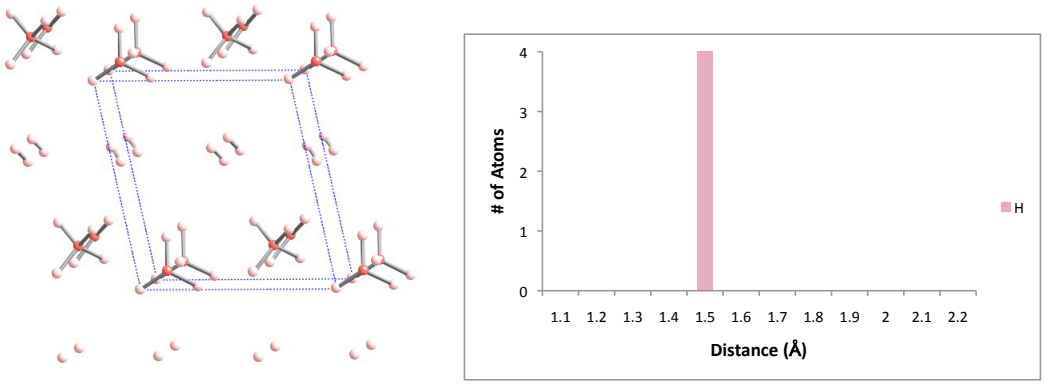

a) b)

Figure 4.5: Lowest-enthalpy structure for SiH_6 at 0 GPa a) The unit cell of the optimized system, extended in this view beyond the unit cell (dashed lines); b) Portions of distance histograms for silicon atoms in the unit cell (in pink Si-H and in red, Si-Si distances).

50 GPa

At 50 GPa, the most stable structure for SiH_6 has molecular hydrogen units, as shown in Figure 5.6. As pressure increases, so does the Si coordination. It goes from tetrahedral to distorted octahedron. The structure can be described as layers of vertex-sharing-octahedra SiH_6 and layers of molecular hydrogen. The axes of H_2 do not lie flat on the layer, however they are oriented within it.

The H-H bond length is 0.75 Å. For this system the equalization factor ξ= 0.71; pure H at this pressure has a ξ= 0.61.

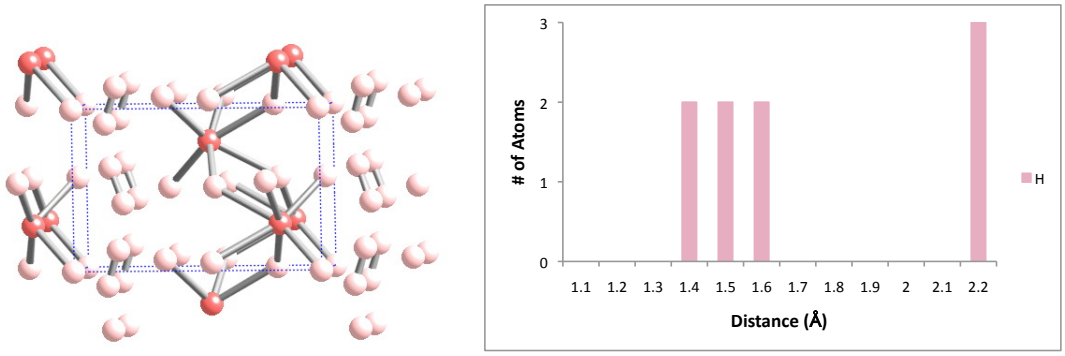

a) b)

Figure 4.6: Lowest-enthalpy structure for SiH_6 at 50 GPa a) The unit cell of the optimized system, extended in this view beyond the unit cell (dashed lines); b) Portions of distance histograms for silicon atoms in the unit cell (in pink Si-H and in red, Si-Si distances).

100 GPa

The lowest-enthalpy structure at 100 GPa is shown in Figure 5.7. Every Si has 6 neighboring hydrogen atoms, with a coordination polyhedron that is a distorted octahedron. But it is difficult to see a clear cut-off for Si-H distances, if one wants to define a coordination number. Within this geometry there are H_2 molecules with bond length 0.75 Å.This structure can be seen as layered; octahedra share edges forming 2-D sheets with layers of H_2 molecules.

The calculated equalization factor for this structure is ξ = 0.73 roughly the same as pure H_2 at 100 GPa which is ξ = 0.72.

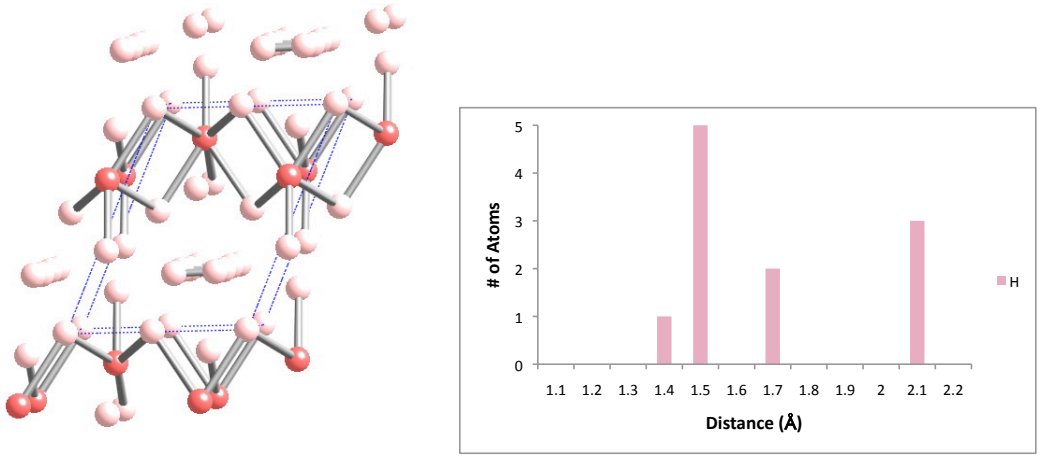

a) b)

Figure 4.7: Lowest-enthalpy structure for SiH_6 at 100 GPa a) The unit cell of the optimized system, extended in this view beyond the unit cell (dashed lines); b) Portions of distance histograms for silicon atoms in the unit cell (in pink Si-H and in red, Si-Si distances).

150 GPa

Si at 150 GPa has a coordination number of 8, Figure 5.8, There are H_2 units within the system. These hydrogen molecules have a bond length of 0.75 Å and their axes lie mostly flat on the layer.

For this system the equalization factor is ξ= 0.76.

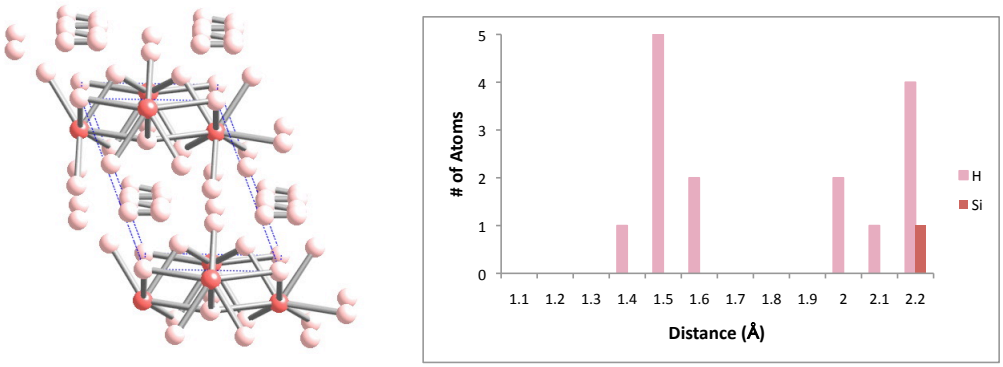

a) b)

Figure 4.8: Lowest-enthalpy structure for SiH_6 at 150 GPa a) The unit cell of the optimized system, extended in this view beyond the unit cell (dashed lines); b) Portions of distance histograms for silicon atoms in the unit cell (in pink Si-H and in red, Si-Si distances).

200 GPa

The lowest-enthalpy structure at 200 GPa is shown in Figure 5.9. Every Si has 8 neighbors hydrogen atoms, with a coordination polyhedron of a distorted do-decahedron. Within this geometry there are H_2 molecules with bond length 0.75 Å.This structure can be seen as layered; octahedra share edges forming sheets of polyhedra in-between layers of H_2. The calculated equalization factor for this structure is $\xi = 0.74$.

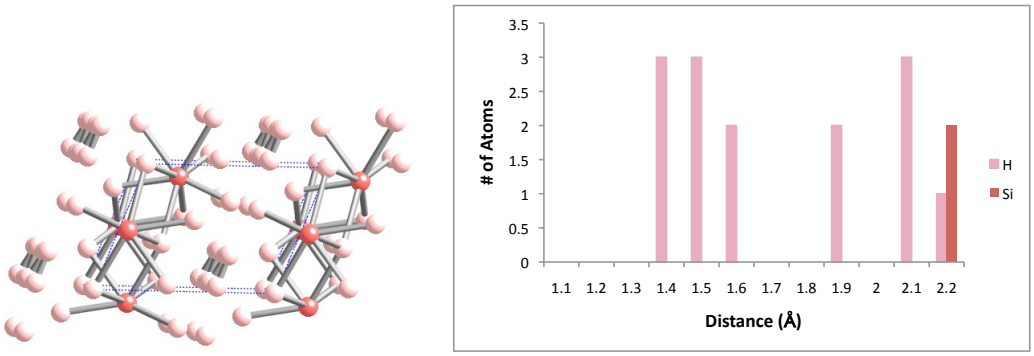

a) b)

Figure 4.9: Lowest-enthalpy structure for SiH_6 at 200 GPa a) The unit cell of the optimized system, extended in this view beyond the unit cell (dashed lines); b) Portions of distance histograms for silicon atoms in the unit cell (in pink Si-H and in red, Si-Si distances).

Throughout the range of pressures considered for the SiH_6 system, layers of H_2 units are a feature in the geometry of the structure. The coordination of Si atoms in the lattice increases with pressure, but the coordination polyhedra arrange themselves in 2-D structures.The equalization factor ξ seem to converge to a value of 0.7 which is reached at 50 GPa.

4.3.3 SiH_8

Ambient pressure

At P= 1 atm, the most stable structure for SiH_8, Figure 5.10, just as it was for SiH_6, can be considered as a molecular crystal composed of silane and molecular hydrogen. Si has 4 neighbors H, in a tetrahedral arrangement, with a Si-H bond length of 1.5 Å, and the closest H-H is 0.75 Å. Using the equalization function introduced in chapter 1, ξ = 0.17. This weakly-bonded van der Waals complex is not a metal; its large gap in the DOS at the Fermi level is shown in Appendix C.

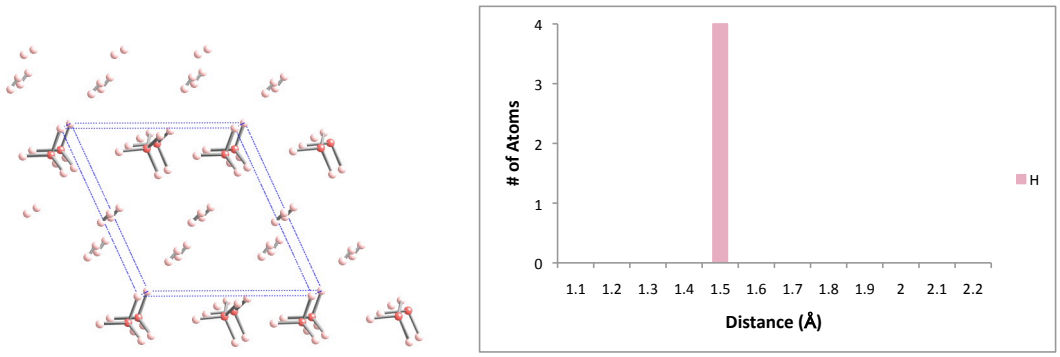

a) b)

Figure 4.10: Lowest-enthalpy structure for SiH_8 at 0 GPa a) The unit cell of the optimized system, extended in this view beyond the unit cell (dashed lines); b) Portions of distance histograms for silicon atoms in the unit cell (in pink Si-H and in red, Si-Si distances).

50 GPa

At 50 GPa, the lowest-enthalpy structure for SiH_8 has molecular hydrogen units, as shown in Figure 5.11. Si has a distorted octahedra coordination. The structure can be described as layers of vertex-sharing-octahedra SiH_6 and layers of molecular hydrogen. The coordination of Si is similar to that of Silane, and SiH_6 at this pressure.

The H-H bond length is 0.75 Å. For this system the equalization factor ξ= 0.68, pure H at this pressure has a ξ= 0.6.

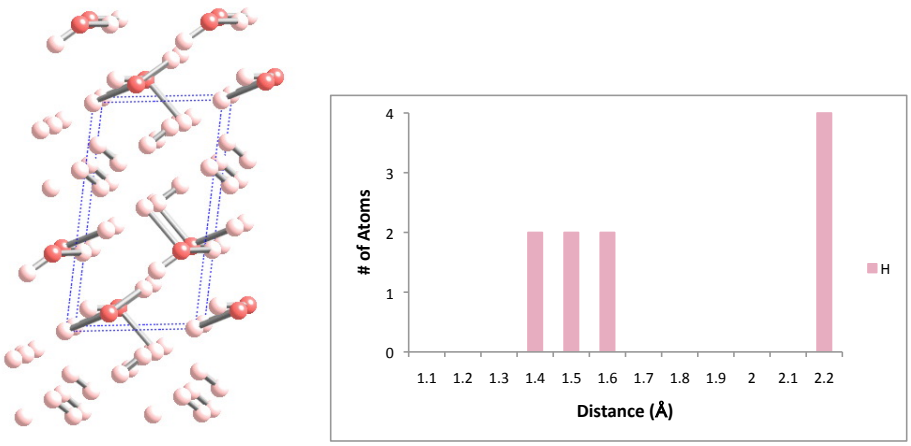

a) b)

Figure 4.11: Lowest-enthalpy structure for SiH_8 at 50 GPa a) The unit cell of the optimized system, extended in this view beyond the unit cell (dashed lines); b) Portions of distance histograms for silicon atoms in the unit cell (in pink Si-H and in red, Si-Si distances).

100 GPa

The lowest-enthalpy structure at 100 GPa is shown in Figure 5.12. Every Si has 8 neighboring hydrogen atoms, with a coordination polyhedron of a distorted dodecahedron. There is clear cut-off in the histogram, Figure 5.11b, at 1.6 Å Within this symmetry there are 2 H_2 in the unit cell with bond length 0.75 Å. Two more H_2 units have a longer separation of 0.81 Å, with one of the H atoms bonding to a Si atom (Si-H separation of 1.66 Å) This structure can be seen as layered; dodecahedra share edges forming sheets between layers of H_2 units.

The calculated equalization factor for this structure is $\xi = 0.77$, pure H_2 at 100 GPa which is $\xi = 0.72$.

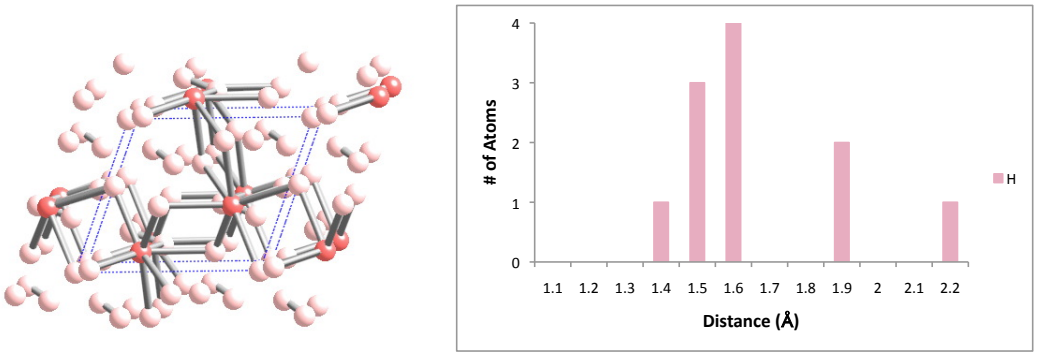

a) b)

Figure 4.12: Lowest-enthalpy structure for SiH_8 at 100 GPa a) The unit cell of the optimized system, extended in this view beyond the unit cell (dashed lines); b) Portions of distance histograms for silicon atoms in the unit cell (in pink Si-H and in red, Si-Si distances).

150 GPa

Si at 150 GPa has a coordination number of 10, as Figure 5.13 shows. Still, there are H_2 units within the system. The structure can be considered as being made out of layers, the polyhedra form sheet by sharing edges, between layers of H_2. These hydrogen molecules have a bond length of 0.75 Å and their axes are oriented within the layer.

For this system the equalization factor is ξ= 0.77.

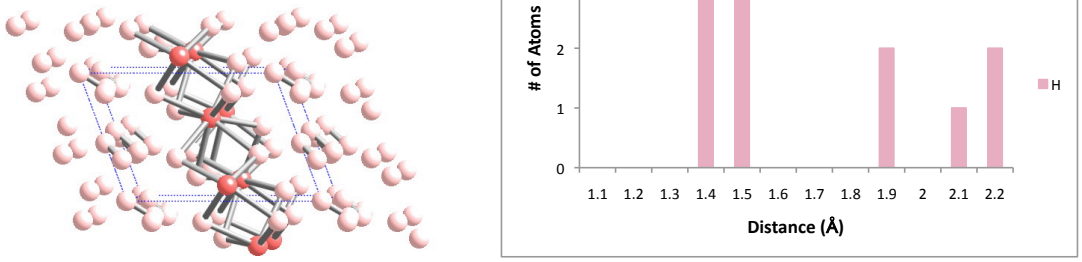

a) b)

Figure 4.13: Lowest-enthalpy structure for SiH_8 at 150 GPa a) The unit cell of the optimized system, extended in this view beyond the unit cell (dashed lines); b) Portions of distance histograms for silicon atoms in the unit cell (in pink Si-H and in red, Si-Si distances).

200 GPa

The lowest-enthalpy structure at 200 GPa is shown in Figure 5.14. Every Si has coordination number of 8, with a coordination polyhedron of a distorted dodecahedron. This structure can be seen as layered; octahedra share edges forming 2-D networks of polyhedra in between layers of H_2, with bond length 0.75 Å. The calculated equalization factor for this structure is $\xi = 0.88$.

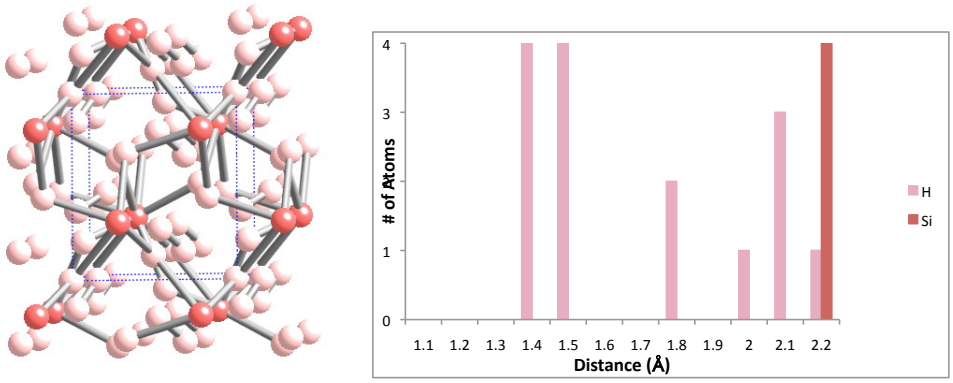

a) b)

Figure 4.14: Lowest-enthalpy structure for SiH_8 at 200 GPa a) The unit cell of the optimized system, extended in this view beyond the unit cell (dashed lines); b) Portions of distance histograms for silicon atoms in the unit cell (in pink Si-H and in red, Si-Si distances). .

At all the pressures considered, there are layers of H_2 in the optimized structures. The Si coordination numbers go up but, polyhedra connect to form 2-D networks. The band-gap starts to close at 150 GPa, but the DOS at the Fermi level is not significant.

4.3.4 Energetics

Figure 5.15 shows the enthalpies of formation for the systems discussed above. It is clear that SiH_4 is more stable than the other systems at the pressure range considered. However the scale for the enthalpy is of formation is arguably small. the largest difference between the systems is of the order of 0.4 eV/SiH_x.

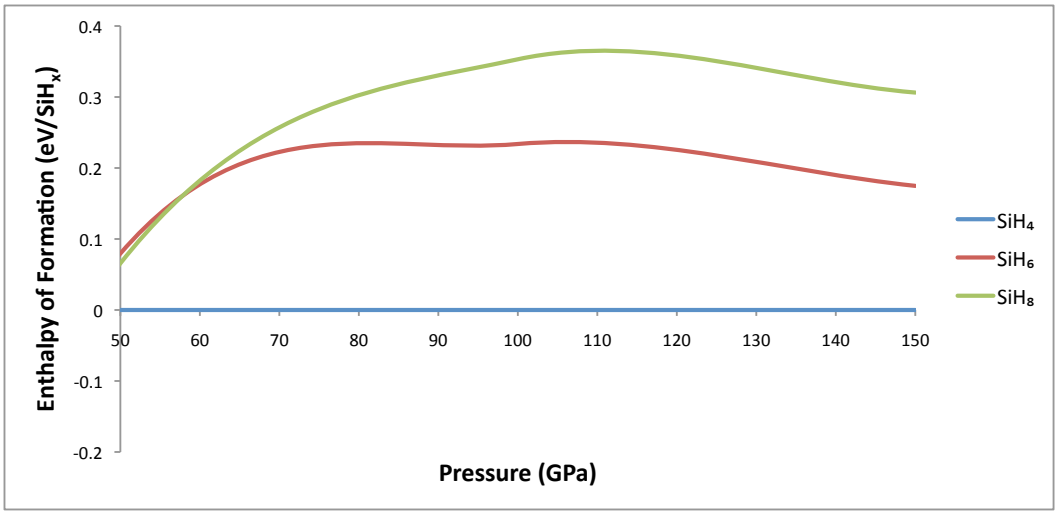

Figure 4.15: Stabilities for the SiH_x, where x= 4, 6, 8 from 50-150 GPa, SiH_4 and H_2 are used as a reference.

4.4 Conclusions

For our systems studied, we found structures in which there is a new segregation, the material is segregating into compounds; silane and molecular hydrogen. At the range pressure considered in this chapter we are not yet finding metallicity. It is clear that higher pressures need to be considered to complete our study.

BIBLIOGRAPHY

[1] C. Narayana, H. Luo, J. Orloff, and A.L. Ruoff. Solid Hydrogen at 342 GPa, No Evidence for an Alkali Metal. *Nature*, 393:46–49, 1998.

[2] P. Loubeyre, F. Occelli, and R. LeToullec. Optical Studies of Solid Hydrogen to 320 GPa and Evidence for Black Hydrogen. *Nature*, 416:613–617, 2002.

[3] N. W. Ashcroft. Hydogen Dominan Metallic Alloys: High Temperature Superconductors? *Phys. Rev. Lett.*, 92:187002, 2004.

[4] T.A. Strobel, M. Somayazulu, and R.J. Hemley. Novel Pressure-Induced Interactions in Silane-Hydrogen. *Phys. Rev. Lett.*, 103:065701, 2009.

[5] C.W. Glass and A.R. Oganov. USPEX-Evolutionary Crystal Structure Prediction. *Comput. Phys. Commun.*, 175:713–720, 2006.

[6] A.R. Oganov and C.W. Glass. Crystal Structure and Prediction Using Ab Initio Evolutionary Techniques: Principles and Applications. *J. Chem. Phys.*, 124:244704, 2006.

[7] J.P. Perdew, J.A. Chevary, S.H. Vosko, K.A. Jackson, M.R. Pederson, D.J. Singh, and C. Fiolhais. Atoms, Molecules, Solids and Surfaces: Applications of the Generalized Gradient Approximation for Exchange and Correlation. *Phys. Rev. B*, 46:6671–6687, 1992.

[8] H.J. Monkhorst and J.D. Pack. Special Points for Brillouin-zone Integrations. *Phys. Rev. B*, 13:5188–5192, 1976.

[9] J. Feng, W. Grochala, T. Jaron, R. Hoffmann, A. Bergara, and N.W. Ashcroft. Structures and Potential Superconductivity in SiH_4 at High Pressure: En Route to "Metallic Hydrogen" . *Phys. REv. Lett.*, 2006:017006, 96.

[10] M. Martinez-Canales, A. R.Oganov, Y. Ma, Y. Yan, A.O. Lyakhov, and A. Bergara. Novel Structures and Superconductivity of Silane under Pressure. *Phys. Rev. Lett.*, 102:087005, 2009.

[11] X-J. Chen, V.V. Struzhkin, Y. Song, A.F. Goncharov, S. Liu M. Ahart, H k. Mao, and R.J. Hemley. Pressure-Induced Metallization of Silane . *Proc. Natl. Acad. Sci. USA*, 105:20–23, 2008.

CHAPTER 5

Lithium, Beryllium and Hydrogen: Metallization By Impurities

5.1 Introduction: LiBe at 80 GPa

Be is the 4^{th} element in the Periodic Table and the head of the alkaline earth metal group. Under ambient conditions Be is unreactive to water and air [1]. It has the highest Debye temperature(Θ_D), and one of the highest melting points among metals, as well as a low superconducting transition temperature, T_C= 26 mK.

If one is interested in increasing the T_C of a system, one strategy is to form alloys in such a way as to increase the density of electronic states at the Fermi level. The guiding idea here is BCS theory, which yields in its most simplified form an expression for $T_C = 1.13\Theta_D \exp[-1/N_F V]$ where N_F is the density of states at the Fermi levels.

Beryllium and lithium do not form either a stoichiometric compound or a random ordered alloy at ambient conditions [2, 3]. High pressures have a considerable effect on electronic structure, reactivity, and compound formation. Compounds that at ambient conditions are not likely to form, may do so under pressure [4–6]. It was in this spirit that alloys of two unlikely elements were studied under pressure by Feng et.al [7]; lithium and beryllium. They found that Li and Be indeed form a number of stable alloys. It is one of those alloys,

LiBe, that is of great interest to us in this chapter.

The computed optimum structure of LiBe at 80 GPa has a space group $P2_1/m$. It can be described as a "layered" structure, as indicated in Figure 5.1. However, the distances within and between the layers (~ 2 Å at this pressure) are comparable, so that structurally LiBe is three dimensional. Remarkably the Density of States (DOS) of the system, Figure 5.2, shows a step-like shape, which is characteristic of 2D-systems. The origins of this two-dimensional electronic structure in a three-dimensional compound are explored in the paper of Feng et. al. [7]

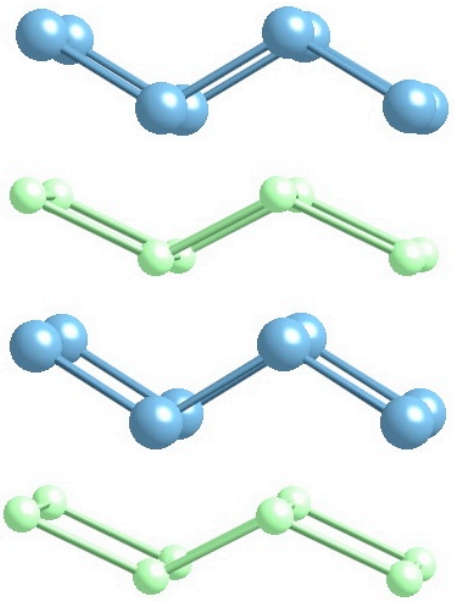

Figure 5.1: Extended structure of LiBe at 86.7 GPa. In this pictures, and from now on, Li atoms are depicted in blue and Be are shown in green.

How can we further increase the DOS at the Fermi level? In other words,

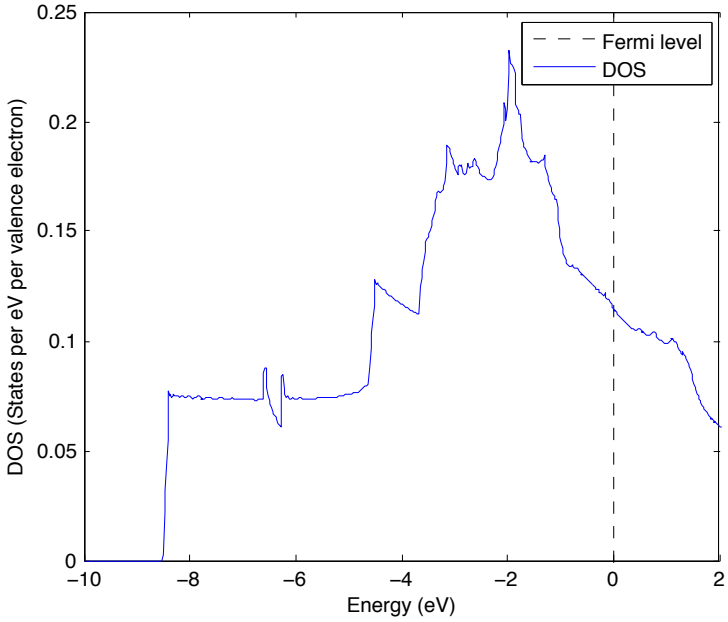

Figure 5.2: DOS for LiBe at 86.7 GPa. DOS plot is normalized to the number of valence electrons of the system and Fermi level is set to zero. Note the step-like shape at around -9 eV, which is characteristic of 2-D systems.

can we enhance metallic behavior in this alloy? As the DOS of Figure 5.2 shows, one way to effectively achieve this is by reducing the number of valence electrons while keeping the overall structure. Lithium has only one valence electron while Beryllium has two. If we wish to reduce the number of valence electrons, it makes sense to replace some atoms of Be by atoms with one valence electron. Hydrogen could be a reasonable substitute for Be. We are not interested in reducing the number of valence electrons in a dramatic way, only to reach a higher DOS region in Figure 5.2. In this way we were led to consider Li_8Be_7H and $Li_{16}Be_{15}H$.

5.2 Methodology

Density-functional theory (DFT) calculations with the Perdew-Wang exchange-correlation functional [8] were performed with Blöchl's projector-augmented wave method (PAW) and a plane wave basis set, as implemented in the Vienna Ab Initio Simulation Package (VASP). Given the size of the atoms involved in the calculations, we included all the electrons.

For the optimization of the structures, the cell parameters, the atomic positions, and the cell volume were all allowed to relax. The stress tensor was also calculated. A defined stress was added to the stress tensor, converging towards a particular pressure. Once an optimized structure was reached, the electronic density of states per electron (DOS) was calculated. The k-point grids were generated via the Monkhorst-Pack scheme [9]. The calculations are for the ground state at 0K, and neglecting the zero-point vibrational energy. The cutoff of the kinetic energy was set at 650 eV, and for the planewaves we set a self-consistent field (SCF) tolerance of 1 x 10^{-5} eV/unit cell. The Wigner-Seitz radii was oriented along the atomic radii given in the PAW potentials.

For structure prediction, we use the genetic optimization algorithm developed by Oganov and Glass (USPEX) and implemented with VASP [10, 11]. Simulations were performed at 40, 60, 80 and 100 GPa for systems with 16 atoms per unit cell. (LiBe: Z=4; Li_4Be_3H:Z=2; Li_8Be_7H:Z=1; Z= number of formula units by unit cell). We selected the lowest-enthalpy structures and further optimized their structures as a function of pressure using VASP and dense k-point meshes.

5.3 Results

What structure might these Be-Li-H alloys have? In this study we considered two approaches: (1) Starting with the LiBe structure studied by Feng et.al. at 86.7 GPa, we constructed super-cells with the desired stoichiometry, substituting a Be atom by a H. (2) Alternatively, we made use of structure prediction algorithms, such as USPEX, for the endeavor. We set up these numerical experiments for stoichiometries Li_4Be_3H and, Li_8Be_7H at 40, 60, 80 and 100 GPa.

While searching for new structures we were particularly interested in analyzing if indeed metallicity was enhanced by swapping H for Be. The following questions arise; Where is hydrogen going to be within the structures? Are layers going to remain structurally and electronically an important feature in our most stable structures?

5.3.1 LiBe block units as starting points

Supercells without Optimization

Using an optimized unit cell of LiBe at P= 86.7 GPa with Z = 2 as a unit block four supercells were created: three supercells with Z= 8 (the supercells were built by taking $1\times2\times2$, $2\times1\times2$ and, $2\times2\times1$ times the unit block), and a larger

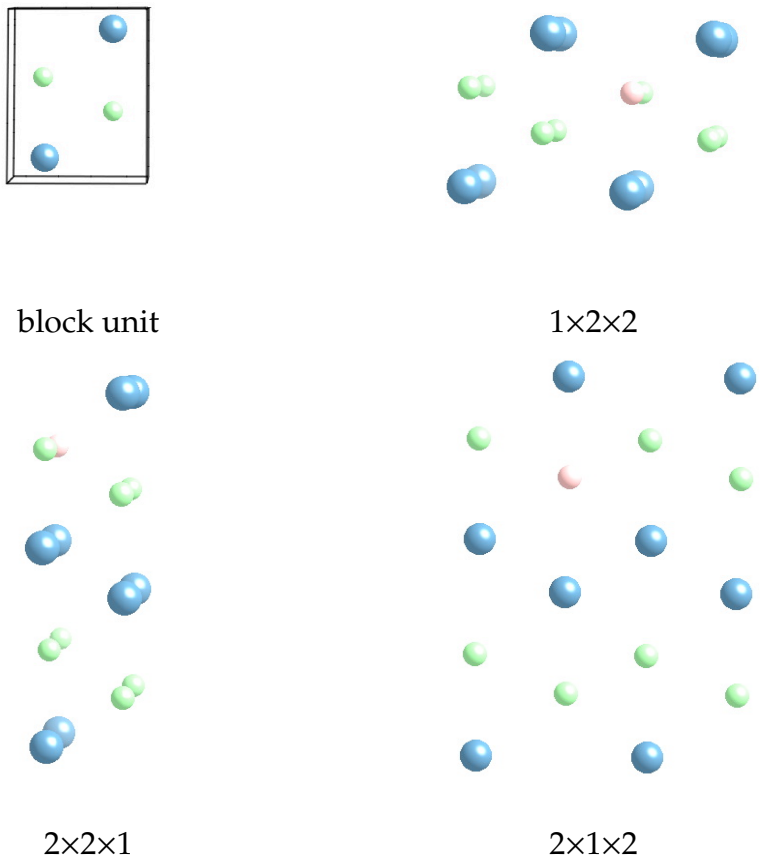

Figure 5.3: Structures of the unit cell used as a block unit and the different systems with stoichiometry Li_8Be_7H . On top, from left to right, the unit cell with Z=2 of LiBe, next the system built from 1×2×2 times the unit cell. On the bottom, the supercells created from $2 \times 2 \times 1$ and $2 \times 1 \times 2$ times the block unit. Note that one Be atom (in green) was replaced by an atom of H (in pink).

supercell with Z =16 ($2 \times 2 \times 2$ times the unit block).

One atom of Be was then replaced by one atom of H in the four supercells. The LiBe block unit cell and the supercells of stoichiometry Li_8Be_7H are shown in Figure 5.3.

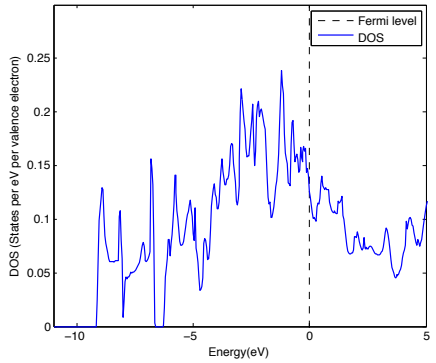

$1\times 2\times 2$

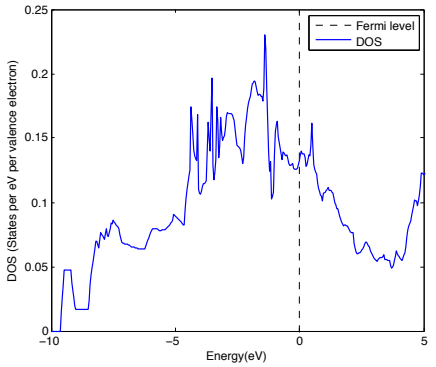

$2\times 1\times 2$

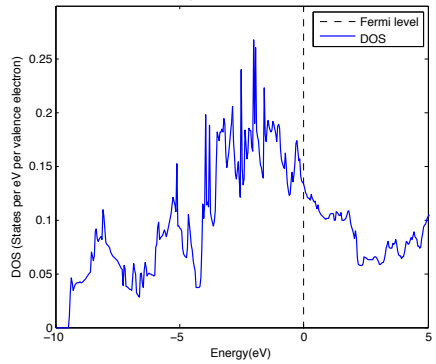

$2\times 2\times 1$

Figure 5.4: Normalized DOS for Li_8Be_7H for non-optimized super-cells as shown in Figure 5.3.

The DOS curves of the above systems (without further relaxation of ions) were also calculated, shown in Figure 5.4. The system Li_8Be_7H, built from the $1\times 2\times 2$ supercell of LiBe, shows an increase of the DOS at the Fermi level. The shape of the DOS no longer shows the characteristic features of a 2-D system

(the rectangular onset) but that of a 1-D system, with Van Hove singularities. The DOS for the Li_8Be_7H structures built from the $2 \times 1 \times 2$ and $2 \times 2 \times 1$ unit block without relaxation of ions still show a step-like shape, more pronounced in the latter case. The three systems with formula Li_8Be_7H are characterized by the same external pressure (as could be expected; having the same stoichiometry and cell volume), but their DOS curves differ substantially.

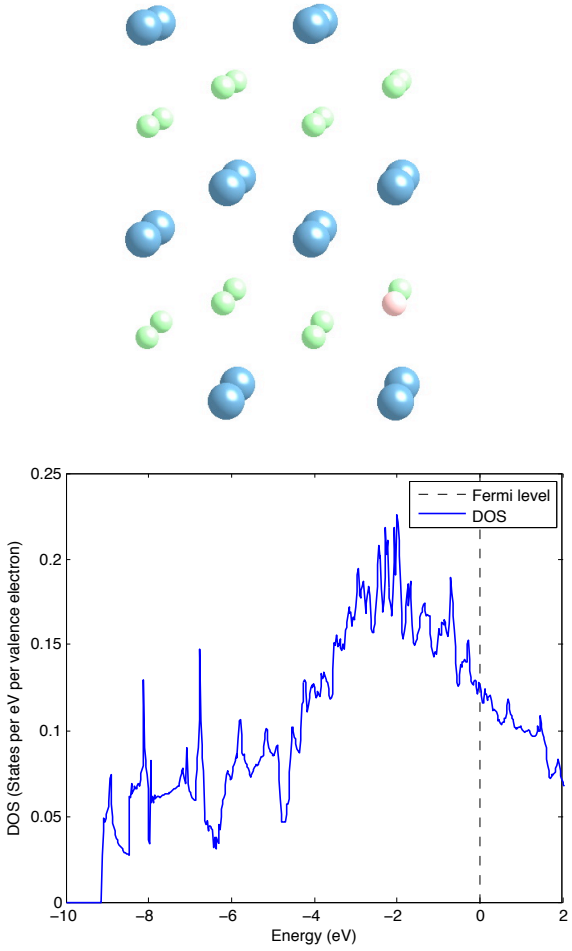

Figure 5.5: Structure and normalized DOS of supercell $Li_{16}Be_{15}H$.

For the larger supercell that leads to $Li_{16}Be_{15}H$, Figure 5.5, we can still notice a step-like shape of the DOS. For this system the pressure is larger than those of

the Li_8Be_7H structures, since the hydrogen atom has a lesser effect on the overall system. DOS calculations were performed without allowing relaxation of ions. The DOS at the Fermi energy is also higher than in the original LiBe case (Figure 5.5).

Some results are summarized on Table 5.1. The DOS at the Fermi energy is normalized per valence electron and, the total energy of the system is normalized by the total volume of each system, so as to allow a rough comparison of structures of different stoichiometry.

We notice from the table that the pressures are different in each systems. The pressures of the supercells calculated are lower than that of the original LiBe cell because initially we allowed neither a relaxation of ions nor a change in the total volume of the system upon substituting a H for a Be.

Table 5.1: Energetics for non-optimized supercells.

System	DOS at the Fermi level per valence electron (eV^{-1})	Pressure (GPa)	Volume $Å^3$	Energy (eV / $Å^3$)
LiBe	0.1042	86.7	24.29	-0.2615
Li_8Be_7H-$1 \times 2 \times 2$	0.1536	75.1	97.16	-0.2881
Li_8Be_7H-$2 \times 1 \times 2$	0.1195	75.2	97.17	-0.2928
Li_8Be_7H-$2 \times 2 \times 1$	0.1248	75.1	97.16	-0.2878
$Li_{16}Be_{15}H$-$2 \times 2 \times 2$	0.1265	78.6	194.34	-0.295

Optimization of super-cells

After geometrical optimization the structures are very different from their simple substitution starting point. The H atom in general moves away from Be layers in the cell towards the closest layer of Li atoms. This movement distorts distances and positions among the Li layer as the H approaches it. In contrast to this movement Be layers remains relatively unaltered, Figure 5.6.

We were also interested in looking at the distances between H atoms (see chapter 1). However the closest H$\cdots$H was of 1.99 Å (on the system which came from $2 \times 1 \times 2$ cell); one assumes that the small hydrogen concentration is responsible for the absence of direct HH bonding.

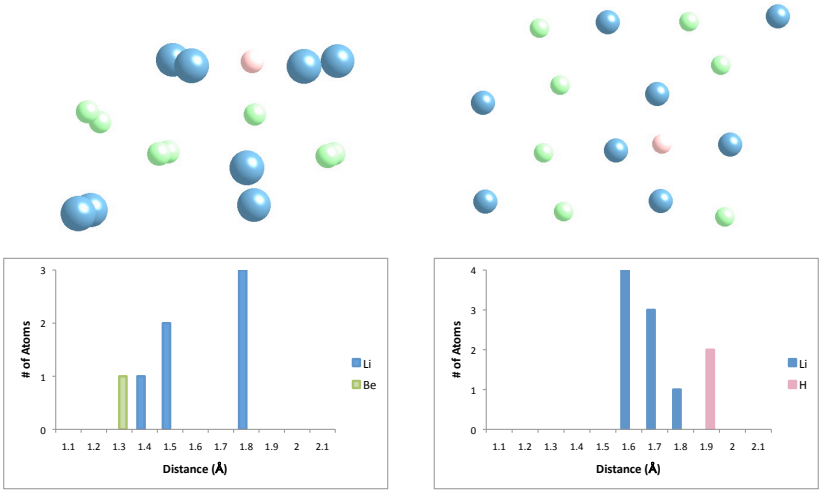

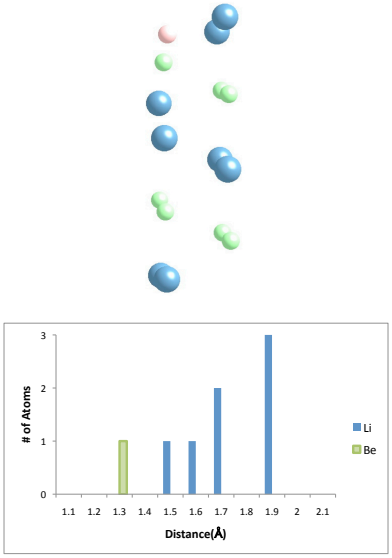

Figure 5.6: Structures and histograms of Li_8Be_7H after optimization of supercell structures at 86.7 GPa. The coordination of the hydrogen is shown in portions of distance histograms (in blue, distances from the reference H to lithium; in green to beryllium; and in pink to another hydrogen).

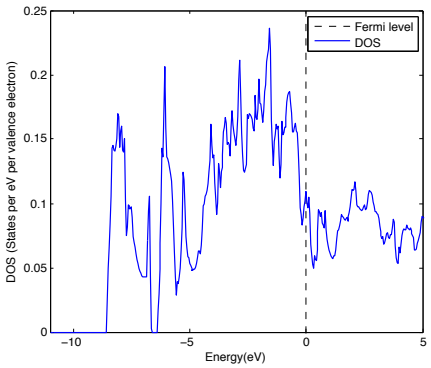

1×2×2 supercell

a)

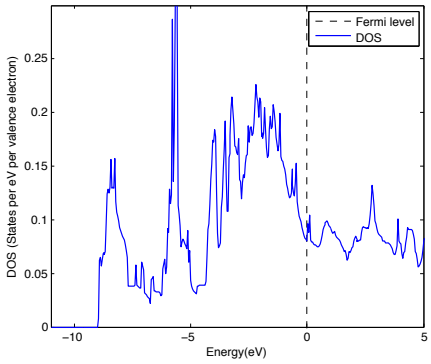

2×2×1 supercell

b)

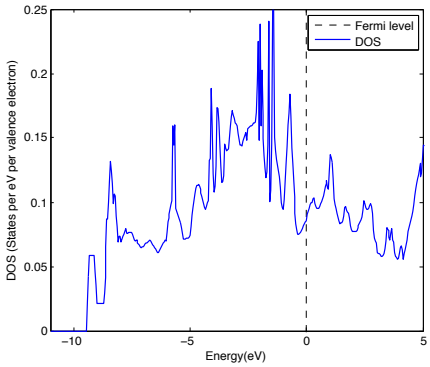

2×1×2 supercell

c)

Figure 5.7: Normalized DOS for the Li_8Be_7H supercell structures optimized at 86.7 GPa.

The DOS were calculated, Figure 5.7, and the results are summarized in Table 5.2. The DOS at the Fermi level are normalized by the number of valence

Table 5.2: Energetics for optimized supercells.

System	DOS at Fermi level per valence electron (eV^{-1})	Pressure (GPa)	Volume $Å^3$	Energy (eV / $Å^3$)
LiBe	0.1042	86.7	24.29	-0.2615
Li_8Be_7H-1 $\times$ 2 $\times$ 2	0.1482	87.6	92.86	-0.306
Li_8Be_7H-2 $\times$ 1 $\times$ 2	0.09	87.8	92.75	-0.304
Li_8Be_7H-2 $\times$ 2 $\times$ 1	0.085	87.7	92.88	-0.2952

electrons and, the total energy of the system by the total volume of each system.

After the relaxation of atoms, we obtained a smaller value for the DOS at the Fermi level. The $1 \times 2 \times 2$ cell has the largest DOS at the Fermi level among the three structures

5.3.2 Random Algorithm Search

We recalculated the LiBe structure with the genetic structure-searching program USPEX [10, 11] as a way to gauge the effectiveness of the algorithm. We were interested in the system at P = 80 GPa, but considered that a larger pressure range was needed to analyze in depth the role of H as in impurity and as a potential enhancer of metallicity for the alloy. The pressures studied were 40, 60, 80 and 100 GPa. We proceeded in the same way as described above for Li_8Be_7H, but we also considered a system with a different stoichiometry: Li_4Be_3H, in

which hydrogen has a stronger presence as an impurity.

LiBe

This stoiciometry was a tet of the methodology, for while LiBe had been considered previously, Ji Feng had not used an evolutionary algorithm in his structure search. We set up our random search, considering 16 atoms total per unit cell, 8 of them Be and 8 Li. The optimized structures are shown in Figure 5.8. In all cases the structure show a "layered" nature, but this may be a prejudice of our visualization program. At 80 GPa we got the same structure found previously by Feng [7]. The distances within and between the layers (~ 2 Å at this pressure) are comparable, therefore LiBe is structurally three dimensional.

Table 5.3: Energetics for LiBe cells found with USPEX

Pressure	DOS at Fermi level per valence electron	Volume	Energy
(GPa)	(eV^{-1})	$Å^3$	(eV / $Å^3$)
40	0.107	117.0	-0.196
60	0.100	106.2	-0.298
80	0.101	98.0	-0.305
100	0.106	91.6	-0.2877

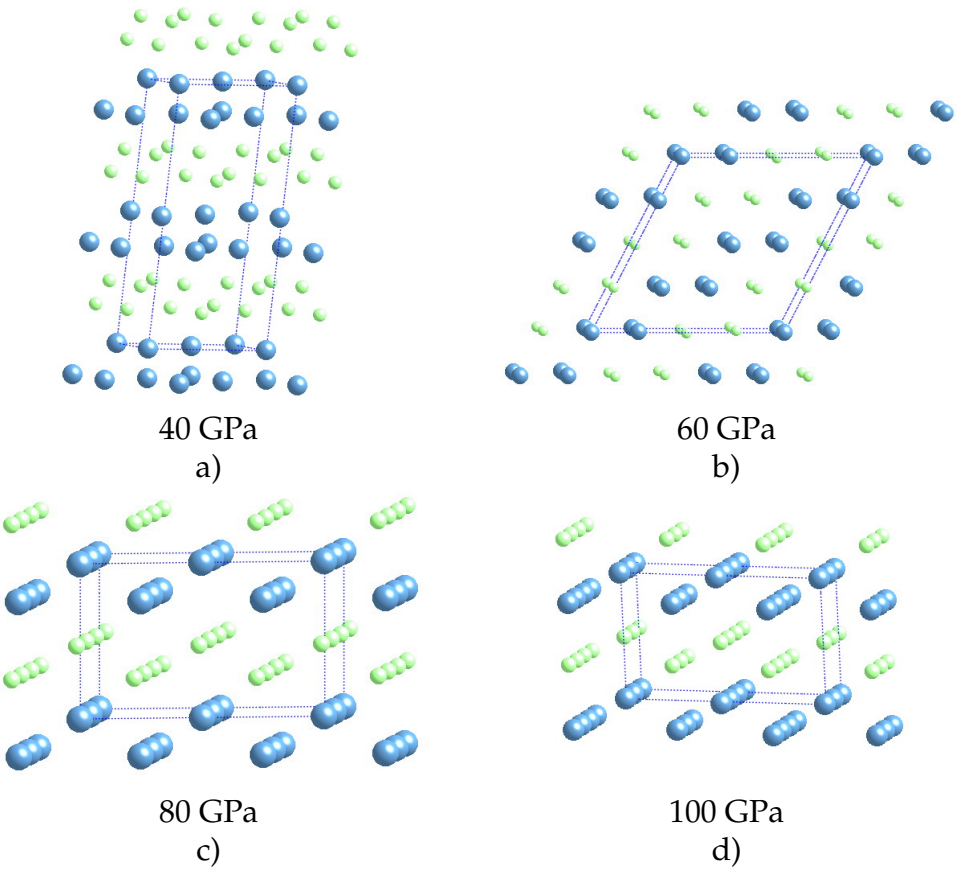

Figure 5.8: The lowest -enthalpy structures for LiBe found with USPEX.

The calculated DOS also shown resembles the ones found by Feng et. al. [7]. The step like functions in the DOS are present at the different pressures considered, as shown in Figure 5.9.

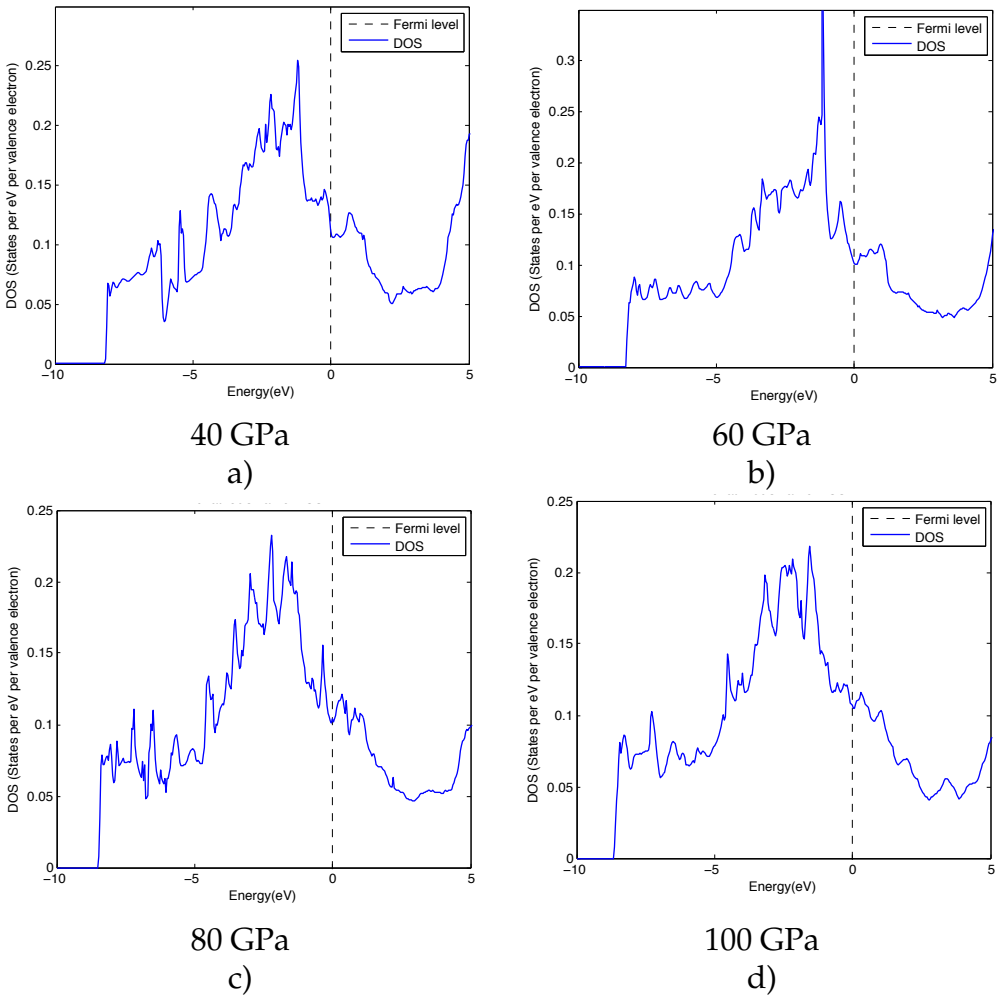

Figure 5.9: Normalized DOS for the LiBe structures found with USPEX.

DOS values at the Fermi level along with volume and energy data are listed in Table 5.3

Li_8Be_7H

The optimized structures of the alloy with composition Li_8Be_7H are shown in Figure 5.10. The distance histograms for the coordination environment surrounding the hydrogen atom are in Figure 5.11. Histograms show that as pressure increases the coordination also increases, as expected [12].

The DOS were calculated, Figure 5.12, and the results are summarized in Table 5.4.

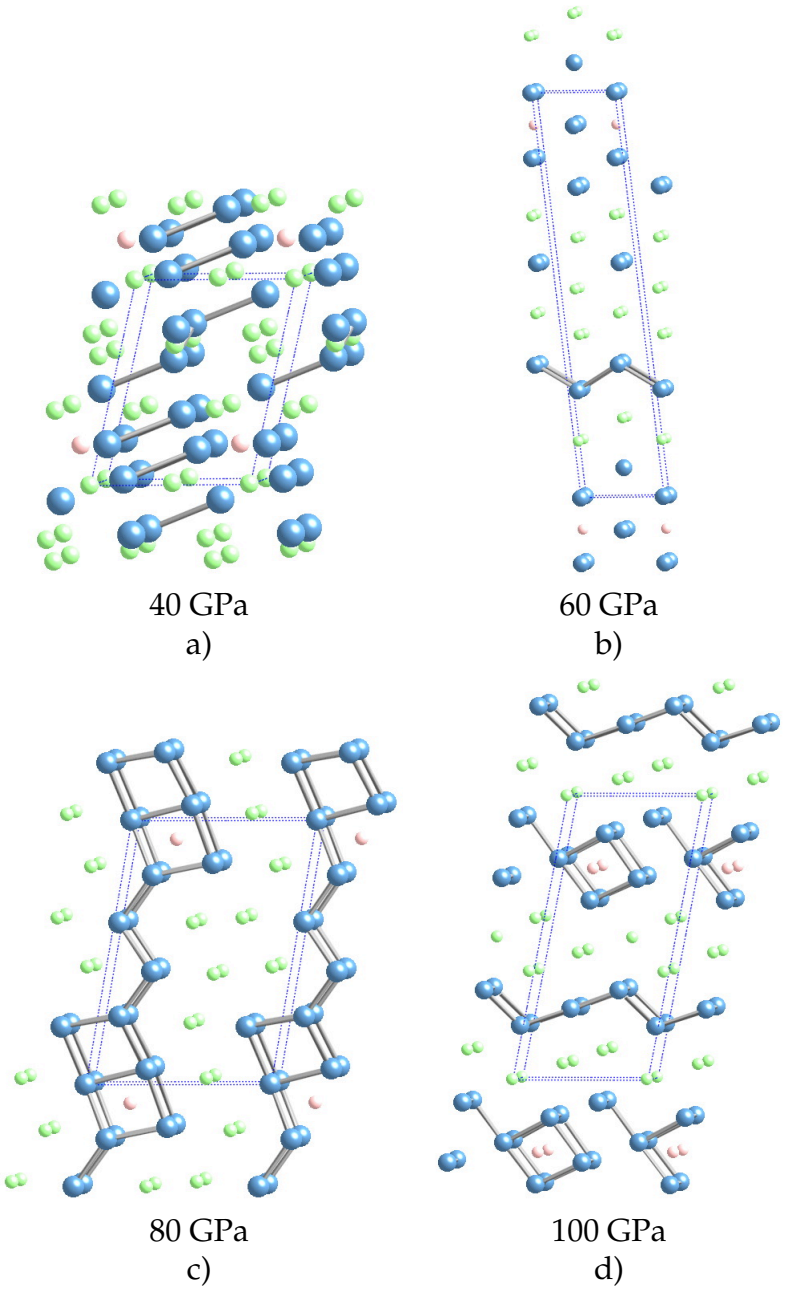

40 GPa
a)

60 GPa
b)

80 GPa
c)

100 GPa
d)

Figure 5.10: The lowest-enthalpy structures for Li_8Be_7H found by USPEX.

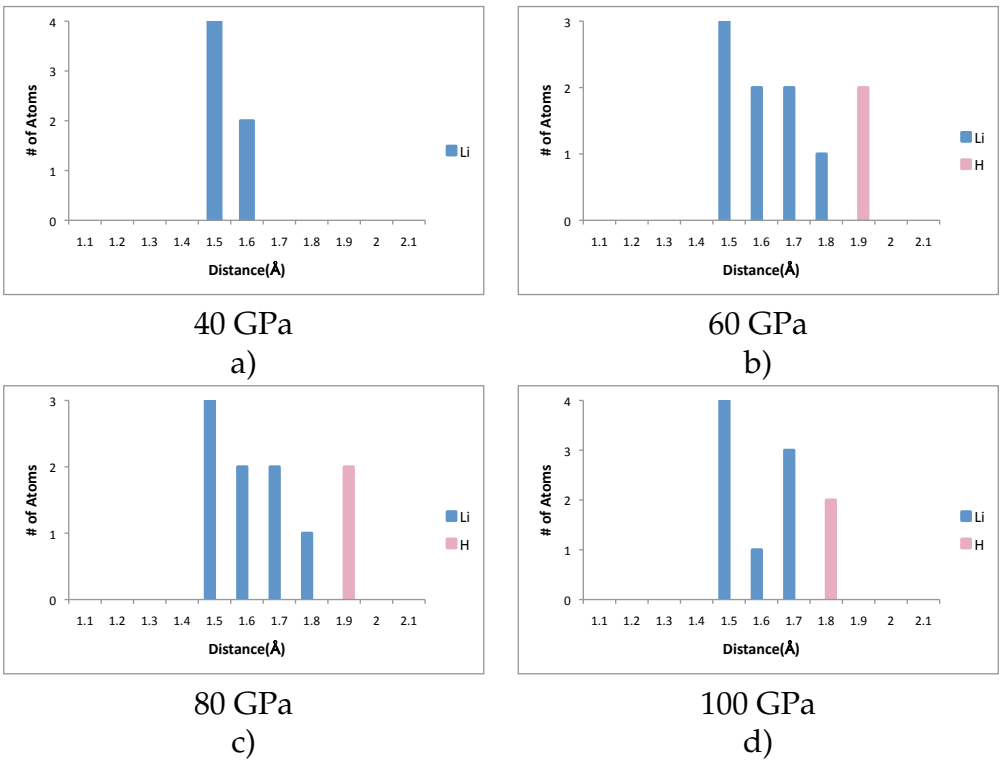

Figure 5.11: Histograms for the lowest-enthalpy structures for Li_8Be_7H found by USPEX. The coordination of the hydrogen is shown in portions of distance histograms (in blue, distances from the reference H to lithium; in green to beryllium; and in pink to another hydrogen).

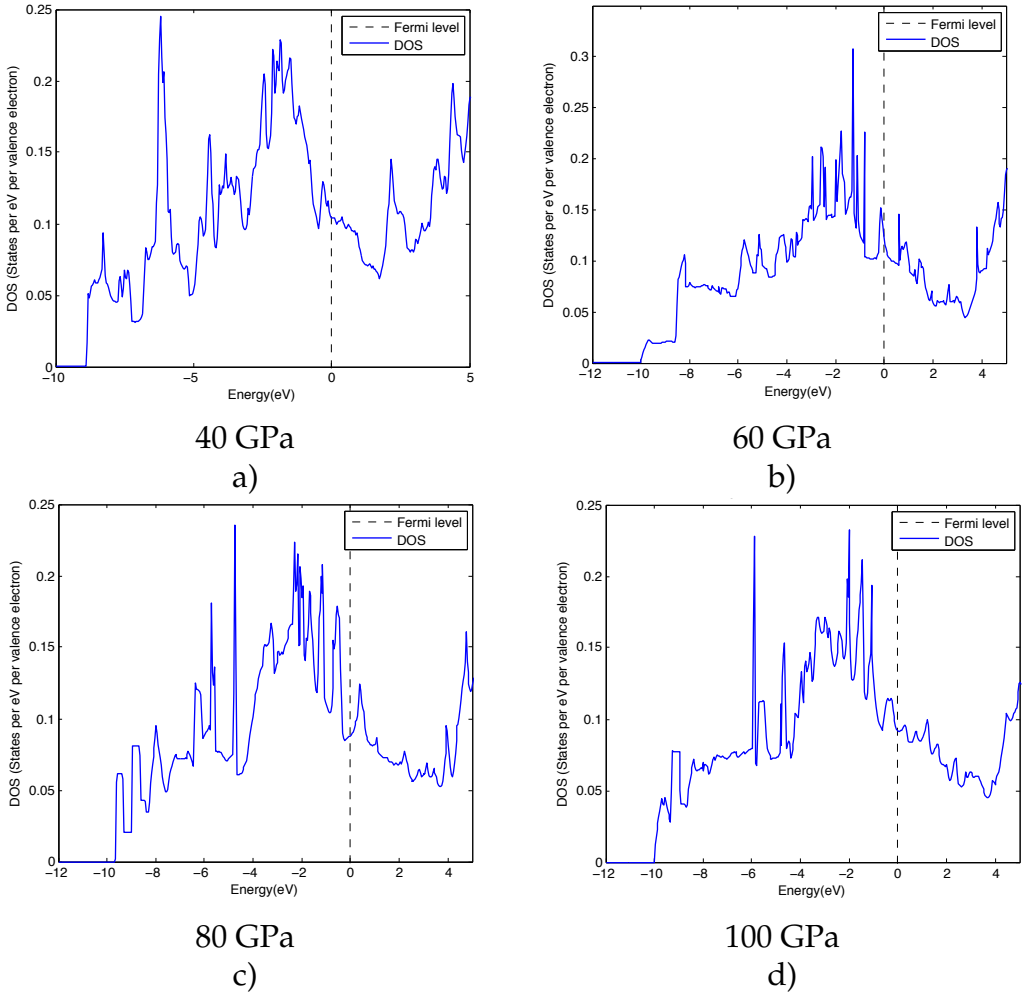

Figure 5.12: Normalized DOS for the Li_8Be_7H structures found with USPEX.

The lowest-enthalpy structure for the alloy Li_8Be_7H do show "layers" (Figure 5.10), but, as in the case of LiBe, these layers can be misleading; the distances within and between the layers are comparable, in the range of 1.9 - 2.2 Å at the pressures considered. These structures should be considered as three-dimensional. However, the DOS shows a step-like shape, as may be seen above in Figure 5.12. The values of the DOS at the Fermi level for these structures are not as high as they were for the unoptimized supercells.

Table 5.4: Energetics for Li_8Be_7H cells found with USPEX.

Pressure (GPa)	DOS at Fermi level per valence electron (eV^{-1})	Volume $Å^3$	Energy (eV / $Å^3$)
40	0.104	115.0	-0.295
60	0.115	101.9	-0.323
80	0.088	93.4	-0.324
100	0.091	87.6	-0.308

Li_4Be_3H

In this stoichiometry and at high pressures our lowest-enthalpy structures have beautiful and whimsical symmetries, as shown in Figure 5.13. Histograms of distances from the hydrogen atoms are shown in Figure 5.14. Once again, the trend observed earlier is repeated; hydrogens seems to move towards lithiums and even more, the hydrogen atoms seem to be nested within lithium cavities or channels . We summarize our results in Table 5.5.

Table 5.5: Energetics for Li_4Be_3H cells found with USPEX.

Pressure	DOS at Fermi level per valence electron	Volume	Energy
(GPa)	(eV^{-1})	$Å^3$	(eV / $Å^3$)
40	0.099	109.5	-0.352
60	0.073	96.8	-0.357
80	0.079	89.3	-0.353
100	0.066	83.3	-0.336

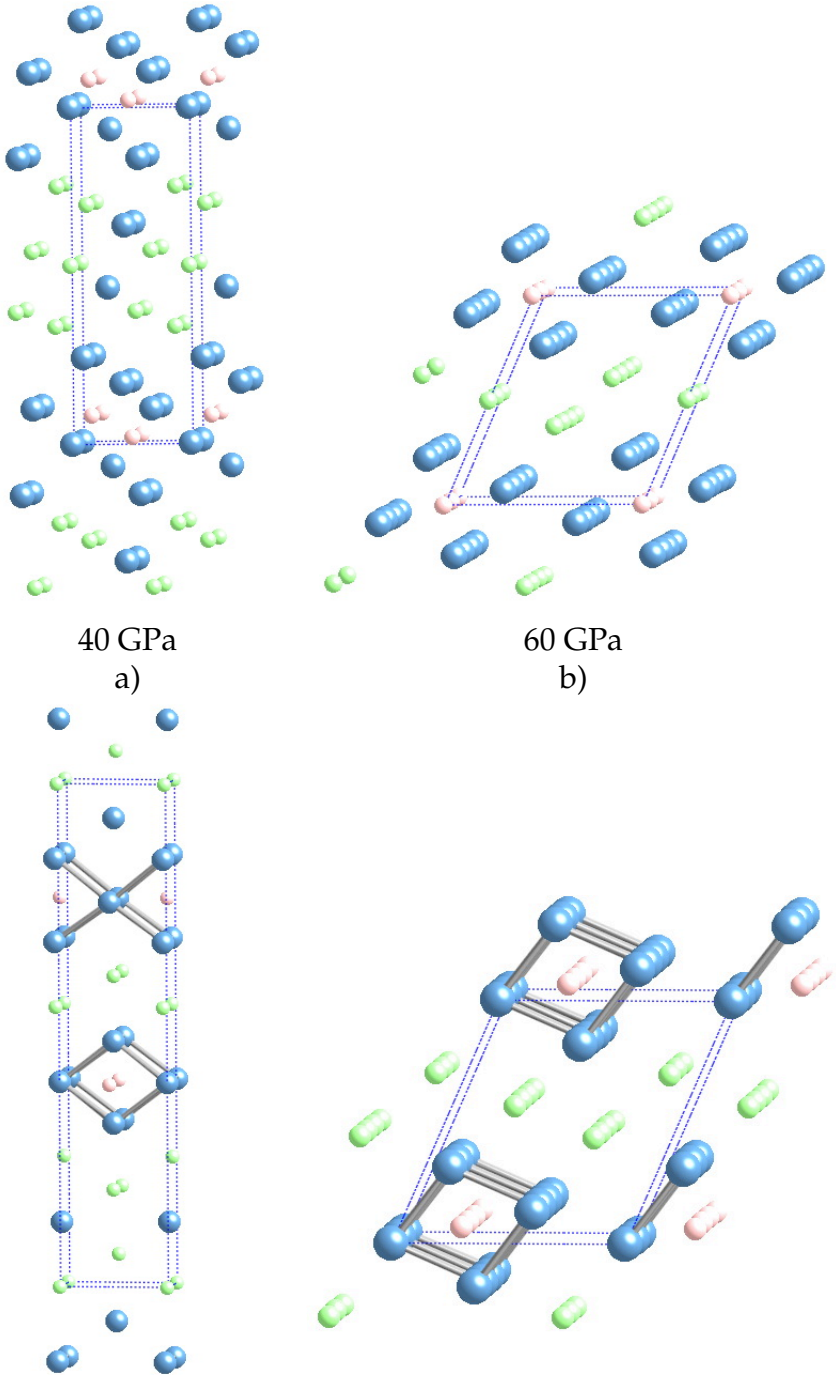

40 GPa
a)

60 GPa
b)

80 GPa
c)

100 GPa
d)

Figure 5.13: The lowest -enthalpy structures for Li_4Be_3H found with USPEX.

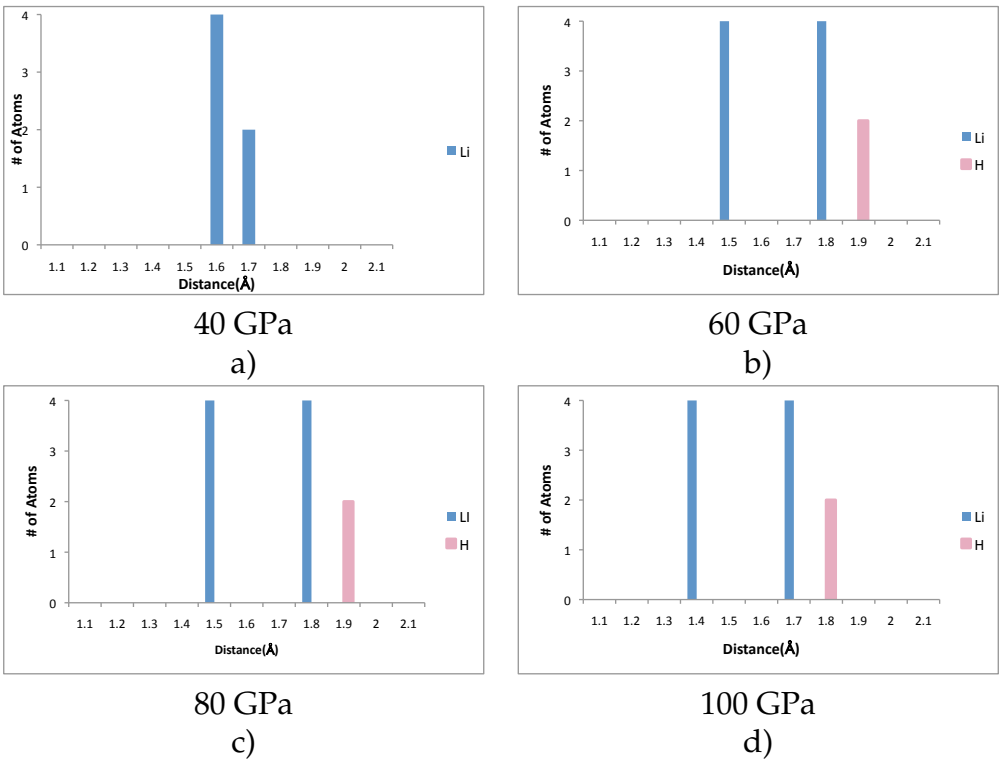

Figure 5.14: Histograms for the lowest-enthalpy structures for Li_4Be_3H found with USPEX. The coordination of the hydrogen is shown in portions of distance histograms (in blue, distances from the reference H to lithium; in green to beryllium; and in pink to another hydrogen).

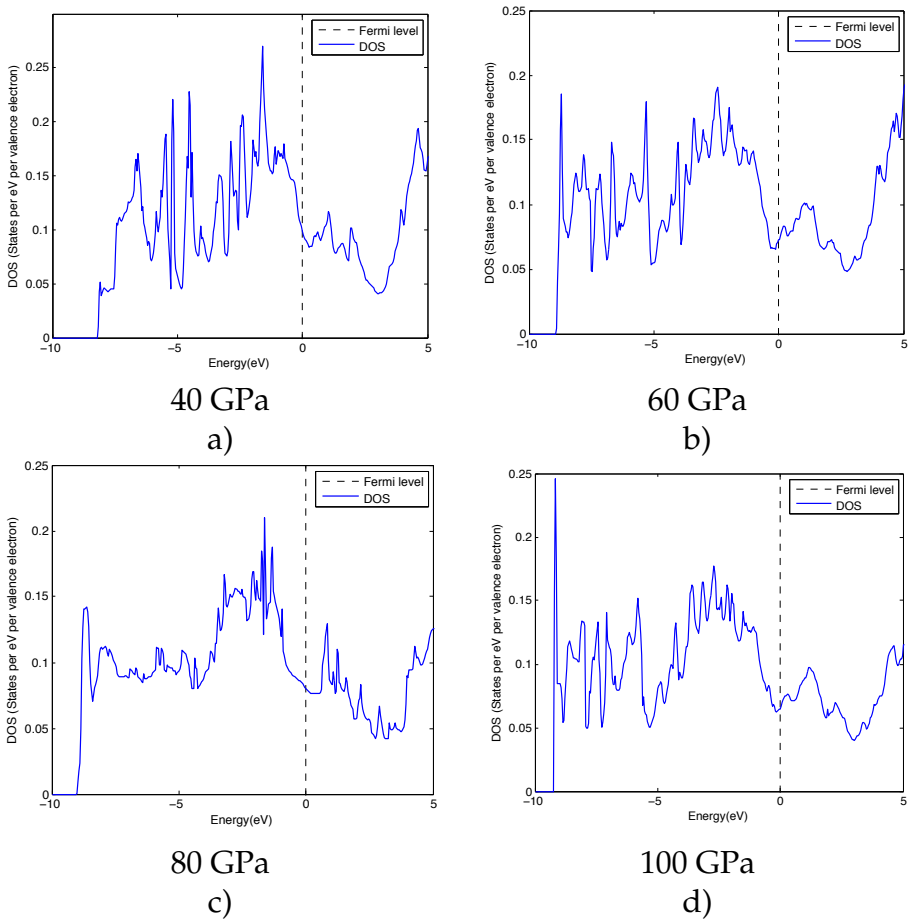

Figure 5.15: Normalized DOS for the Li_4Be_3H structures found with USPEX.

The structures found with the help of USPEX for the LiBe alloy are very similar to the ones previously found by Feng et.al. [7]. But the structures, although lower in enthalpy, for the $Li_xBe_{x-1}H$ with x= 4, 8 are very different from the ones we initially considered. A trend worth noting in our structures is that, as shown in our histograms, the closest nearest neighbor for H are Li atoms. Some hydrogens are ensconced within beautiful cages of Li.

The structures also seem to remember their "layered" nature in the LiBe alloy and all of our most stable symmetries have layers of Be. Interestingly enough,

the DOS for the system Li_8Be_7H at pressures 40, 60, 80 GPa and Li_4Be_3H at 40 GPa also shown a marked step-like shape.

In Table 5.6 we list the differences of the DOS at the Fermi level for our most stable systems at their corresponding pressures. Here a positive number means that the hydrogenated system has a lower density of states at the Fermi level, while a negative value implies a higher DOS. From Table 5.6 only one system has a higher density at the Fermi level than of LiBe, Li_8Be_7H at 60 GPa.

Table 5.6: Differences of DOS at the Fermi level for the systems found with USPEX.

Pressure (GPa)	LiBe - Li_8Be_7H (eV^{-1})	LiBe - Li_4Be_3H (eV^{-1})
40	0.002	0.007
60	-0.014	0.027
80	0.013	0.022
100	0.015	0.040

5.4 Conclusions

Our aim was to find some compounds related to the Li/Be alloy previously studied in which we could raise the DOS at the Fermi level. We achieved this, although not with any spectacular improvements, by building super-cells and replacing a Be atom by a H atom.

By using a genetic algorithm structural search program, USPEX, we found a

number of interesting, lower-enthalpy structures for these Li/Be/H alloys. Further studies are needed to find new ways of enhancing the density of states at the Fermi level in these compounds.

BIBLIOGRAPHY

[1] N.N. Greenwood and A. Earnshaw. *Chemistry of the Elements*. Oxford: Butterworth- Heinemann, 1997.

[2] M. Hansen. *Consittution of Binary Alloys*. Mc Graw-Hill Book Company, Inc., 1958.

[3] D.G. Pettifor. The Structures of Binary Compounds: I. Phenomenological Structure Maps. *J. Phys. C: Solid State Phys.*, 19:285–313, 1986.

[4] L.J. Parker, T. Atou, and J.V. Badding. Transition Element-like Chemistry for Potassium Under Pressure. *Science*, 273:95–97, 1996.

[5] T. Atou, M. Hasegawa, L.J. Parker, and J.V. Badding. Unusual Chemical Behavior for Potassium under Pressure: Potassium -silver compounds. *J. Am. Chem. Soc.*, 118:12104–12108, 1996.

[6] A.V. Tsvyashchenko, L.N. Fomicheva, M.V. Magnitskaya, V.A. Sidorov, A.V. Kuzenetsov, D.V. Eremenko, and V.N. Trofimov. New Ferromagnetic Compound synthesized at High Pressure. *JETP Lett.*, 68:908–914, 1998.

[7] J.Feng, R.G. Hennig, N.W. Ashcroft, and R. Hoffmann. Emergent Reduction of Electronic State Dimensionality in Dense Ordered Li-Be Alloys. *Nature(London)*, 451:06442, 2008.

[8] J.P. Perdew, J.A. Chevary, S.H. Vosko, K.A. Jackson, M.R. Pederson, D.J. Singh, and C. Fiolhais. Atoms, Molecules, Solids and Surfaces: Applications of the Generalized Gradient Approximation for Exchange and Correlation . *Phys. Rev. B*, 46:6671–6687, 1992.

[9] H.J. Monkhorst and J.D. Pack. Special Points for Brillouin-zone Integrations. *Phys. Rev. B*, 13:5188–5192, 1976.

[10] C.W. Glass and A.R. Oganov. USPEX-Evolutionary Crystal Structure Prediction. *Comput. Phys. Commun.*, 175:713–720, 2006.

[11] A.R. Oganov and C.W. Glass. Crystal Structure and Prediction Using Ab Initio Evolutionary Techniques: Principles and Applications. *J. Chem. Phys.*, 124:244704, 2006.

[12] W. Grochala, R. Hoffmann, J. Feng, and N. W. Ashcroft. The Chemical Imagination at Work in Very Tight Places . *Angew. Chem. Int. Ed*, 46:3620–3642, 2007.

APPENDIX A

SiH_4

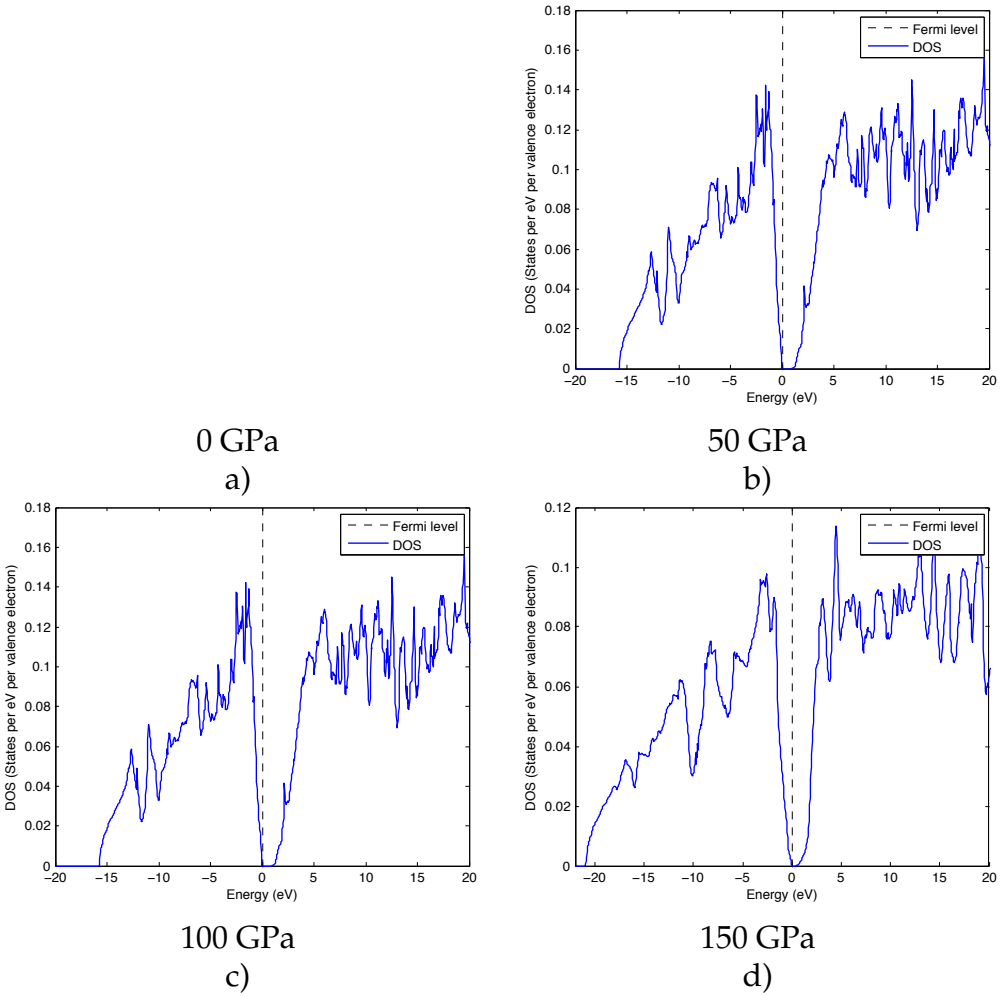

Figure A.1: Normalized DOS for the SiH_4 structures found with USPEX.

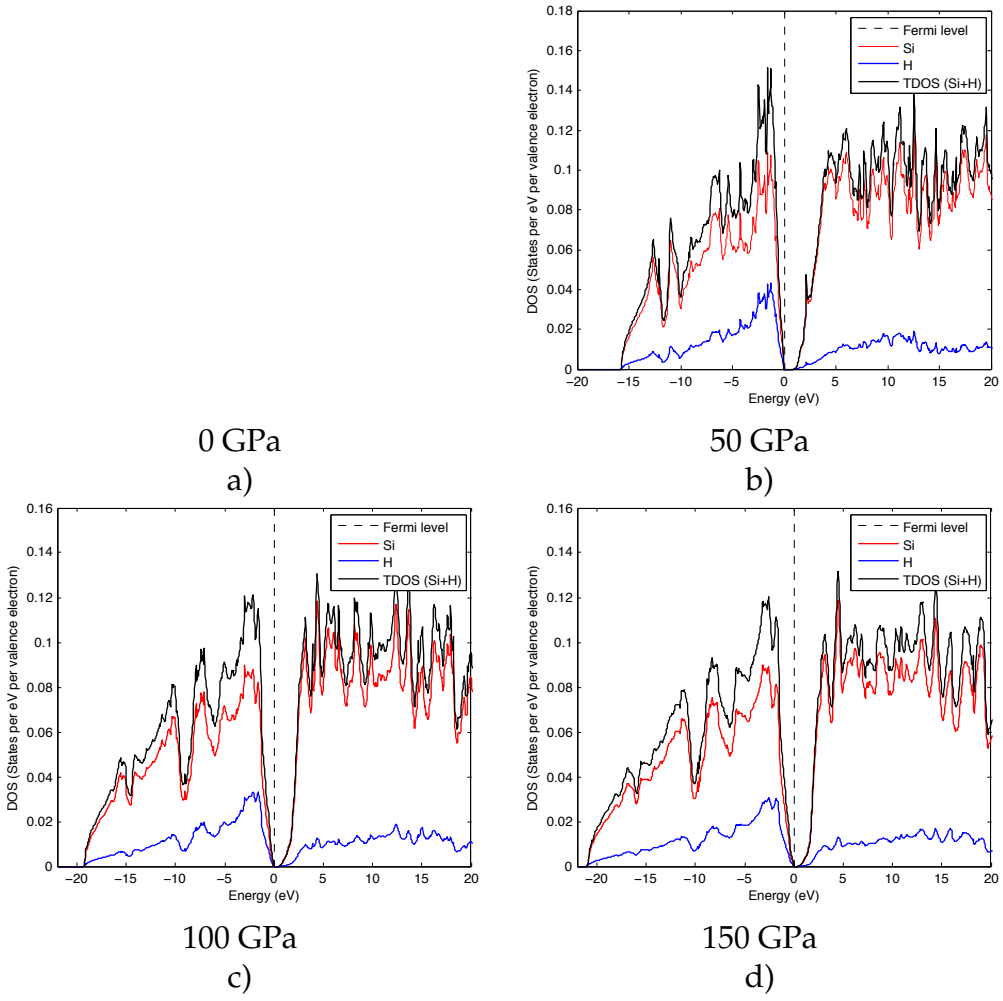

Figure A.2: Normalized PDOS for the SiH_4 structures found with USPEX, RWIGS values used as set on VASP. In red, the contribution of Si; in blue for H.

APPENDIX B

SiH_6

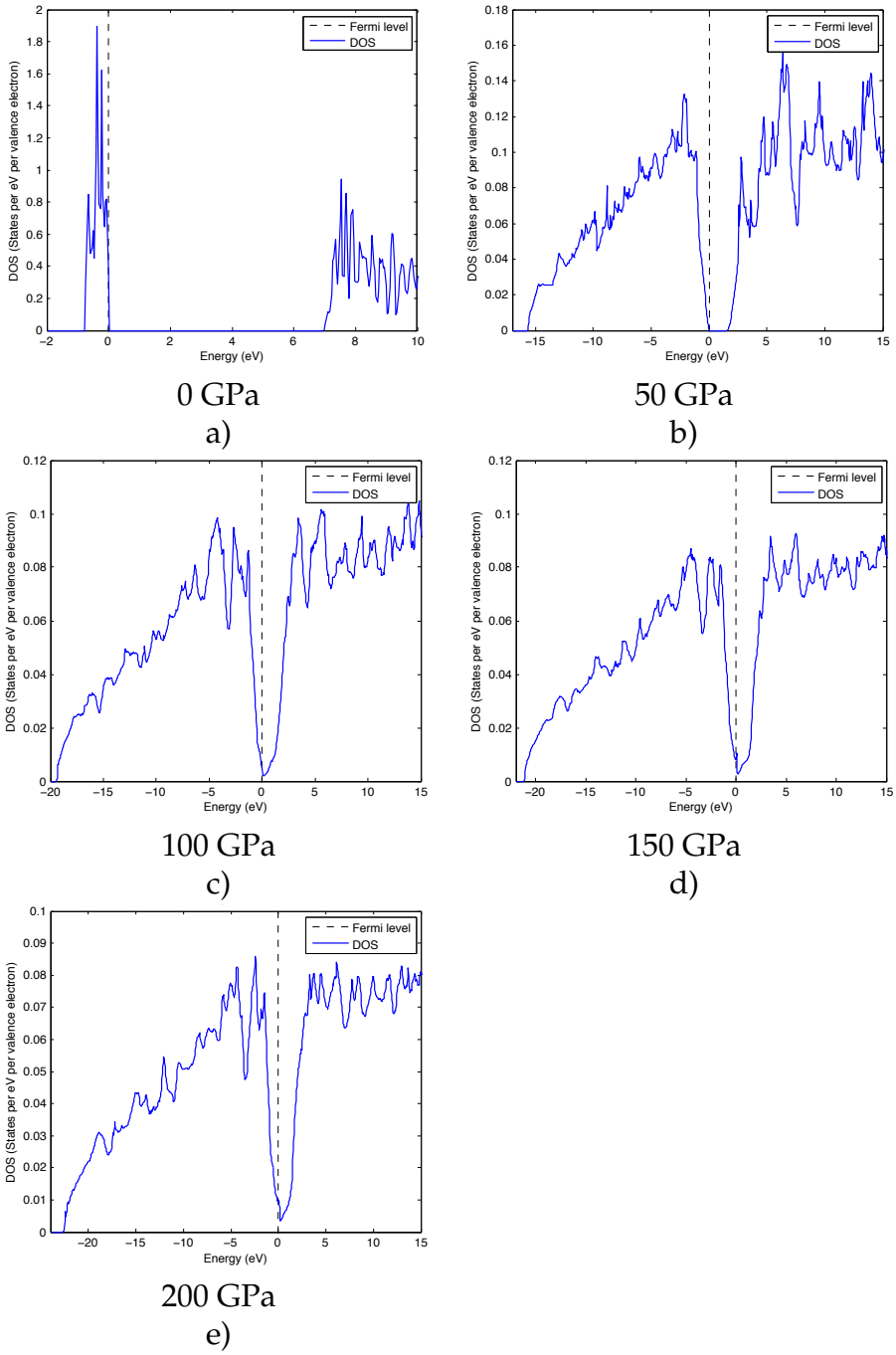

0 GPa
a)

50 GPa
b)

100 GPa
c)

150 GPa
d)

200 GPa
e)

Figure B.1: Normalized DOS for the SiH_6 structures found with USPEX.

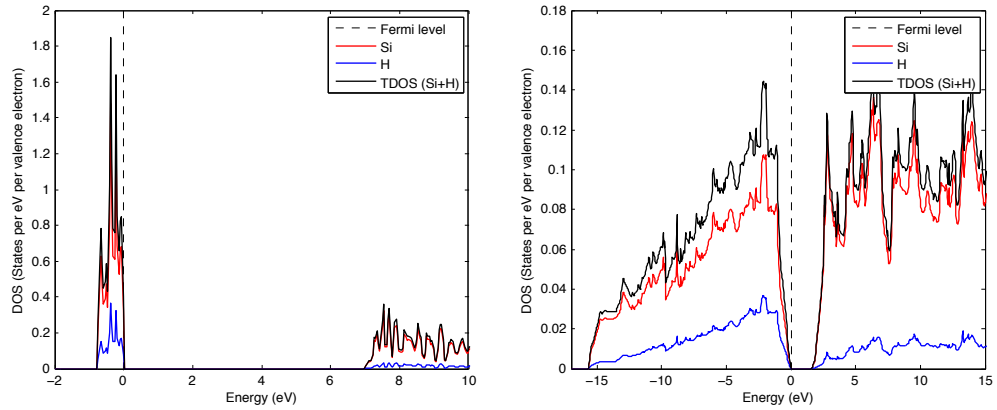

0 GPa

a)

50 GPa

b)

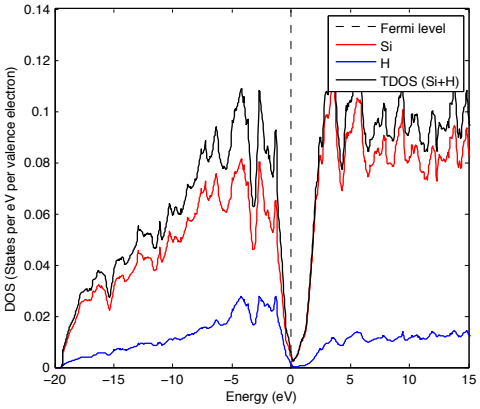

100 GPa

c)

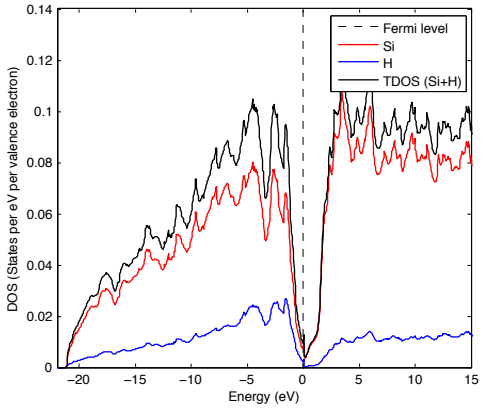

150 GPa

d)

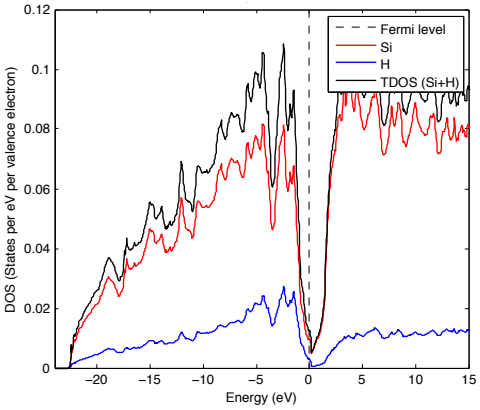

200 GPa

e)

Figure B.2: Normalized PDOS for the SiH_6 structures found with USPEX, RWIGS values used as set on VASP. In red, the contribution of Si; in blue for H.

APPENDIX C

SiH_8

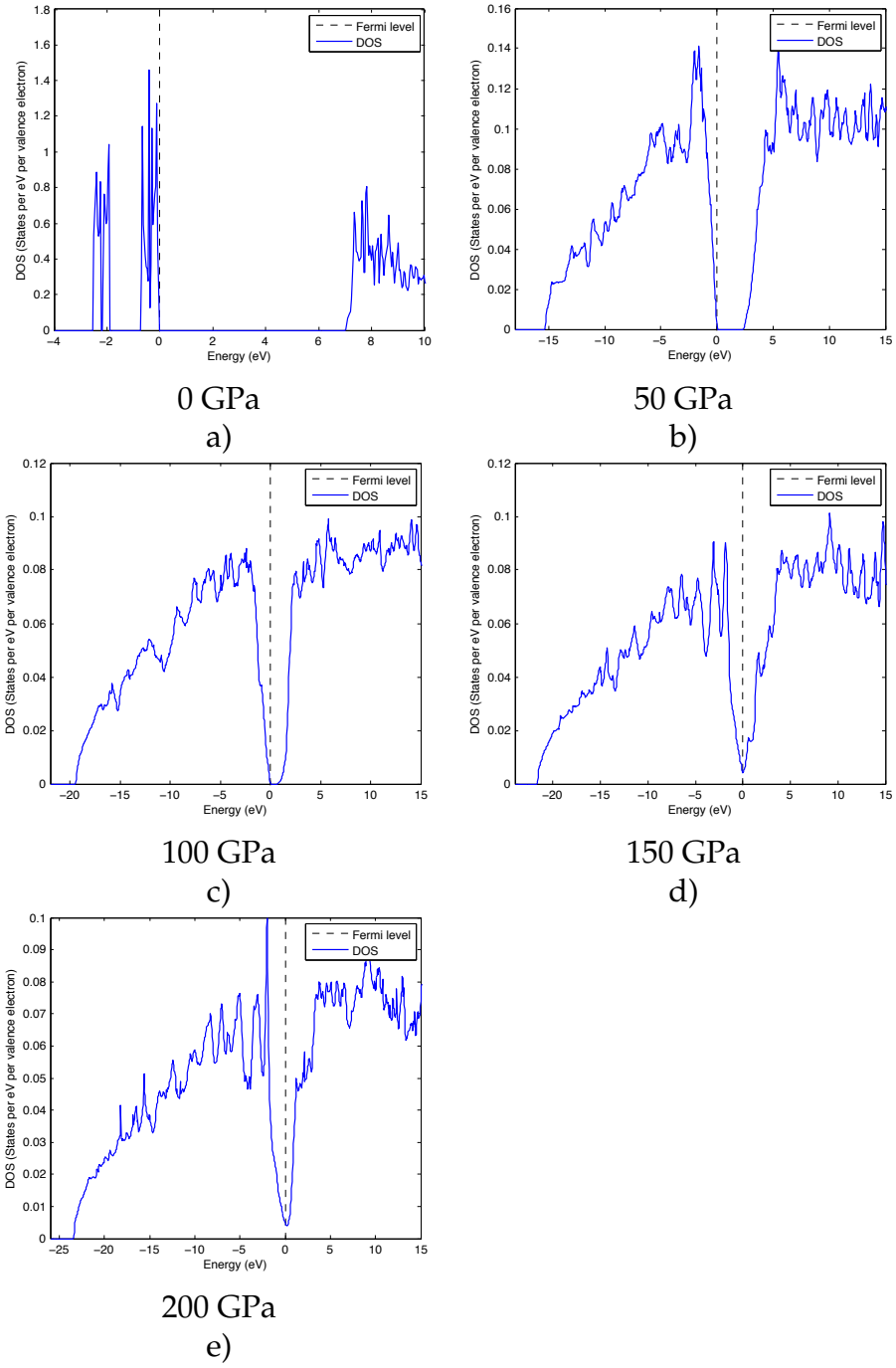

0 GPa
a)

50 GPa
b)

100 GPa
c)

150 GPa
d)

200 GPa
e)

Figure C.1: Normalized DOS for the SiH_8 structures found with USPEX.

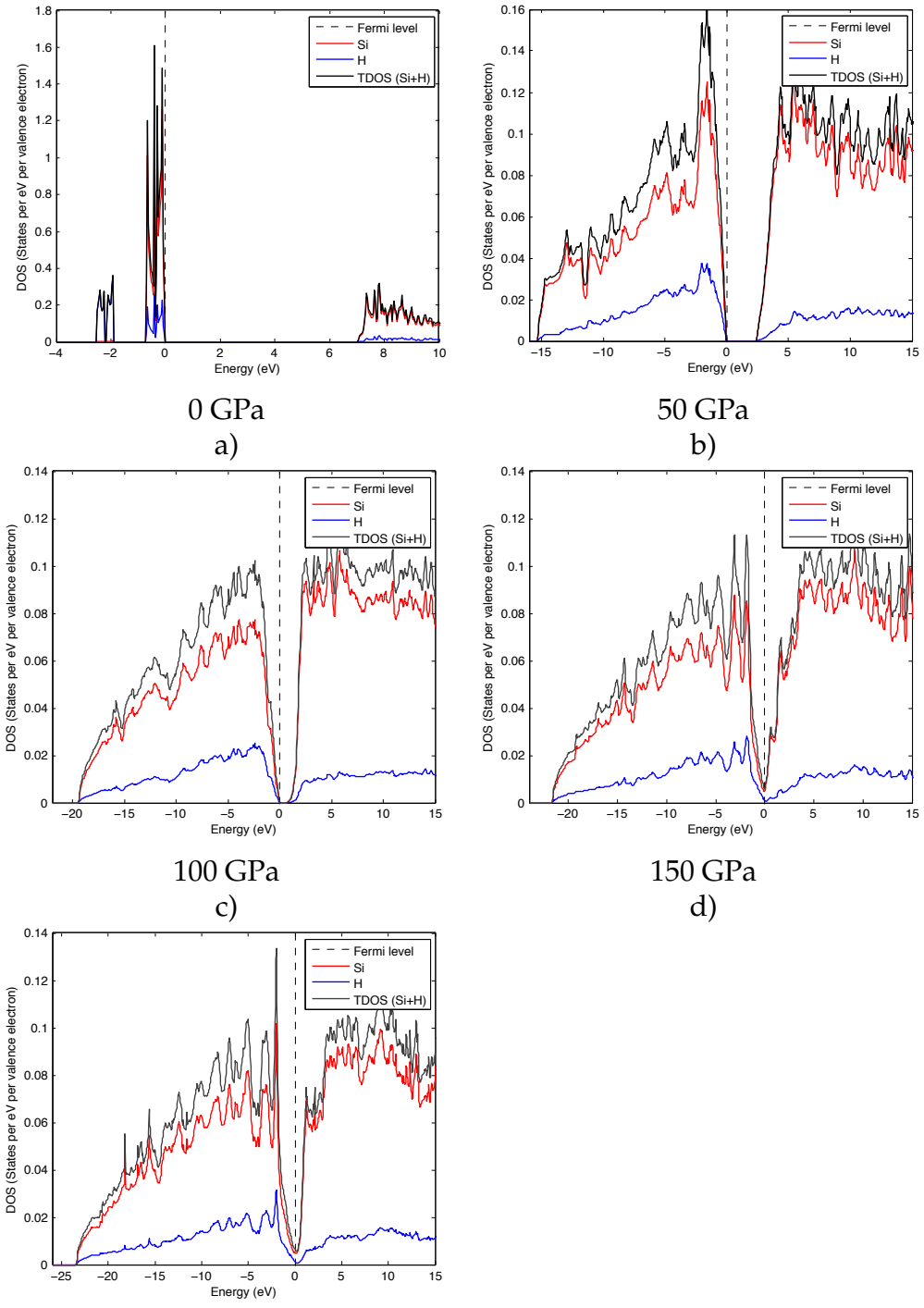

Figure C.2: Normalized PDOS for the SiH_8 structures found with USPEX, RWIGS values used as set on VASP. In red, the contribution of Si; in blue for H.

APPENDIX D

LiBe

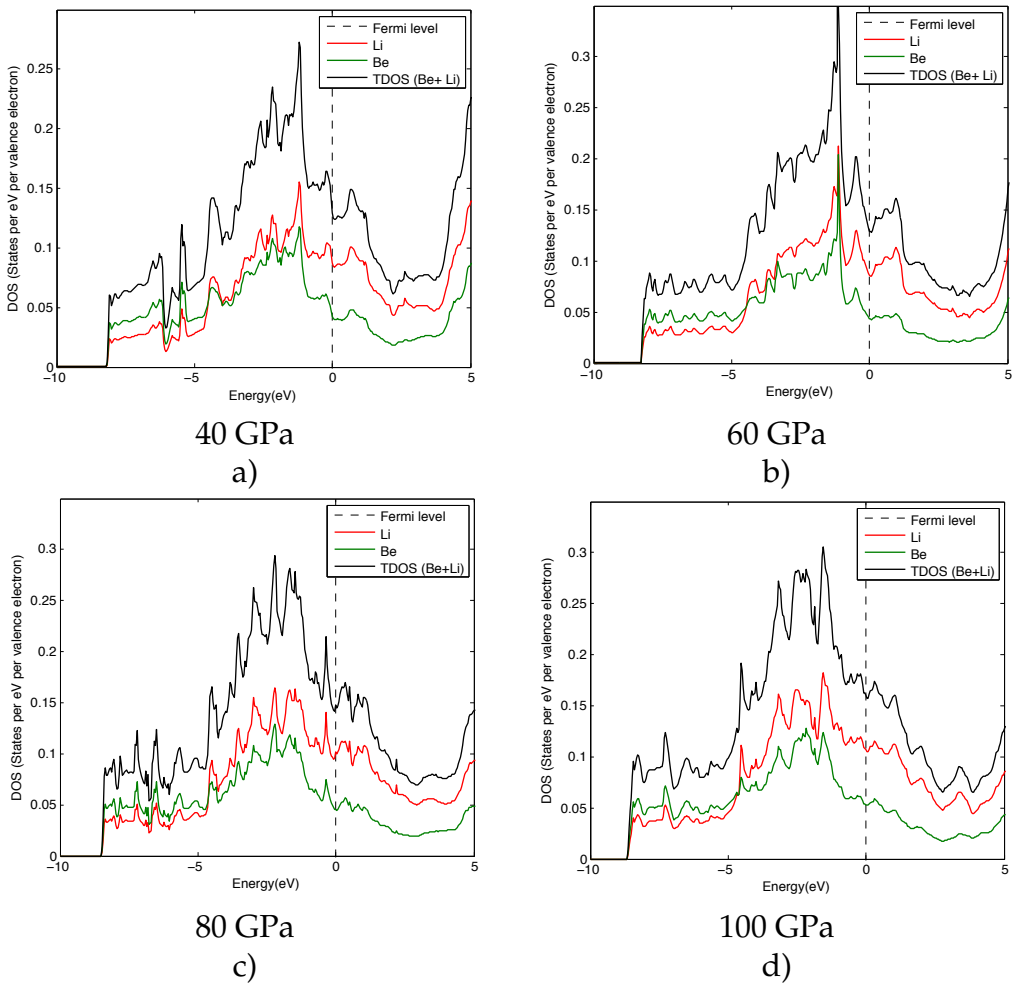

Figure D.1: Normalized PDOS for the LiBe structures found by USPEX, RWIGS values used as set on VASP. In red, the contribution of Li; in green, for Be.

APPENDIX E

Li_8Be_7H

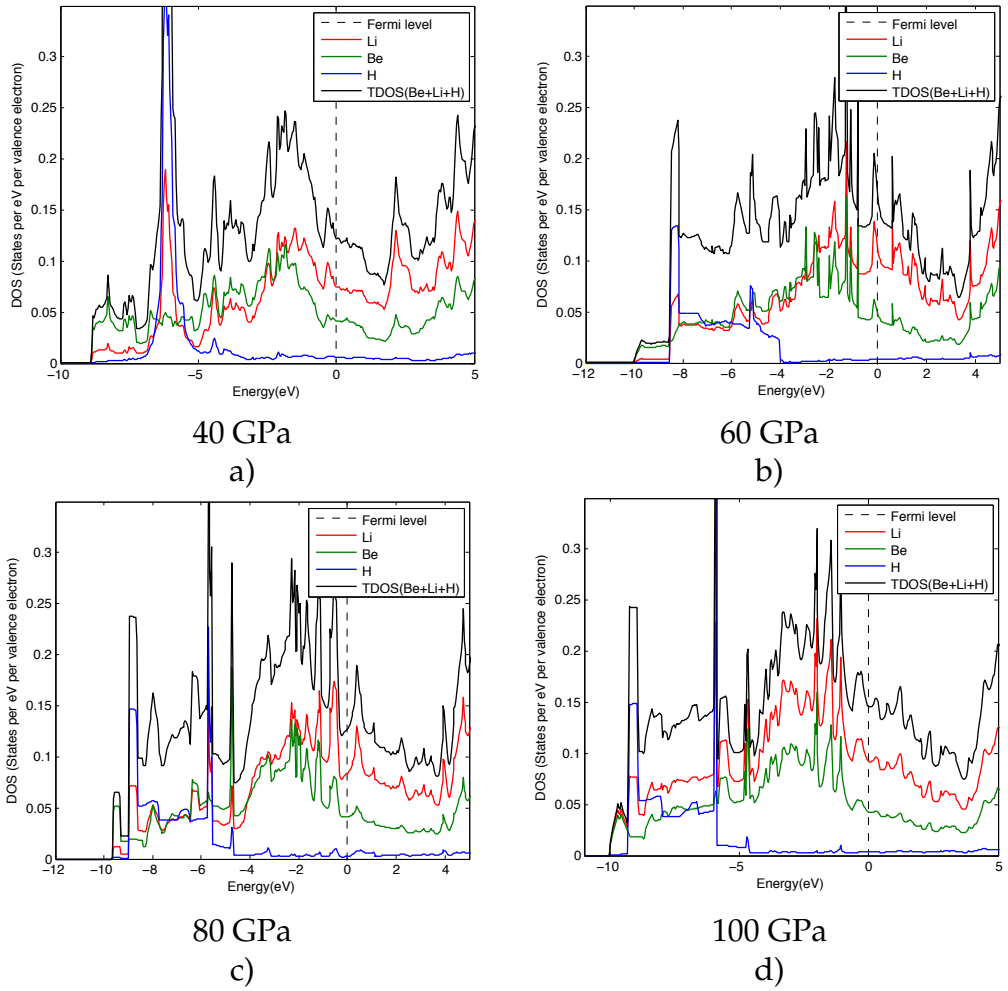

Figure E.1: Normalized PDOS for the Li_8Be_7H structures found by USPEX, RWIGS values used as set on VASP. In red, the contribution of Li; in green, for Be; in blue for H.

APPENDIX F

Li_4Be_3H

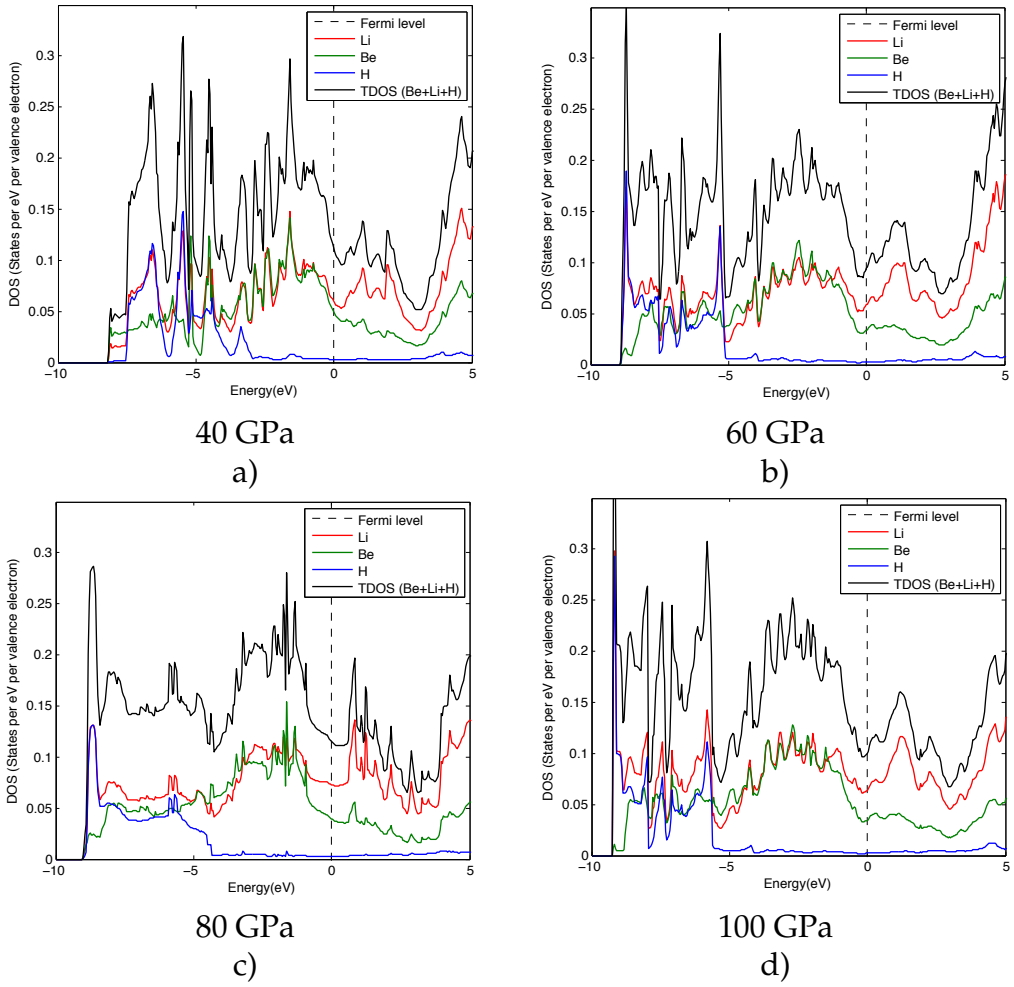

Figure F.1: Normalized PDOS for the Li_4Be_3H structures found by USPEX, RWIGS values used as set on VASP. In red, the contribution of Li; in green, for Be; in blue for H.